Board Level Drop Testing of Advanced IC Packaging

PEK WEE SONG ERIC

NATIONAL UNIVERSITY OF SINGAPORE

2004

Board Level Drop Testing of Advanced IC Packaging

PEK WEE SONG ERIC

(M.Eng, NUS)

A THESIS SUMITTED

FOR THE DEGREE OF MASTER OF ENGINEERING

DEPARTMENT OF MECHANICAL ENGINEERING

NATIONAL UNIVERSITY OF SINGAPORE

2004

Acknowledgements

The author would like to express his heart-felt gratitude to the following people without whom the project would not have been a success.

Associate Professor Lim Chwee Teck and Dr. Vincent Tan B.C. for their wisdom, guidance and supervision.

Mr. Tee Tong Yan, Dr. Luan Jing En, Mr. Daniel Yap and Mr. Goh Wee Lee from ST. Microelectronics for their assistance and guidance to the project.

Mr. Joe Low, Mr. Simon Seah and Mr. Alvin Goh from Impact Mechanics Lab for their patience and technical support during the course of experimentation.

Mr. Tan Long Bin, Mr. Ong Yeow Chon, Ms. Ang Chia Wei, Mr. Ridha, Mr. Alvin Ong and Mr. Norman Lee for their kind help in various issues of the project.

Ms. Ng Fong Kuan for her assistance in the conduct of experiment.

Huiying and my family members for their love and encouragement

People who have helped me in one way or another.

Table of Contents

List of Symbols and Abbreviations

f_n	natural frequency of vibration
v_b	rebound velocity
G_m	maximum G level of impulse profile
x_o	initial amplitude of deflection of a vibrating beam
AFOP	Gold (Au) on Finger, Organic solderability Preservative on ball pad
BLR	Board Level Reliability (pg. 10)
BGA	Ball Grid Array
CABGA	Ceramic Array BGA
CRO	Cathode Ray Oscilloscope
CSP	Chip Scale Packaging
DNP	Distance to Neutral Point
EIA	Electronic Industries Association
FBGA	Fine-pitch BGA
FCOB	Flip Chip On Board
G level	$1G = 9.81\ m/s^2$
JEDEC	Joint Electron Device Engineering Council
PDA	Personal Digital Assistant
PCB	Printed Circuit Board
SMT	Surface Mount Technology
TFBGA	Thin Fine-pitch BGA
VFBGA	Very thin Fine-pitch BGA
X-, Y- strains	strains in along the width and length directions of the PCB respectively

List of Figures

List of Tables

Summary

With the increase in demand for smaller telecommunications products like cellular mobile phones and PDAs, the use of microelectronic packaging such as BGA in electronic products has been widespread. As a result, accidental drop of these products may contribute to failure of the microelectronic packaging.

This project aims to investigate the drop impact responses of the microelectronic packaging such as during a drop impact. The components are tested on different drop heights and drop orientations. A number of drops are conducted on each PCB to investigate the number of failures induced on the different types of packaging. Their corresponding position and the number of drops at which the packages fails are examined. Strain gauges are also mounted at the center of the PCB to find the maximum strains induced in the principal axes of the PCB.

Drop impact responses (input and output acceleration levels, strains, velocity, flexing of PCBs etc) are analyzed and correlated to gain insight into the failure mechanisms of these electronic packages. Drop tests are conducted according to the new standards proposed by JEDEC. In addition, the effects of using different strike surfaces and varying different drop heights are also studied to simulate the likely conditions that a product drop test can encounter during an accidental drop impact.

Failure analysis is done on the samples to examine the possible failure modes encountered during impact. This is done using the cross-sectioning methods on the failed samples. A greater depth of understanding of the most likely regions of failure at the solder interconnects can be obtained.

Chapter 1 Introduction

1.1 Background and Motivation for Research

The usage of portable electronic products is getting more and more prevalent in the present society. Examples are portable digital assistants (PDAs), MP3 players, minidisc (MD) players and cellular phones. However, such mobility-enhancing products are susceptible to accidental drop impact. They are still expected to function even when that has occurred. Therefore robustness becomes an important issue in investigating the reliability of these products. A portable product normally houses a printed circuit board (PCB) with many components mounted on it. One common failure mode due to drop impact is the failure of the solder joints in some of these components. Testing for solder joint reliability is an important part in determining the failure of portable products during drop impact.

There are usually two main types of drop impact for these products. It could arise from mishandling during transportation of these products or from consumers who accidentally drop these products. Normally, for some products such as mobile phones, they are designed to withstand a few accidental drops onto a floor at a height of 1.5m, without causing major mechanical or functional failures [42-44].

Traditionally, board level reliability usually refers to solder joint fatigue strength during thermal cycling or thermal shock tests [13]. There are many researchers who have applied viscoplastic modeling to achieve accurate fatigue life prediction of solder interconnects in this area of research. However, there are few research work and publications related to drop test and modeling of solder joint reliability, although drop test should be as important as thermal tests, especially for the telecommunications industry. There is also very little study on correlation between simulation and experimental testing.

The motivation of this project lies in the fact that little is known on how microelectronic packages fail when electronic products are subjected to accidental drops. This study aims to find out how these components fail compared to other modes involving thermal cycling and key-press failures (usually found on mobile phones).

From this study, it is desired that we determine the factors that affect drop impact reliability and how these can help to obtain a more robust design of the IC package.

1.2 Objectives

The objectives of this research project are to:

- develop a standard methodology to study solder joint reliability by performing a board level drop test
- develop a method of in-situ resistance monitoring of the components during drop impact
- obtain relationship of the drop response parameters and the survivability of the components
- study how different mounting configurations of PCB can affect solder joint reliability

1.3 Scope of Thesis

This thesis comprises seven chapters. Chapter 2 presents an overview on the past research done on experimental board level drop tests and computational modeling of these tests. Past and recent board level drop test standards for different test conditions, size of PCBs and type of mounting are discussed. For board level drop tests, the effects of underfill, lead-free solders and thermally aged packages on drop reliability are discussed. Different board level modeling and simulation methodologies from various work and their correlation to actual experiment is studied. In addition, other mechanical tests closely related to board level drop tests are also reviewed.

Chapter 3 introduces the experimental setup and procedures for the drop tests. The drop test setup includes the drop tester, various fixtures, drop response monitoring equipment like strain gauges and accelerometers, and high-speed camera apparatus. The chapter also discusses the setup conditions to refine the board level drop tests in achieving consistency and ideal test requirements. Mechanics of drop impact are being discussed in detail and the maximum G level and impact time duration derived from momentum equations. Test plans for Thin Profile Ball Grid Array (TFBGA) and Chip Array BGA (CABGA) boards are also discussed.

Chapter 4 discusses the drop impact responses obtained from experiments. These responses include the shock experienced by the whole drop table, which is termed input G level, the in-plane strains at the center of the PCB and other points of interest on the PCB and the electrical resistance level of the components during the duration of drop impact. Output G levels are measured directly on some of the components located at critical locations of the PCB. The damping effect of the board is investigated and the high-speed images captured during drop impact are used in calculating impact velocity and board bending frequency. In-situ resistance measurement is conducted on packages during drop impact and the trend of these measurements is discussed.

Chapter 5 discusses the effects of board bending arising from different mounting configurations. These include different screw mounting and clamped edges configurations. In addition, the effect of knocking of the PCB against the fixture is studied and compared to cases where the PCBs have clearance to bend during impact. For CABGA packages, the effect of having underfill encapsulation is investigated.

Chapter 6 presents a new modeling methodology of using G levels as input boundary conditions and numerical results obtained are correlated with experimental data. The extent of board bending, solder joint stresses and frequency of cyclic bending can be predicted from the model if the correlation of the drop impact responses from experiment to modeling is accurate. The deflection of the board bending can be estimated to a beam-bending situation under certain assumptions with appropriate boundary conditions. This is discussed at the end of Chapter 6.

Chapter 7 then concludes the thesis and also provides recommendations for future work.

Chapter 2 Literature Review

This chapter presents a review of the past research work done on drop impact and other mechanical related tests for components. The topics include current standards used for board level drop tests, drop tests done thus far on various kinds of packages and board sizes, an overview of vibration and cyclic bending tests of PCBs and their effects on packaging material, and other mechanical loading tests that have been used to evaluate solder reliability.

2.1 Overview of shock and drop test standards

The EIA standard [1] suggests several acceleration waveforms for drop tests. For a half sine pulse waveform with time duration less than 3ms, the maximum value of the measured pulse must be within ±20% of the specified ideal pulse amplitude and its duration must be within ±15% of the specified ideal pulse duration. However, this standard does not provide much detail on how the test specimens are to be mounted and tested for reliability.

Military Standard for microelectronics [3] has various shock test conditions. Among these conditions, shock condition B requires an input of 1500G with impact duration of 0.5ms to be used in free-fall drop test conditions. This condition is in line with the JEDEC proposed standard [7] and is quite close to the shock levels experienced by small electronic products due to accidental drop as reported by Low [46].

The JEDEC standard “Board Level Drop Test of Components for Handheld Electronic Products” [7] is not to be used as a component qualification test. Instead, the test procedure is more suited for relative component performance against board level drop impact. Previous JEDEC standards [5, 6] did not provide enough details on the testing procedures nor specify a standardized board.

In [7], the specified overall board size is 132 mm x 77 mm. It has a nominal thickness of 1 mm and can accommodate up to 15 components (3 rows by 5 columns). It is not necessary to mount all 15 components on the board. 1-component and 5-component configurations are provided in this standard. The maximum component is limited to 15

mm in length or width and there must be at least 5 mm and 8 mm gaps between the components in x- and y-directions, respectively. There are four holes on the board for mounting the board on the drop test fixture. The locations of these holes are shown in Figure A.8 of Appendix A. The board is tightened by 4 shoulder screws with washers and supported by 4 spacers. The spacers are fixed onto a fixture plate. In the actual testing of components reported in this thesis, a metric system is adopted instead of the suggested Imperial unit as hardware is more readily available in the metric system. While shoulder screws ensure a higher degree of tightening than normal screws, the test board must still be tightened at regular intervals as high G level drop tests causes large board flexure during and after drop impact which causes the shoulder screws to loosen.

The horizontal board orientation with components facing downward results in greatest tensile force at the solder joints of a component placed at the center of the board due to the board flexure downwards after impact and the inertia of the whole component moving downwards. Thus, this is the orientation that is most likely to cause failures. Therefore, the standard requires that the board be fixed horizontally with components facing downwards during the test. Pre-test characterization is required to achieve JEDEC Condition B of 1500G amplitude and 0.5 milliseconds time duration with half sine waveform. The characterization requires monitoring of output acceleration and in-plane strains of the component at the center region of the PCB. In this thesis, the input acceleration and the center in-plane strains are always monitored. The hardness of the strike surface is adjusted to achieve the desired impact time duration.

During drop testing, the board is to be dropped for a maximum of 30 times or until 80% of all devices have failed, whichever is earlier. If there are no failures, JEDEC also proposes other drop conditions like Condition H of amplitude 2900G with 0.3 ms duration. However, the failure rate depends on a lot of factors including weight of the components, adhesion strength of the solder joints and the number of I/O.

Initial testing was done on small lightweight BGA components in the facedown orientation and it was found that Conditions B and H are not severe enough to cause failures in these components. A more severe condition is required to accelerate the

failure rate of these components. Thus, the most severe condition possible from the available drop tester of amplitude 4000G with 0.3 ms duration is used most of the time.

2.2 Review of board level drop tests

In a typical drop test of boards that are shaped like motherboards in mobile telephones, maximum compressive board strain of about 3800 microstrains were measured when the motherboard experienced a direct fall of 1m drop height from Mishiro et al. [28]. Three types of packages were tested using the same motherboard for many drops and their failure rates recorded. It was found that proper underfilling reduced the motherboard strain and stress of the solder ball. Yasuhisa et al. [49] reported extensive reliability data on key pressing and drop testing of a mobile telephone. Different loading rates were applied in 3-point bending tests to evaluate the failure reliability of the CSP devices in the PCB. Strain gauges were mounted on a cellular phone to determine the strain at various points of interest (where the CSP is located) during drop test. These strain profiles are for cross comparing with other cellular phones of similar mounting specifications of the motherboard and size.

Challenges abound when conducting proper drop tests. For example, drop tests of packages with BGA solder joints by Yu et al. [29] did not achieve good repeatability of shock levels at drop heights 0.8m and higher due to air resistance. However, if the friction of the jigs' bushes with the sliding rods of the drop tester was kept constant, repeatability can still be ensured and the failure results will be more representative of the drop height used. Hiraiwai and Minamizawa [30] evaluated fine pitch ball grid array (FBGA) packages and good reliability was achieved when the packages are mounted above the PCB. Hiraiwai and Minamizawa also dropped PCBs on their edges and found surface cracks on the board side.

Another problem that researchers often overlook is that a large PCB is not representative of PCBs in miniaturized mobile products. Furthermore, different products will have PCBs with different components of different sizes [24]. Testing with large PCBs is not recommended in the JEDEC standard [7]. Larger PCBs generally experience higher deflection and should not be used to compare with product drop tests, where the PCBs are much smaller. The position of components on a large PCB and the size of the components are important factors in drop impact performance.

It is therefore difficult to design a single board level drop test to evaluate the impact reliability of a component that may be used in different products.

Extremely thin CSPs (etCSP), where the height from the top of the package to the surface of the board was only 0.5mm thick, were tested under JEDEC condition B by Yoshida et al. [33]. The cross section of the package is shown in Figure 2.1. This etCSP is cross-compared with that of a standard size CSP where the height of the package from the board is 1.2mm. In the cumulative failure plots given in the paper, it was found that etCSP had better drop reliability than the referenced CSP. This may be due to the heavier weight of the standard package resulting in greater inertia forces and higher peeling stresses at the solder joints. The etCSP is lighter and more flexible as its height is only 0.5mm and the molding area is just around the die. etCSPs were also found to be more reliable in cyclic bending tests.

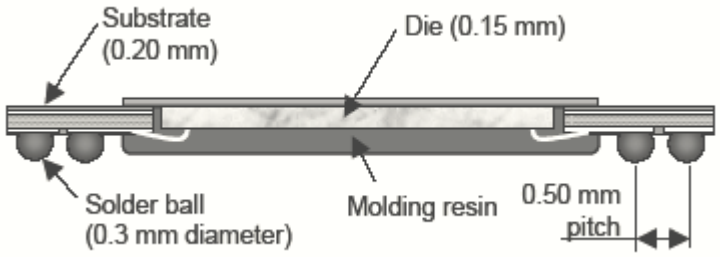

Figure 2.1: Cross section of extremely thin CSP

2.2.1 High-speed photography

High-speed imaging was deployed to monitor displacements of selected points of interest on the PCBs during drop impact testing by Wang et al. [27]. The frame rate used is 4500 frames per second. The velocity profile could be derived from the displacement plots. The displacement fluctuates in a cyclical manner at the center of the free edge, suggesting a dominant fundamental mode of vibration shortly after drop impact. Pradeep et al. [40] also used a high-speed camera setup to ensure good repeatability of the drop tests by monitoring the displacement and velocity of the PCBs. The velocity before impact could also be monitored so that the effects of friction along the guiding rods of the drop tower are taken into consideration. High-speed camera photography was also used to estimate the deflection of the PCB upon drop impact as done in Tan's work [18].

2.2.2 Effect of underfill material on drop reliability of packaging

FCOB packages were reported to possess good drop impact reliability because of the presence of underfill encapsulation in these packages [27]. However, the input G level reported in the paper was too low to cause any failures. JEDEC recommends a minimum input of 1500G. In the experiment work presented in this thesis, much higher G levels are used to accelerate failures of BGA packages. Higher G levels will also mean higher maximum in-plane strains and higher deflection velocities of the PCB, resulting in higher strain rates in the solder joints eventually.

FCOB packages with underfill material generally have better drop reliability than FCOB packages without underfill as reported by Jang et al. [35]. Two conventional underfill technologies are capillary underfill and no-flow underfill. Jang et al. tested reworkable underfill for FCOB packages and found they had poor adhesion. However, they are still being used for SMT applications to reduce costs.

An alternative of using pre-applied underfill is discussed by Hannan et al. [36] where four different types of pre-applied underfill were evaluated. They are underfill preapplied to solder bumps (PSB), partial underfill (PUF), underfill preapplied to solder bumps with partial underfill (PSB-PUF) and perimeter underfill (TP). Drop tests were conducted on these four types of underfills with a CSP of dimensions 12 x 12 mm with 168 I/O at 0.8mm pitch. The test conditions were set at a G level of 1500G with a time duration of 30ms. Failures were detected using an event detector with a threshold limit of 1500Ω. The Weibull plot of failures against number of drops is shown in Figure 2.2. In general, the drop reliability of the preapplied underfill CSPs is much better than similar CSPs without underfill. Figure 2.2 also summarizes the number of drops needed to get 63.2% failure for all cases. The number of drops for the control, i.e. no underfill, was around 100, compared to around 233 for PSB, 497 for TP, 342 for PUF and 492 for PSB-PUF. Additional drop test studies for evaluating underfill material are also found in [40] on lead and leadfree solders.

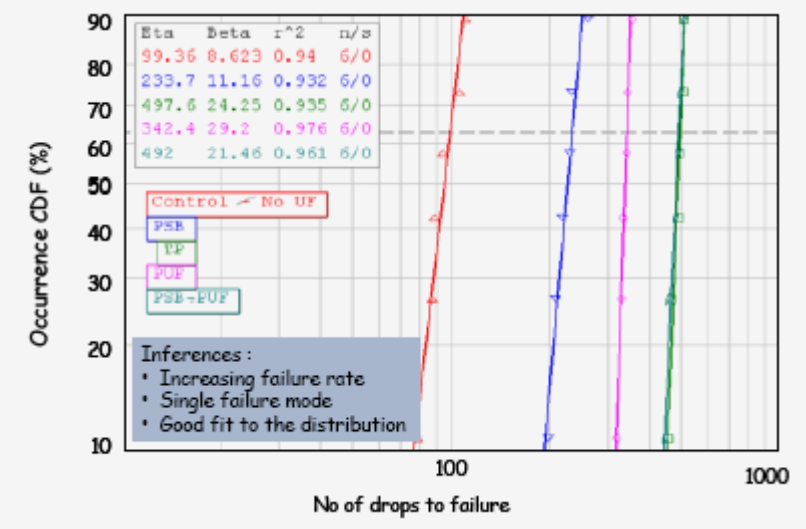

Figure 2.2: Weibull plot of number of drops to failure for various preapplied solders [36]

2.2.3 Effects of thermal aging on drop reliability

Drop tests on lead-free solder showed that as the percentage of silver increases, the drop reliability generally decreases as reported in Amagai et al. [25]. This means that soft solder has an advantage over hard solder for drop test performance. However, it seems that in bending and thermal cycling tests [25], a relatively higher percentage of silver helps in the reliability of these solders. The suggested optimum solder composition for all three tests (drop, thermal cycling and bend tests) is about 1.0-1.5% Ag. Sn-Ag-Cu was also found to be better suited for dynamic loading as compared to Sn-Ag-Ni lead free solder. It is further shown that indium can reduce Kirkendall voids and nickel can reduce the thickness of the Cu_3Sn layer in lead free solder [41]. With a correct solder composition, the drop performance can increase by 20% after thermal aging at 150°C.

The effect of thermal aging on CSPs was studied in [38]. This study was conducted to investigate the influence of intermetallic compound (IMC) growth on the solder joint reliability of Pb-free BGA (SnAgCu solder on Cu pads) packages under drop loading conditions. Thermal aging of the test board assembly was performed at 125°C for 3, 10, 20 and 40 days to induce solid state IMC growth in solder joints. The shock pulse used for the drop condition is a triangular pulse with peak acceleration of 1500G and 1ms duration. It is found that the components near the test board mounting locations (at the corners) have higher drop lifetimes than components at the center of the test

board due to the lower vibration amplitude near board mounting points. Figure 2.3 shows the board level drop mean life as a function of aging time. It shows the drop performance (BLR- Board Level Reliability) degraded 80% from time 0 to 10 days of 125°C aging. After 40 days of thermal aging, the failure occurred at the first drop. This includes the corner components failing at the 1st drop. This is due to the formation of voids at the pad-solder interface under high temperature aging.

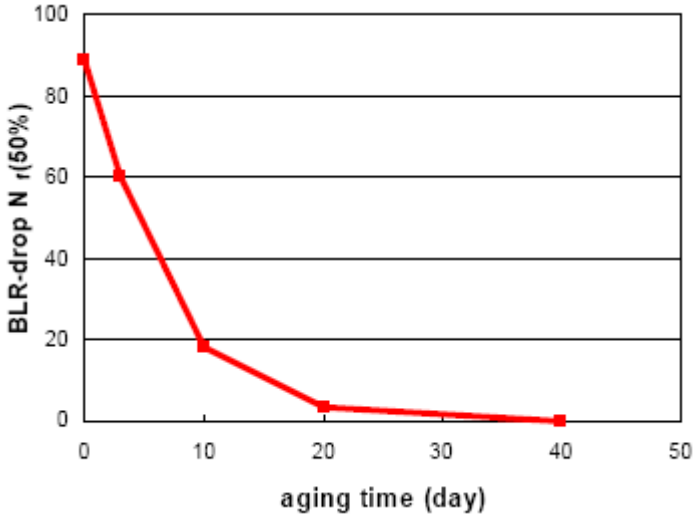

Figure 2.3: Mean cycles to failure for board level drop test as a function of aging time

2.3 Review of board level drop test simulation

Zhu [19] used a sub-modeling method in LS-DYNA to analyze impact reliability to reduce CPU time. The time-history dynamic response from a macro global model is transferred to a micro local solder model in the sub-modeling approach. Two types of impact loading were tested. The first uses a guide tube to drop a sphere onto the center of the PCB. The second simulates a PCB free fall onto a hard surface. The second type of simulation is more relevant to the work presented in this thesis. The paper shows that the solder-to-component interface is where the maximum plastic strains occur and a crack is likely to initiate. This is in agreement with typical keypad loading tests. However, the failure location may not be the same for all cases as adhesion strength and degree of bending of the PCB are important factors as well. The sub-modeling technique was also used to evaluate the stresses in solder joints of different shape profiles. He found that a larger neck size at solder-to-component interface than the neck size at solder-to-PCB interface would decrease plastic strain as compared to a larger neck size at the solder-to-PCB interface. This will improve impact related

reliability. The simulation also determined that the solder ball most likely to fail is the one at the corner of the grid array.

Tee et al. [17] did a simulation of board level drop test on Integrated Passive Devices (IPDs), using orthotropic properties for rectangular-shaped PCB and viscoelastic properties for eutectic and lead-free solder joints. The drop condition follows the JEDEC standard of an input acceleration peak of 1500G with time duration of 0.5ms. The results show the solder ball stress level is the highest when the PCB has the largest deflection, because of the inertia force after impact. High stress concentration is observed along both the solder/PCB and solder/IPD pad interfaces unlike [9] where high stress concentration is observed only at the solder/component interface. It is found that solder balls along the PCB length direction has a higher bending stress level (see Figure 2.4) because the board bends more along the length direction.

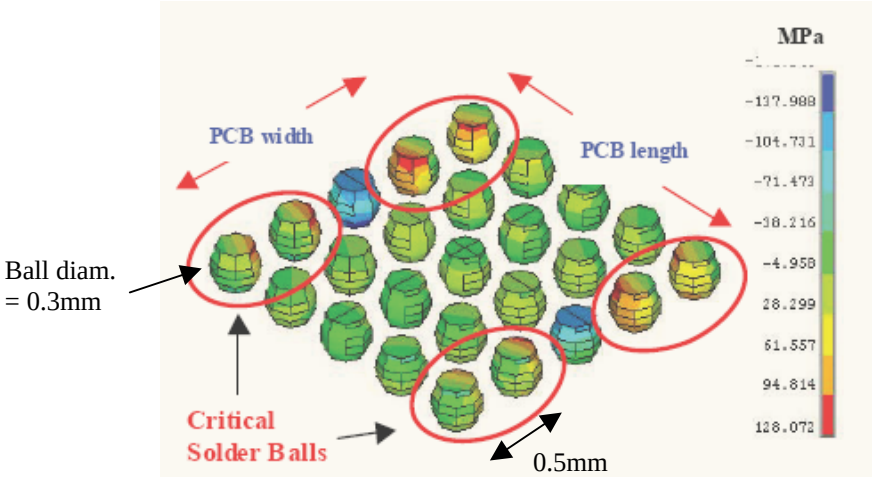

Figure 2.4: Stress distribution of solder joints during maximum PCB bending

Wang et al. [27] used a small hybrid model and a full detailed model to simulate board level drop tests Only the FCOB assembly including the PCB and silicon chips were modeled in the hybrid model (see Figure 2.5). The displacement data at the two longer clamped edges of PCB was obtained from video camera measurements. The results show that the detailed model yielded larger error than the hybrid model when compared to the experimental results. This is because a lot of factors in the detailed model are not considered such as friction along the guiding rods, effect of strike surface material and shape and rebound effect of the drop table. The hybrid model may pose some problems if the displacement profile used as the input for model does not have a small time step to accurately predict the level of acceleration in the FCOB

assembly. This gave results close to the output acceleration of the component itself, but it did not show a true picture of the stress levels in the solder joints because displacement was obtained from high-speed photographs. Acceleration data acquired by accelerometers is preferred as input data for simulation in the proposed G-input method mentioned in this thesis.

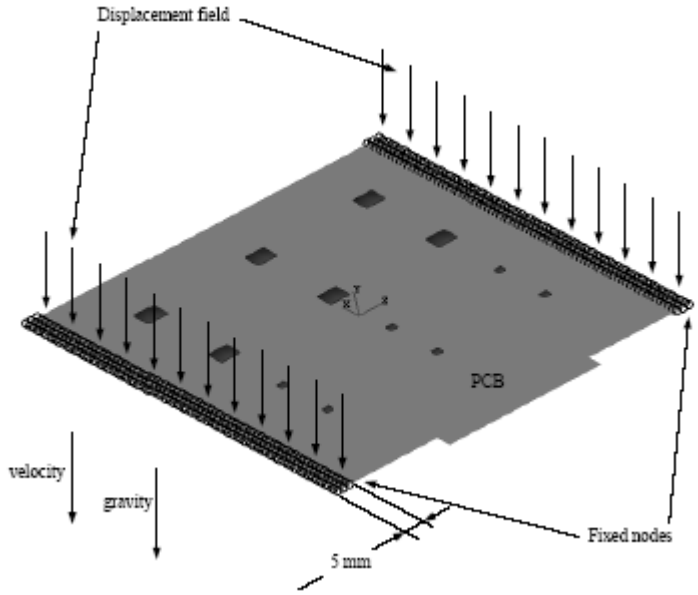

Figure 2.5: Hybrid model for FCOB assembly

Xu et al. [26] studied the effects of solder ball height and pad size on the stress levels of the solder joints under similar drop load conditions. The board is fixed with 4 screws at the corners with the component at the center of the board. Von Mises stresses and peeling stresses were compared. With 4-screw supports and the component at the center, peeling stress is more of a concern as board flexure is expected to be greatest at the center of the board. The difference in curvatures of the board and component induces large peeling stresses in the solder joints. It is believed that peeling stress in the joints (shown by the experiments in this thesis) is the dominant factor in the drop reliability of these packages. The paper shows that higher solder ball height, i.e. an increase in solder volume, results in higher peeling stresses at the solder/component and solder/board interfaces. This is further supported by the simulations reported in [36]. Increasing the pad size decreases the peeling stress but increases the Von Mises stress on the board side [26]. Xu et al. also mentioned that while shorter solder ball height might have lower peeling stress, it is likely that it will experience higher shear stress, which is a concern when thermo-mechanical loading is present. The weight of

the package is also an important factor determining the magnitude of the peeling stress in the solder ball [36].

A model of PCB with mounted components using shell elements was proposed by Ren and Wang [31]. In the drop simulation, it was found that the relative difference in the peak Von Mises stress between the shell-element model and a solid-element model is only less than 3.5%. The computational time of the shell-element model only took 14% of the time to run the detailed 3D solid-element model. It is also found that the outermost corner solder experiences the most severe stress during drop impact, as shown in Figure 2.6.

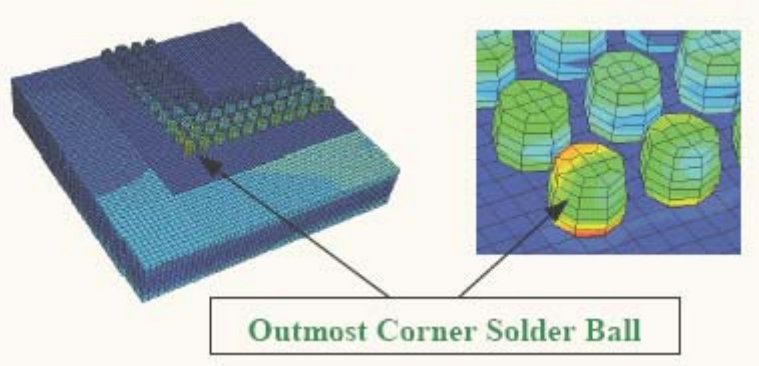

Figure 2.6: Von Mises Stress due to drop impact [31]

2.4 Review of other mechanical loading tests on PCBs

2.4.1 Cyclic bending and vibration tests

Bending and vibration tests were conducted by Hin et al. [51] to characterize the effect of board mounting locations as well as the mass effect on the PCB flexure. In the paper, three bend modes were studied, i.e. spherical bend, diagonal bend and planar bend as shown in Figure 2.8. The standoffs are spacers that give a specific clearance of the PCB to the fixture to allow board flexure. An example of the layout of the spherical bend test is shown in Figure 2.7. The rectangular rosette directions are shown next to the figure. For spherical bend, the bending effect due to the masses and mounting positions will induce equivalent strains for all three strain components E1, E2 and E3 due to symmetry. The strain component E2 is dominant in the diagonal bend test. However, components are seldom placed in the diagonal bend test configuration and thus the work discussed in this thesis will only focus on the spherical and planar layout for board level drop tests. In the planar bend tests, the dominant strain occurs on E1

direction while E3 strain is a result of Poisson's effect. Stresses are induced at the package edges.

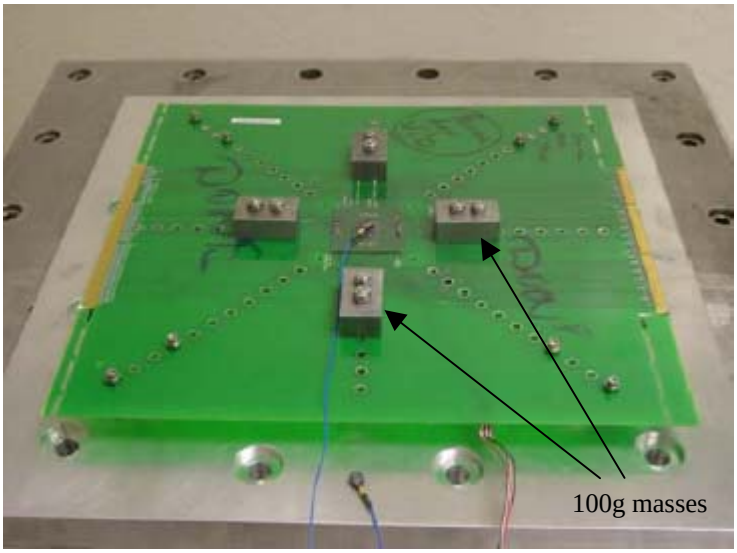

Figure 2.7: PCB setup with simulated masses and mounting position (spherical bend)

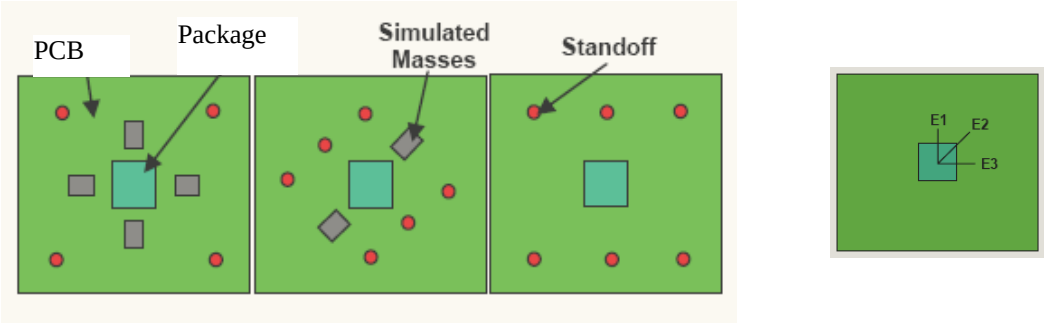

Figure 2.8: Spherical Bend, Diagonal Bend and Planar Bend

A detailed vibration test was done on PCBs by Phil et al. [52]. They studied the mass effect at the center of PCB on the resonant frequency of the board by varying the weight at the PCB center. A comprehensive study of modal testing was also conducted by varying package sizes and orientations. Of the three variables tested, i.e. mass, orientation and package sizes, the mass on the board was determined to be the most dominant factor for resonant frequency. Larger masses yielded smaller board resonant frequencies. The experimental results also show good correlation to simulation results.

A 3-point cyclic bend test was conducted with maximum out-of-plane displacement of 1mm at the board center with a FBGA (Fine-pitch Ball Grid Array) component on the

other side of the board by Sidharth et al. [32]. The test was conducted for 3000 cycles. Failure was defined by the detection of an open circuit. There was no increase in the electrical resistance of the FBGA for the 1st 250 cycles and no failures were recorded after 3000 cycles although the resistance had increased. The board support span is only about 51mm and thus for a small board, the PCB will bend with a larger radius of curvature as compared to a longer board. Hence, the peeling stress at the solder joints is higher when the deflection is the same for a shorter support span.

2.4.2 Ball shear tests

A miniature Charpy impact test was conducted by Date et al. [61] to evaluate the impact toughness of different types of lead-free and conventional solders. The Charpy test was compared to normal ball shear test. The Charpy test induces a high shear rate of 1 m/s while the conventional ball shear test gives a very slow shear rate of 0.2 mm/s. The schematics of the conventional shear test and the Charpy test are shown in Figure 2.9.

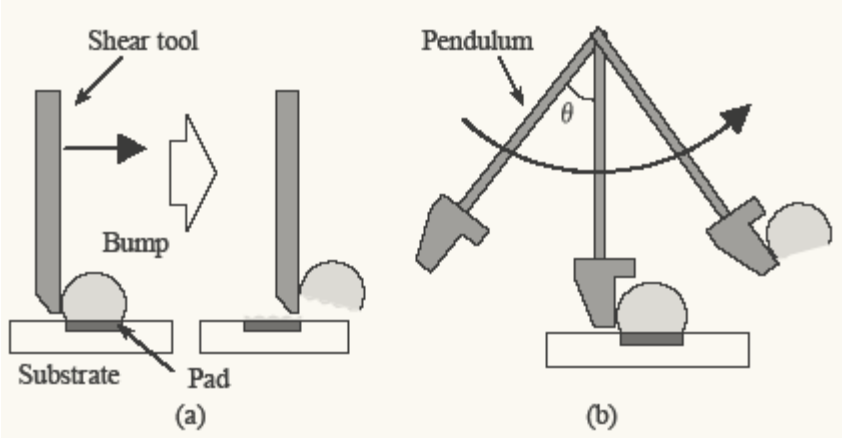

Figure 2.9: Schematics of (a) conventional shear test and (b) miniature Charpy test

The impact toughness, J, was calculated as the kinetic energy absorbed by the bump during fracture as follows:

$$J = \frac{1}{2} m_p \left(v_1^{\,2} - v_2^{\,2} \right)$$

where m_p is the weight of the pendulum, and v_1 and v_2 the velocities of the pendulum immediately before and after the impact, respectively. Four types of solders were tested in this paper; SnPb, SnAgCu, SnZn and SnZnBi. These solders were separated into two main groups - reflowed and aged. It was found that the solder joints had a

greater tendency to break at the interface from the impact test than from the conventional shear test.

During the tests, SnPb solder showed lower shear strength and impact toughness (about 0.2-0.3 mJ) than the SnAgCu solders. The SnPb and the SnAgCu solders showed similar interfacial reactions, regardless of bond pads, but the latter was prone to fracture at the interface from the impact test because of higher solder bulk strength. The SnZn(Bi) solder on the Cu pad was degraded markedly with aging time, which is due to the rapid growth of γ-Cu_5Zn_8 and substantial void formation at the interface. But the solder on the Au/Ni-P pad exhibited high shear strength and impact toughness even after aging, due to the formation of a Zn-rich phase. The effects of aging were also discussed in the paper. It showed that aging makes the solders brittle.

Ball shear and pull tests were conducted on SnAgCu lead free solder on Cu pads to investigate the effects of thermal aging by Chiu et al. [38]. In the shear tests, the shear strength dropped slightly after three days of thermal aging and no significant changes were found when the aging time increased beyond three days. Failure mode of the solder was dependent on the aging temperature for the shear tests. However, at higher temperatures, the pull strength did not reduce monotonically as the aging time increased. This may be attributed to the failure mode changing from pad-solder interfacial fracture to pad lift off.

Hanabe and Canumalla [62] performed shear tests on three packages (BGA1, BGA2 and LGA) mounted on a single board. BGA1 had 144 solder balls while BGA2 had 168 solder balls with a 4x4 solder ball array at the center of the component. The shear strength of BGA1 was relatively strain-rate insensitive and the failure was always at the buildup layer. The LGA packages showed the greatest strain-rate sensitivity because they had the lowest shear strength at low loading rates but the highest shear strength at high loading rates.

Chapter 3 Experimental Setup and Procedures

3.1 Experimental setup

The experiment involves conducting board level drop tests using a drop tester. This involves mounting PCBs on a fixture. The fixture was screwed tightly to a drop table. Accelerometers were mounted on the fixture and the packages to monitor the acceleration levels during drop impact. Strain gauges were mounted on the bare side of the PCB without any components to monitor the in-plane strains of the board. The electrical resistances of the components on the boards were monitored in-situ during drop impact. A power supply of low voltage provides a potential difference across the components and any fluctuations in the potential difference during drop impact can be monitored through an oscilloscope. The fluctuations of the potential difference can be related to changes in electrical resistances of the components. A high-speed camera is used to capture the side view of the drop table to monitor the board flexure during drop impact.

For this project, a Lansmont drop tester capable of dropping test specimens up to a maximum drop height of 1.5m is used. The drop tester consists of a motor for raising the drop table, a 15kg drop table with pneumatic brakes, a control panel for raising and lowering the drop table, two guiding rods for drop table to fall along and a base for mounting appropriate strike surfaces. A picture of the drop tester is shown in Figure 3.1.

The drop table is mounted on the drop tower by means of side jigs that slide along the guiding rods. The drop table is held tightly to the side jigs by means of cap screws. When the drop table drops is subjected to high-G level drops repetitively, the tightening screws tend to break off via shearing due to inertia of the side jigs falling downwards while the drop table rebounds upon impact. This problem occurs quite frequently and screw threads can deteriorate over time.

A new drop table is designed and fabricated to eliminate the problem of broken screws. The new drop table incorporates two side jigs together with the drop table into one piece. The main advantage is that there is no need to use screws to tighten the side jigs

to the main block. In addition, it is lighter than the old drop table and thus prevents heavy impact damage to the drop tower apparatus. The same hole arrangement is used for fixing fixtures on top and has two side copper bushings for smooth free-falling motion along the sliding rods when the drop table is released.

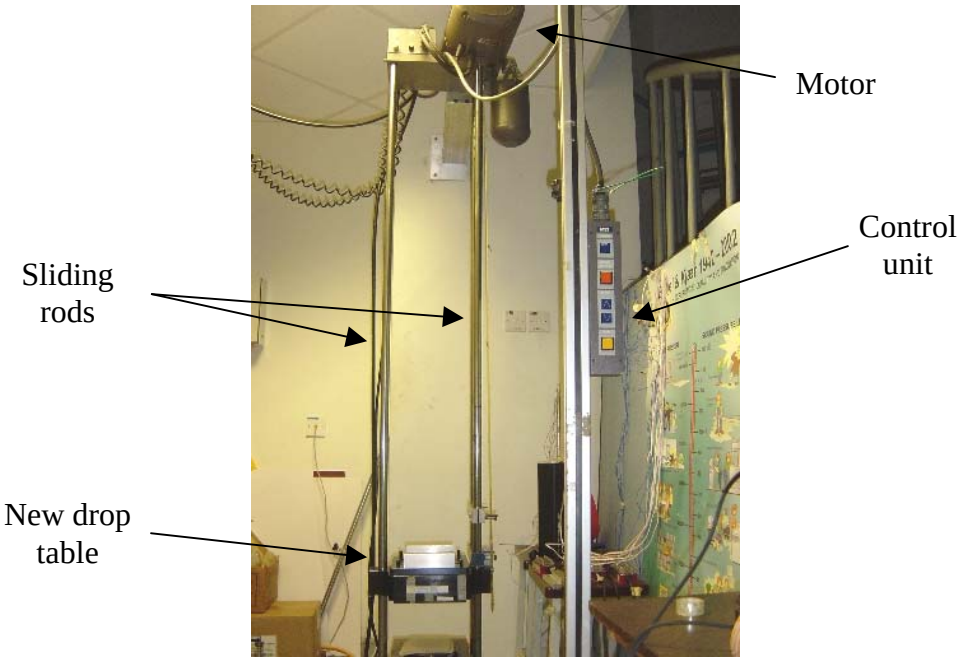

Figure 3.1: Lansmont drop tester

The weight of the new drop weight is 12.5kg and is capable of reaching a maximum G level of 4500G using a single layer of felt as the strike surface. Figure 3.2 shows a picture of the new drop table aligned to the sliding rods of the drop tower. A technical drawing of the drop table is shown in Appendix A.1.

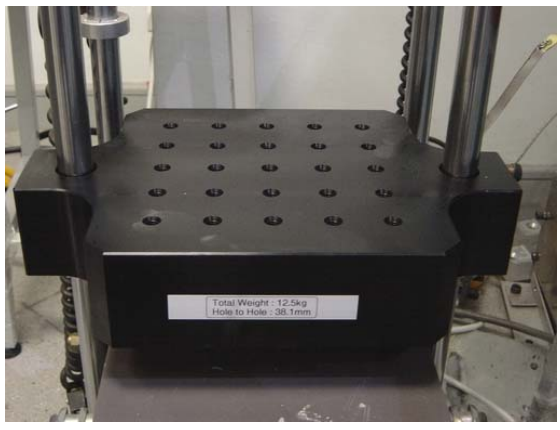

Hole to hole: 38.1mm
Hole thread: 10mm

Figure 3.2: New Drop Table

The high-speed camera setup is a novel method of monitoring velocity changes in the test specimens upon impact. An APX high-speed camera capable of capturing up to 100,000 frames per second is used. For this project, a frame rate of 6000 frames per second is used. Higher frame rates will require much stronger lighting for the high-speed images to be clear and resolution will also be smaller. Figure 3.3 shows a picture of the high-speed camera apparatus.

Figure 3.3: APX High-Speed Camera Apparatus

The camera is connected to a control unit and a controller. The controller is able to control the frame rate, resolution, type of triggering and other functions. The control unit is able to connect an external trigger switch if the activating is to be done from some distance away from the controller. The control unit also links to a laptop so that high-speed images can be instantly downloaded to the laptop for viewing and storage. Suitable lenses are used together with the camera for best effects. It is recommended that a lens with a good depth of view be used with the high-speed camera so that more details can be captured on the test specimens.

During drop impact of microelectronic packaging, drop responses and failure data are acquired by means of certain measuring devices. This data is important for comparing drop tests and evaluating the drop reliability of these components. Measuring devices include accelerometers, strain gauges and resistance checking through multimeters and oscilloscopes. Accelerometers are mounted either on the fixture itself or the package.

As accelerometers are extremely susceptible to mechanical damage or mishandling, extra care is required to mount them properly to the places of interest. Figure 3.4 shows a picture of the accelerometers used in this experiment.

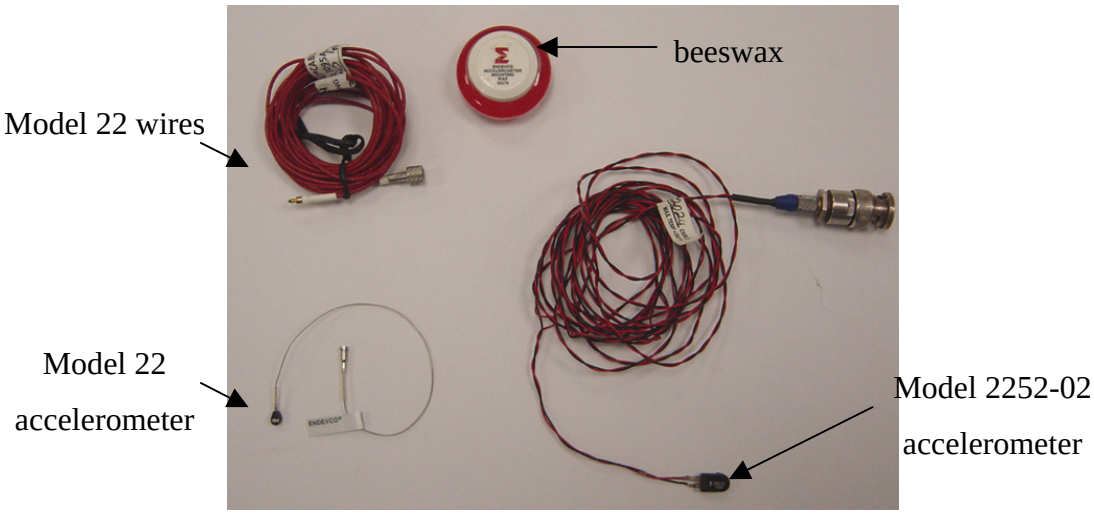

Figure 3.4: Endevco Accelerometers with Petrol Wax

The two types of accelerometers used are the Endevco Model 22 and Model 2252-02. Model 22 accelerometers and small and lightweight and thus useful for mounting on packages to monitor the output acceleration. Model 2252-02 accelerometers are bigger in size and more robust and are thus useful in monitoring the input acceleration of the drop table. Usually, the acceleration value measured at the fixture is similar to the acceleration level measured on the drop table if the fixture is secured tightly to the drop table.

Coaxial strain gauge rosettes used in experiment testing are of 1mm or 2mm gauge length. The small size is required because the PCBs tested usually have many components mounted on them. Smaller strain gauges are also more lightweight and do not affect the results of drop impact testing of PCBs. The rosettes are connected to strain bridges powered by strain meters and signals are registered on the oscilloscope. Figure 3.5 shows a picture of the strain gauges used.

Figure 3.5: Coaxial strain gauge (1mm gauge length)

The strain gauges are connected to strain bridges and bridges connected to the strain meters. The strain meters are linked back to a cathode-ray oscilloscope (CRO) for capturing signals. The settings of the strain meters are to be calibrated with the CRO before testing. Similarly, the accelerometers are connected to a charge amplifier and then connected to the CRO. Figure 3.6 shows a picture of a strain meter, charge amplifier and CRO. The signals from the CRO could be extracted out in tabular form for analysis.

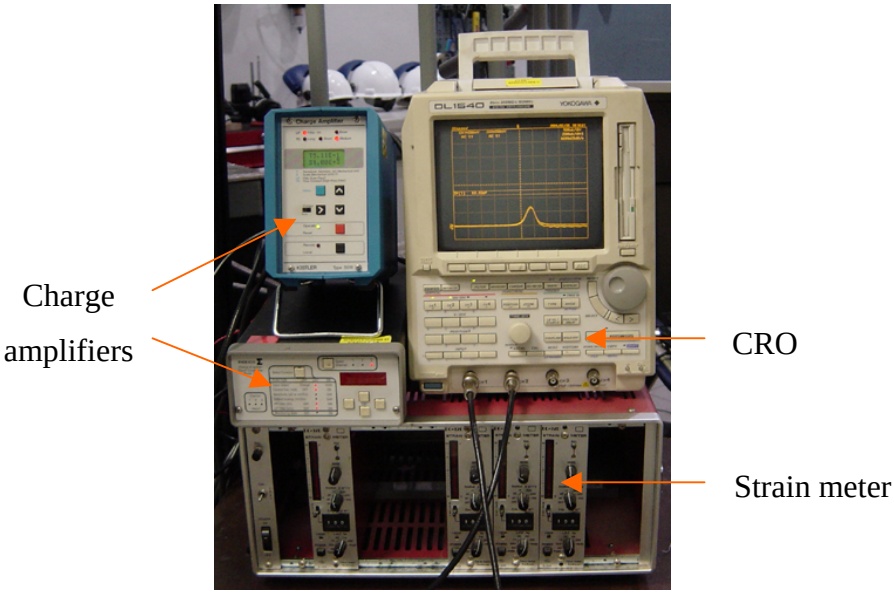

Figure 3.6: Charge Amplifiers, Strain Meters and a CRO

3.2 Test specimens

Several types of packages are being tested. They include mainly TFBGA/VFBGA and CABGA (with and without underfill) packages. Figure 3.7 shows the PCBs with the packages mounted on them. The TFBGA board has dimensions of 100x48x1.6mm, while the CABGA board size has dimensions of 115x77x1.6 mm. These two types of PCBs have different dimensions because of different sources from which these

packages are manufactured. Each PCB comes in two configurations; they either house 10 components or 1 component only.

Both types of packages are tested using the same testing procedures. Strain readings are taken usually at the center of the PCB where maximum deflection occurs in a typical 4-screw fixation. Their resistances at the interconnections are also monitored during drop impact through the CRO and their drop reliability evaluated. TFBGA/VFBGA packages do not have underfill material in them, and are separated by leaded and lead-free solders. CABGA packages have either no-underfill or with underfill material in them. Different types of underfill materials have been tested till the packages failed. Output acceleration is also monitored at the packages to correlate with simulation findings.

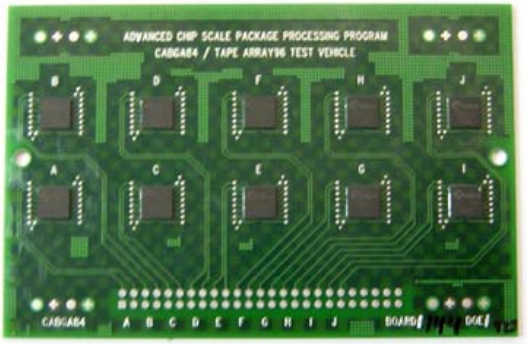

PCB dimensions
length: 114.3mm, width: 76.2mm,
thickness: 1.6mm

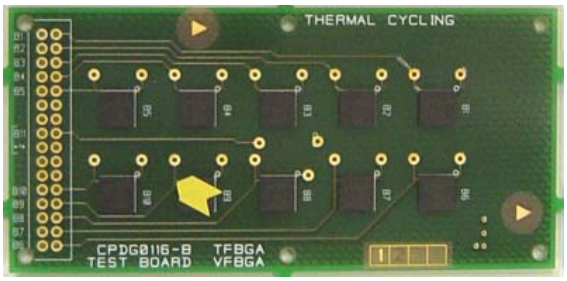

PCB dimensions
length: 100mm, width: 48mm,
thickness: 1.66mm

Figure 3.7: CABGA (left) and TFBGA (right) packages on PCBs

3.3 Basic mechanics of drop test

Some background experiment is conducted to better understand the drop responses acquired during drop tests. First, it is important to achieve uniform G level throughout the whole drop table and fixture upon drop impact. This is to ensure the whole carriage experiences the same shock level so that consistency in the board level drop test can be achieved. The strike surface consists of a circular toughened steel plate with a round tip at the center as shown in Figure 3.8. The steel plate should be toughened as multiple drops might cause the steel plate to crack at the center and propagate outwards. The reason for the curved surface is to ensure a single impact between the drop table and the strike surface. If the strike surface is flat, it is difficult to ensure perfect contact between the two surfaces.

Figure 3.8: Curved strike surface (toughened steel)

Achieving appropriate G levels and impact time duration is another important element of control. Varying the height as well as the type of strike surface will vary the G level. From kinematics, theoretical impact velocity during free fall just before impact, V_b, can be related to drop height, H, by

$$V_b = \sqrt{2gH} \qquad (3.1)$$

where g is free fall acceleration (9.81m/s^2). Assuming the input will yield a half-sine acceleration curve (from JEDEC standard [7]) with the following equation:

$$G(t) = G_m \sin\frac{\pi t}{T} \qquad (3.2)$$

where $G(t)$ is acceleration at time t, G_m is peak acceleration, and T is impact duration. When the potential energy is fully converted into kinetic energy, the peak acceleration, G_m, for perfectly plastic case (no rebound) may be shown to be as

$$G_m = \frac{\pi\sqrt{gH}}{T\sqrt{2}} \qquad (3.3)$$

For a perfectly elastic case (full rebound), G_m is 2 times larger than values given in the above equation.

Actual products experiencing accidental drops result in high acceleration forces induced in the product because the impact surface is usually rigid (ground). At fixed drop height, according to the law of conservation momentum and impulse, the product G_mT is a constant

$$G_{m1}T_1 = G_{m2}T_2 \qquad (3.4)$$

where $G_{m1}T_1$ denotes a set of prescribed drop impact conditions of peak G and time duration and $G_{m2}T_2$ denotes another set of impact conditions at the same drop height. Usually there is a need to fine-tune the felt thickness, drop height, and impact surface

conditions (including type of material, shape and flatness of surface), so that desired acceleration profile (G_m and T values) can be achieved. Generally, thicker felt generates lower peak acceleration and longer impact duration. Other rubber materials have been tested but they cannot achieve a nice sinusoidal acceleration profile as felt material.

According to impulse and momentum theory, the velocity after impact, V_a, is in the range between 0 (zero rebound) and $-V_b$ (full rebound). Assuming V_a is some fraction of V_b, $V_a = cV_b$, then according to impulse-momentum theorem,

$$-mcV_b - mV_b = -\int_0^T mG(t)dt \qquad (3.5)$$

$$V_b = \frac{1}{1+c}\int_0^T G(t)dt \qquad (3.6)$$

where c is the coefficient of restitution, and its value is between 0 (perfectly plastic impact) and 1 (perfectly elastic impact), $G(t)$ is the acceleration at time t during impact, T is the impact duration, and m is mass. By substituting Eq.(3.1) into Eq.(3.6),

$$A = \int_0^T G(t)dt = (1+c)\sqrt{2gH} \qquad (3.7)$$

where A is the area under $G(t)$.

3.4 Characterization of the drop tester

3.4.1 Drop height characterization

Figure 3.9 shows the impact pulses under different drop height from 0.5m to 1.5m. Larger sudden change of acceleration occurs at higher drop heights. The time duration varies very little compared to the change in G levels as the felt layer is thin and unable to cushion much of the drop impact.

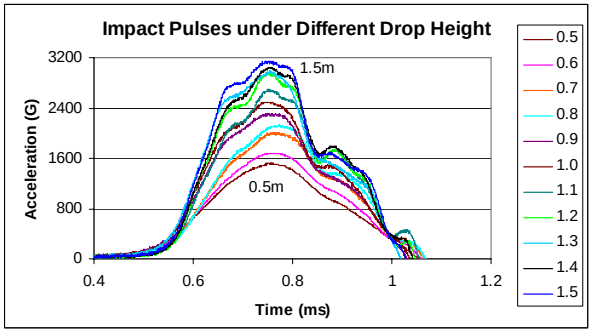

Figure 3.9: Impact pulses under different drop height

The relationship between drop height and *A*, which is actually the change in velocity during impact, can be described by a power law equation (see Figure 3.10). Equation (3.7) shows that *A* varies with $H^{0.5}$. Actual curve in Figure 3.10 has slightly higher coefficient of $H^{0.58}$, and the difference is partly due to the friction of the guiding rods that partially slows down the falling of the drop table. The peak acceleration, G_m, has a similar relationship with drop height as the two curves in Figure 3.10 are almost in parallel. This implies that the fluctuation in pulse duration is small in this case.

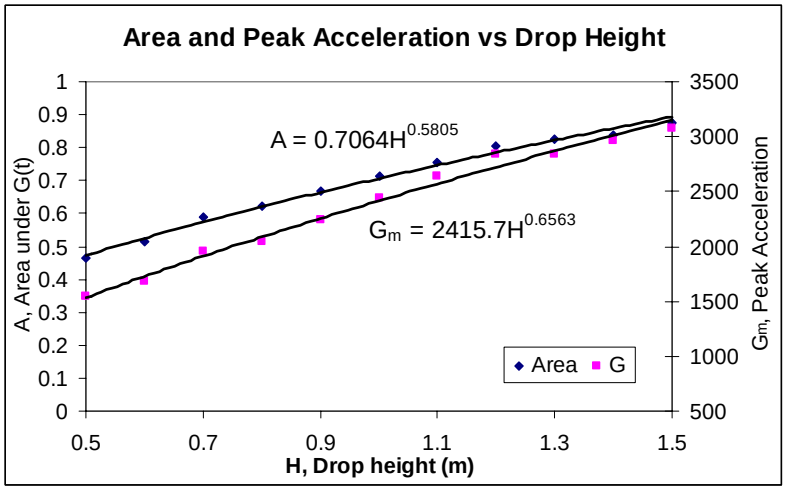

Figure 3.10: Comparing *A* and G_m from plot of *A* against drop height, *H*

The drop height and strike surface are usually adjusted to achieve a specific G level and pulse duration. Figure 3.11 shows that the actual impact pulse measured can be approximated as a half-sine curve or a triangular curve. By assuming constant area under the curves and maintaining same peak acceleration, the area under *G(t)* is

$$A = \frac{2}{\pi} G_m T = 0.6366 G_m T \qquad (3.8)$$

For a triangular impact pulse, the area is simply

$$A = 0.5 G_m T \qquad (3.9)$$

T is the impact pulse duration. Actual impact pulse measured by the accelerometer is usually between a half-sine pulse and a triangular pulse (see Figure 3.11). The pulse durations of half-sine pulse and triangular pulse are computed using eqns (3.8) and (3.9), assuming constant *A* and G_m. For simplicity, either half-sine pulse or triangular pulse can be applied for quick approximation of actual impact pulse.

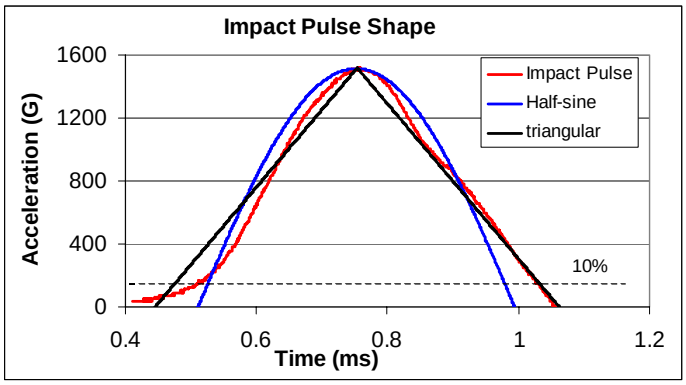

Figure 3.11: Approximation of impact pulse shapes

The relationship between pulse duration and drop height is linear and the slope of the line is very small (see Figure 3.12). Pulse durations for different drop heights are directly extracted from the measured impact pulses (see Figure 3.12), according to pulse duration definition of JEDEC standards, i.e. the interval between instance when the acceleration first reaches 10% of the specified peak level and the instant when the acceleration first returns to 10% of the peak level. It is less than the duration of a triangle pulse and more than the duration of a half-sine curve, according to eqns (3.8) and (3.9).

Comparing Figures 3.10 and 3.12, the sensitivity of peak acceleration is much higher than pulse duration to variation in drop height. This implies that if large variation in pulse duration is required (e.g., 0.3ms to 0.5ms), adjustment in drop height alone is insufficient. Instead, different felt material or extra felt layers may be needed.

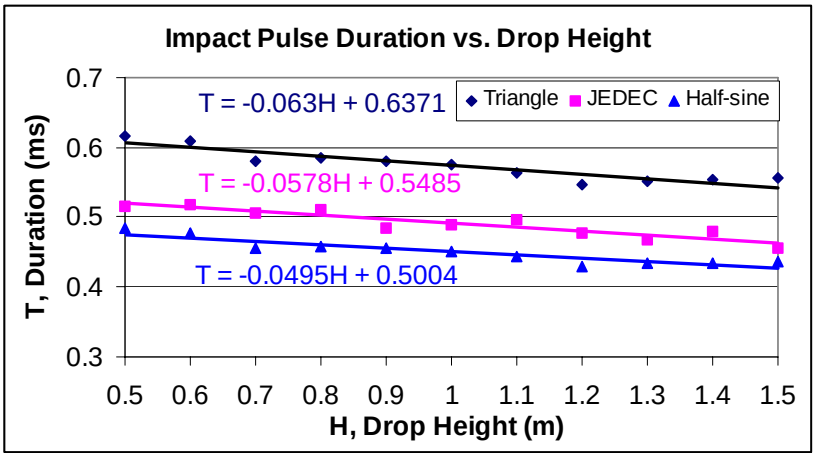

Figure 3.12: Impact pulse duration vs. drop height

In actual experiment, there is some rebound of the drop table after impact. How much the drop table rebound is governed by the coefficient of restitution, c. The coefficient of restitution can be derived from Figure 3.10 (*A* vs. *H*), according to Eqns (3.2) and (3.5), as

$$c = \frac{A}{V_b} - 1 = \frac{V_a + V_b}{V_b} - 1 = \frac{V_a}{V_b} \qquad (3.10)$$

and it is equal to 0.58 for this particular drop test configuration if theoretical impact velocity of 5.425m/s is achieved from drop height of 1.5m. The post impact velocity is measured through a high-speed camera apparatus. Due to friction effect along the guiding rods, the high-speed camera measures the actual impact velocity to be 4.78m/s. Thus, the actual value of *c* is found to be 0.79.

3.4.2 Strike surface characterization

Besides drop height, felt material, and strike surface, thickness or number of felt layer can also be used to adjust and achieve the required G level and pulse duration. Figure 3.13 shows the impact pulses using one, two, and three layers of felt material. The areas under *G(t)*, peak accelerations, pulse durations, and coefficients of restitution for different number of felt layers (see Table 3.1) can be extracted. In general, with increasing number of felt layer, the peak acceleration is reduced and the pulse duration is longer (flatter impact pulse). In addition, the area under G(t) graph or change in velocity during impact, *A*, and coefficient of restitution, *c*, are lower with increasing number of felt layers. Pulse duration is more sensitive to variation in number of felt layers than to drop height (see Figure 3.12). Therefore, a combination of number of felt layer and drop height can help to vary both peak acceleration and pulse duration, and obtain a specific impact pulse. However, if a larger time duration (>1ms) is required, it may be necessary to change the felt material.

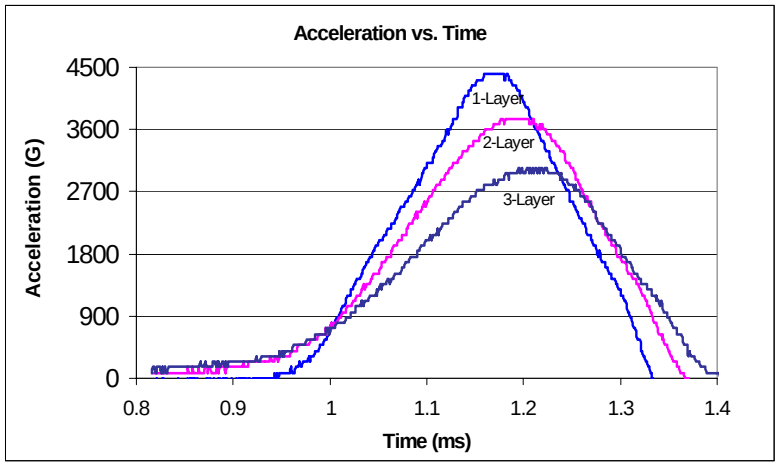

Figure 3.13: Effect of number of felt layers on impact pulse

Table 3.1: Effects of number of felt layer

Number of Layer	A (m/s)	G_m (G)	T (ms)	c
1	8.524	4400	0.334	0.571
2	8.243	3760	0.393	0.519
3	7.852	3040	0.456	0.447

3.4.3 Drop conditions for 1500G peak level

According to JEDEC standard in board level drop test [7], JEDEC requires an input of 1500G with an impact duration of 0.5 ms with a half sine pulse. Calibration of the drop tower was done using different layers of felt material at the strike surface to vary the time duration. Varying the drop height could easily vary the G levels. From Figure 3.14, a single layer of thick felt of thickness 10mm is used at the strike surface. At a drop height of 0.75m, the JEDEC requirement can be approximately achieved. Adjusting the time duration could be difficult as varying the thickness of felt material may not vary the time duration accurately as felt material tends to be flattened after many cycles.

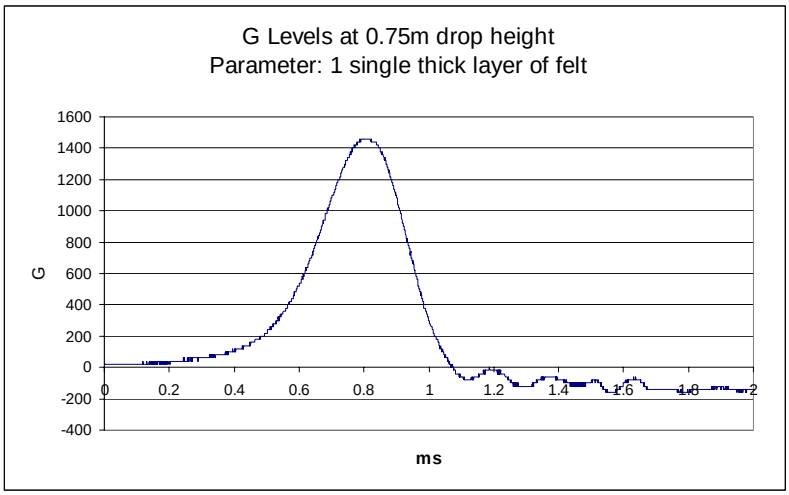

Figure 3.14: JEDEC standard of 1500G using Lansmont drop tower

In addition, other conditions were also tested maintaining the same G_m. From Figure 3.15, thin layers of felt are placed on top of the thick layer of felt to increase the thickness. Condition M denotes the condition where a thin layer of felt is placed over the original thick layer of felt and the drop table dropped from a height of 0.9m. Condition N denotes the condition where two thin layers are used over the thick layer of felt and drop table dropped from a height of 1.3m However, the impact duration did not vary much as compared to the change in drop height to maintain the same G level using different numbers of felt layers. In actual board level test, this JEDEC condition might not be appropriate to yield failures within a reasonable number of drops for certain packages and thus higher G levels and shorter impact durations might be necessary for the tests.

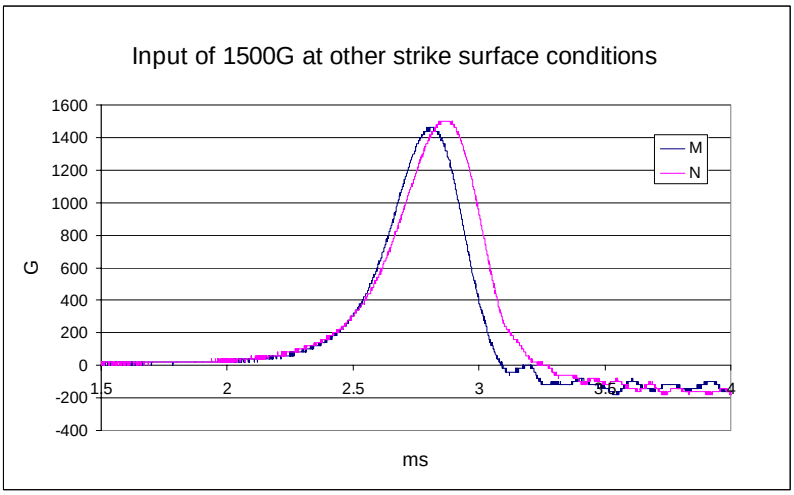

Figure 3.15: Plot of G level against time for peak acceleration of 1500G for different number of layers of felt material

Once the tester is characterized and the relationships among drop height, area under acceleration curve, peak acceleration, and pulse duration are known, the drop height required can be estimated easily for a specific set of G levels and impact durations. Therefore, avoiding the "trial and error" approach can shorten the subsequent test setup time.

3.4.4 Repeatability of drop test

Six drops were conducted to ensure the repeatability of test results. Impact pulses as well as strains along the PCB length and width directions are measured. In this experiment, drop height is 1.5m with one layer of felt material and four corner PCB mounting screws. Figure 3.16 shows the six shock impact pulses. The tolerances of peak acceleration, G_m, and pulse duration, T, are within ±5% and ±1%, respectively.

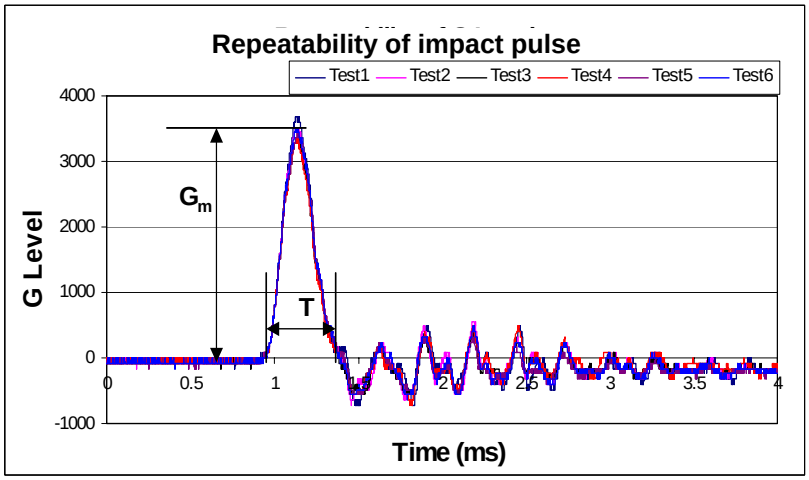

Figure 3.16: Repeatability of shock pulses at 1.5m drop height

3.5 Overview of drop test plan

3.5.1 Test plan for TFBGA components

TFBGA boards will be tested using 2-, 4- and 6-screw supports. The 4- and 6-screw supports are described in Chapter 4. The mounting screws are held on by spacers to make sure the board does not knock onto the fixture underneath it. A pair of strain gauges is mounted at the center and top surface of the board while the components are on the bottom surface of the board as shown in Figure 3.17. An accelerometer is placed in a downward direction on a TFBGA package that is mounted at the center of the board to monitor the output acceleration during drop impact for the 4-screw configuration.

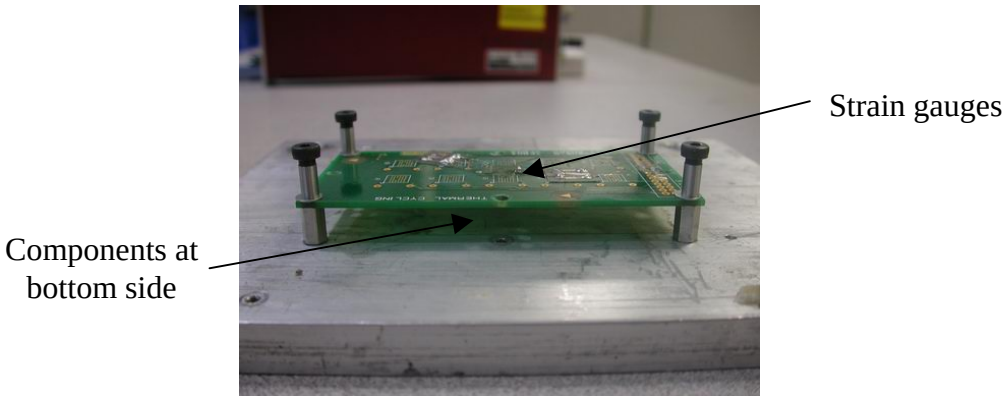

Figure 3.17: 4-screw support layout

Ten batches of packages are being tested. Each batch has 3 to 5 boards. The batches are grouped under normal TFBGA and LFBGA (low profile and fine pitch) packages. The solder interconnects come in eutectic solder or lead-free solder (SnAgCu). Some boards have AFOP (Gold on Finger, OSP on Pad) treatment. These batches are subjected to a drop test of 1500G with 0.5ms duration (JEDEC standard) for 20 to 40 drops. All the packages are checked for failure after the test. The detailed test layout is described in Chapter 4.

3.5.2 CABGA components test plan

The CABGA components consist of those with underfill and those without underfill. There are 12 batches of CABGA packages with different types of underfill and 1 batch of CABGA packages without any underfill material. Each batch consists of two PCBs with 10 components consisting of a specific type of underfill material. The fixture has two boards mounted on the drop table for each drop. The boards are tested at a drop height of 1.5m and subjected to at least 300 drops for each batch. The packages without underfill are also tested at the same condition. Resistances of these components are checked at regular intervals. Due to the large number of drops required to complete the tests of these packages, the components were checked for resistance every 2 drops up to 100 drops. From 100 to 300 drops, the resistances were checked once every 5 drops.

In addition to batch testing to evaluate the drop reliability of these components with underfill material, other drop tests were also conducted. The effect of different screw supports including clamped edges was studied and the drop responses compared. The

effects of loose mounting screws and knocking of the PCB board with the fixture were also studied and explained in details in Chapter 5.

Chapter 4 Board Level Drop tests for TFBGA Packages

In this chapter, the dynamic responses of printed circuit boards (PCBs) mounted with Thin-profile Fine-pitch BGA (TFBGA) packages under board level drop tests were investigated. Data captured during the tests include accelerations, in-plane strains and in-situ change in solder interconnect resistance. PCBs were mounted on the drop table using either 4-screw or 6-screw supports. In addition, a high-speed charge-coupled device (CCD) camera was used to capture the drop impact process. The PCB bending modes, frequency, velocities before/after impact, impact duration, and deflection were derived from the high-speed photographs. The results are used to verify the measured strains and accelerations. In-situ solder joint resistance is monitored using an oscilloscope. In-situ resistance measurement is an important tool to monitor resistance as a solder joint crack may close up again after impact. For the 4- and 6-screw supports, the in-plane strain magnitudes are found to be similar, but the flexural frequency and failure rate of the solder interconnects are different. This is mainly attributed to the bending of the PCB that resulted in solder joint failure.

As discussed in Chapter 2, JEDEC has developed a standard to perform board level drop test of components used in handheld electronic products. However, this current test standard for mechanical shock of components and subassemblies is not adequate because it does not consider other screw fixations such as the 6-screw support that is commonly adopted in electronic products, especially in the case of mobile phones. It also does not allow direct comparison of board level drop test performance among various board sizes. This test standard is probably more suited for component qualification, rather than to understand the actual impact strength and weakness of IC packages on actual boards used in the products. In terms of board sizes, the TFBGA test board is smaller than the JEDEC proposed board size due to its availability and are therefore stiffer and undergoes a lesser flexural bending. As a result, a much higher input peak acceleration is usually required to cause the packages to fail. At the moment, many manufacturers propose their own test boards and procedures. This chapter aims to discuss the board level drop tests using the smaller TFBGA PCBs.

4.1 Setup of the TFBGA packages

A typical setup of the board level drop tester is shown in Figure 4.1. One package is mounted at the center of a PCB dimensions 100 x 48 x 1.65 mm. The PCB is mounted onto a drop block using screws with standoffs of 10mm spacing to allow for PCB bending. The test will involve two types of screw supports: 4- and 6-screw supports as shown in Figure 4.2. In this test, the drop table is dropped freely from a height of 1.5m along two vertical guiding rods onto a rigid surface covered with a felt layer. JEDEC standard [7] proposes a maximum of 30 drops or failure rate of 80% of the components (whichever is earlier). However, preliminary test shows that 30 drops are insufficient to achieve significant amount of failures at the maximum drop height. Therefore, the board is tested until all components have failed, or up to a maximum of 50 drops as it is found that components tend to fail between 30 to 50 drops. If necessary, the test can be extended to 100 drops, but the resistance measurement interval can be larger. During impact, an accelerometer is mounted on the fixture to measure the shock level induced.

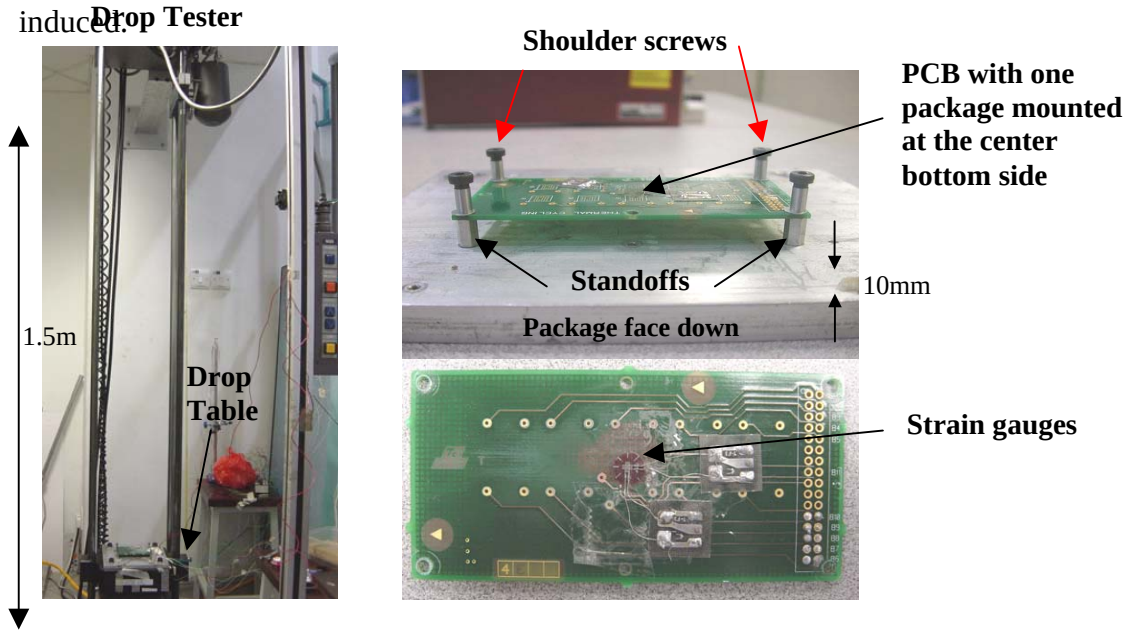

Figure 4.1: Setup of board level drop test

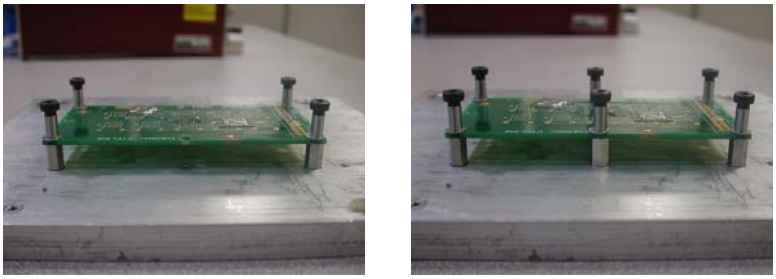

4-screw support | 6-screw support

Figure 4.2: Types of screw fixations of PCB on fixture

During impact, an accelerometer is mounted on the fixture near a corner screw to measure the shock level induced. For the TFBGAs studied, the peak acceleration is 4200G (1G=9.81m/s^2), with about 0.4ms impact duration. The input acceleration is also measured at the top corner of the drop table, and the variation from that mounted near the corner screw is within ±200G or 5%. Due to some minute clattering between fixture and drop table, the acceleration measurement on the fixture usually has a slightly higher noise level. The input acceleration is closely monitored and controlled at a consistent level for each test. Strain gauges are mounted on the reverse side of the PCB. Measured strains change from positive to negative and back to positive in a cyclical manner suggest that the PCB flexes upon drop impact. The bending frequency of the PCB is verified with high-speed video footage using the motion analysis software.

The resistance of the daisy-chain circuit is measured before and after each drop. When the resistance exceeds 300Ω (usual failure limit used by the industry), it is considered to have failed. In addition, in-situ resistance measurement is conducted to detect any sudden changes in resistance induced during impact as an open circuit may close up again after a drop impact, or remain in partial contact after the drop. The in-situ resistance method monitors the stages of failure (slow increase in static resistance, intermittent sharp increases in resistance and permanent failure) closely.

4.2 Strain measurements during impact

Strains measured in the X and Y directions indicate the strains induced along the width and length of the board, respectively. The strain gauges are mounted at the center of

the PCB directly at the reverse side of the TFBGA package to monitor the in-plane strains induced at the center of the PCB.

Figure 4.3 shows the strains induced for the 4-screw support case after the initial impact. From the graphs, the strain in the Y direction fluctuates cyclically at a frequency of approximately 450Hz. This cyclical fluctuation is much slower than the strain in the X direction (approximately 3000Hz). From the high-speed images captured, the PCB flexes in the fundamental mode along the length side of the PCB. Thus, this explains the cyclical trend in the Y direction strain as the PCB flexes. There is also a higher tendency for PCB to flex more along the length where it is more compliant to bending upon impact due to inertia. This is shown by the much higher strain and lower frequency in the Y direction. The bending mode along the width of PCB is hard to discern from the high-speed images and is believed that more than one mode of vibration exists during drop impact.

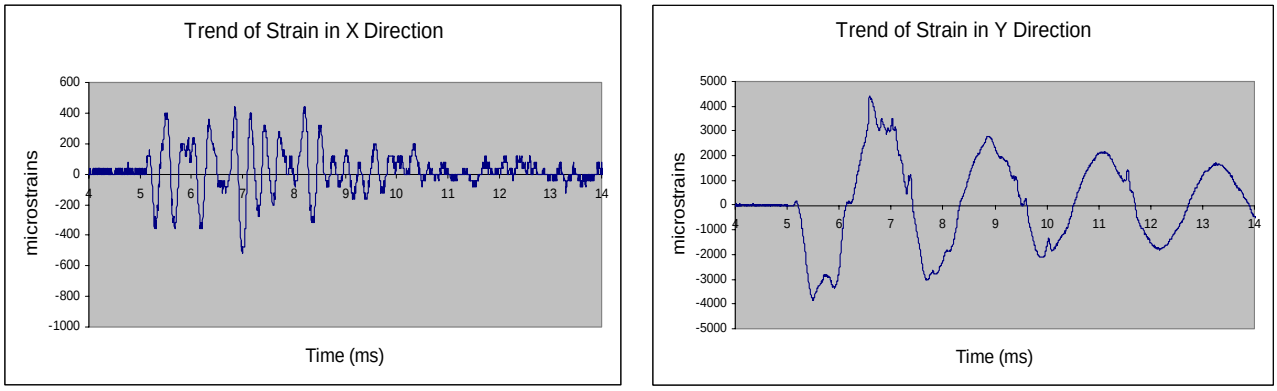

Figure 4.3: Strains induced in the X and Y directions on the PCB for the 4-screw suppport

Since the dominant bending mode is the fundamental mode shown by the strain data along the length of PCB, the strain data also will show a good estimation of the damping ratio of the system (board with components). The damping ratio C/C_C is given by

$$\frac{C}{C_C} = \frac{1}{2\pi n}\ln\left(\frac{x_o}{x_n}\right) \qquad (4.1)$$

where n denotes the number of cycles, C and C_C are the damping coefficient and the critical damping coefficient of a system respectively, x_0 and x_n are the amplitudes of the first and nth cycle respectively. In Figure 4.4, the trend of a Y direction strain is taken from the strain reading. This graph shows more cycles than in Figure 4.3 for

more accurate approximation of the damping ratio. In this case, the 6th cycle is taken as an example. The initial amplitude is about 4000 microstrains and the 6th cycle amplitude is about 1000 microstrains. The damping ratio is thus computed to be 0.0368. Taking other cycles and recalculating the damping ratio, it is found that the damping ratio is about 0.036 for a TFBGA board for the 4-screw support. The effects of damping must be known for an accurate simulation of board level drop test.

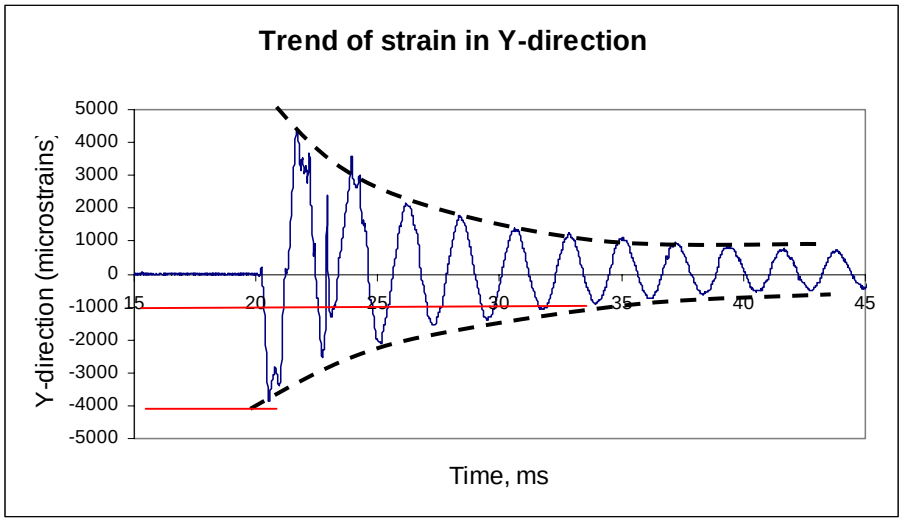

Figure 4.4: Trend of the plot of Y-strain against time for the 4-screw support case

Figure 4.5 shows a pair of strain plots taken from one drop for a 6-screw support case. From Figures 4.3 and 4.5, the mode of vibration for the 6-screw support is different from a 4-screw support. In a 6-screw support, the peak strains in the X-direction are about twice as much as that in the Y-direction and 180° out of phase from each other (although the frequency is the same). The similarity in frequency of vibration (approximately 1400 Hz) for both strains in the 6-screw support suggests that the flexural stiffness is approximately the same in both directions because the distance between the fixing screws are almost equal. Its higher frequency (compared to 4-screw support) also suggests faster cyclic bending at the center of the PCB.

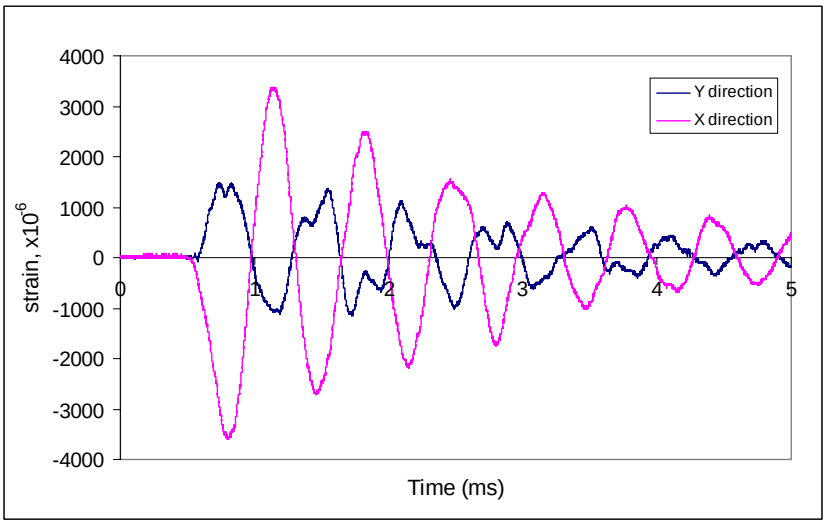

Figure 4.5: Plots of strains against time for the 6-screw support case

4.3 Study of board level drop test using high-speed photography

The extent of bending can be visually studied using a high-speed CCD camera. The frame rate used in this test for capturing is 6000Hz. For the 4-screw support case, the amount of bending can be seen clearly from the high-speed images when viewed along the length of the PCB. Figure 4.6 shows the bending and vibrating motion as the drop table impacts the surface. The PCB bends downwards initially due to its inertia because of the sudden change in velocity upon impact. It then flexes up and down but the oscillation dampens after tens of cycles. The frequency of vibration can be verified and the impact velocity can be estimated using this method. However, this method cannot determine the extent of bending accurately as the center of the board could not be seen clearly from the side.

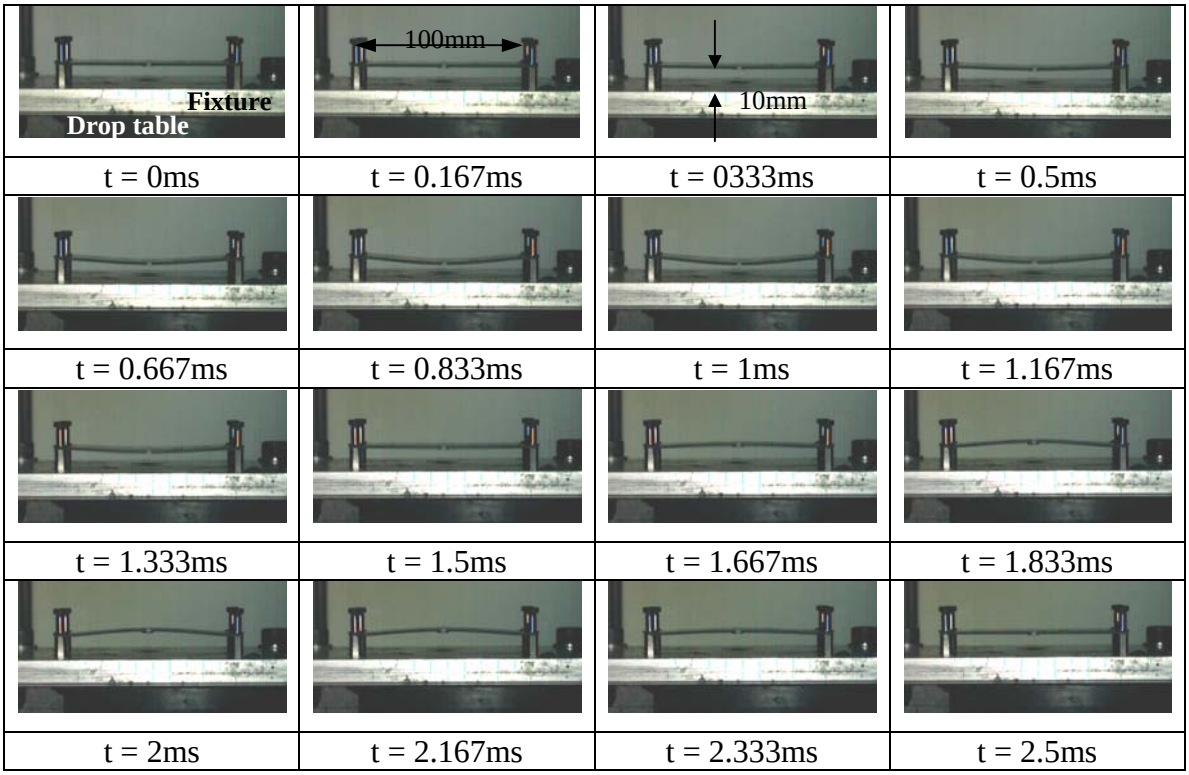

Figure 4.6: High-speed images showing bending of PCB upon impact for the 4-screw support

From the high-speed footages, the PCB for the 4-screw support undergoes cyclic bending in the fundamental mode. The deflection is the greatest at the center. The center package cannot be seen clearly from the high-speed footage due to lack of contrast and picture quality. However, it is observed that the dominance in cyclic bending lies along the length rather than along the width. The freqeuency of this dominant cyclic bending is 450Hz as verified earlier in the strain graph (see Figure 4.3). From the high-speed images, the maximum deflection was estimated to be about 2.9mm downwards.

In the 6-screw support case, the extent of bending is not very apparent from the high-speed images. Thus, the trend of cyclic bending cannot be verified with that of the strain plots. Figure 4.7 shows the PCB upon impact along the length direction of PCB. High-speed images were also obtained along the width of PCB but the extent of bending and the vibration mode cannot be determined visibly during and after impact.

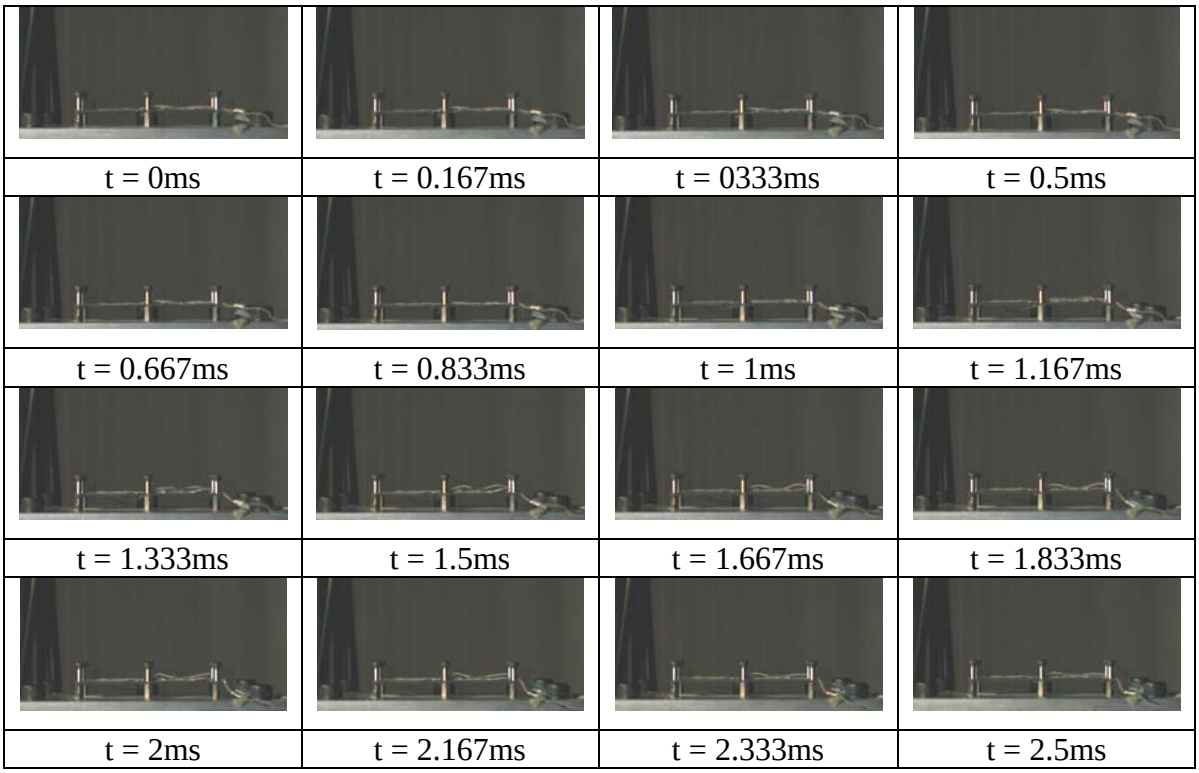

Figure 4.7: High-speed images showing bending of PCB upon impact for the 6-screw support

4.4 Monitoring change of velocity during impact

Velocity changes during drop impact are also detected using motion analysis software. The points of interest are at the whole drop table and the center of PCB for the 4-screw support case. The drop direction is denoted as the negative Z direction. However, errors arise when computing the acceleration values using motion analysis software, as the number of frames during the impact is inadequate to calculate the peak acceleration (upwards) accurately.

Figure 4.8 shows the position of the two tracking points used for the 4-screw support set-up. Point 1 is at the center of the length of PCB while Point 2 is near to a screw support. It is assumed that the screw is completely rigid and thus, the velocity of the screw support is the same as the whole drop block.

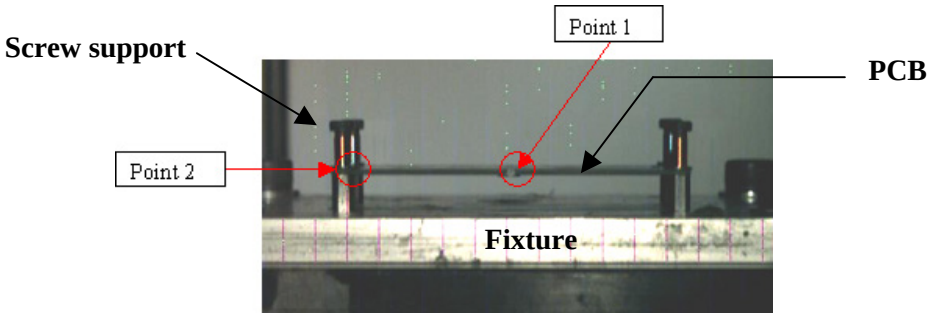

Figure 4.8: Location of two tracking points on the PCB and near the screw support

Figure 4.9 shows the absolute velocity profiles upon impact. The sharp change in the second series of the graph (Z velocities at screw support) shows the moment before and after impact. The fluctuations in the velocity of the PCB center are due to the PCB flexing after impact. The frequency of the fluctuations at the PCB center is about 450Hz. This is the same as the frequency found from the strain plots earlier (see Figure 4.3). For the 6-screw support, the two center screws restrict bending at the center of the PCB.

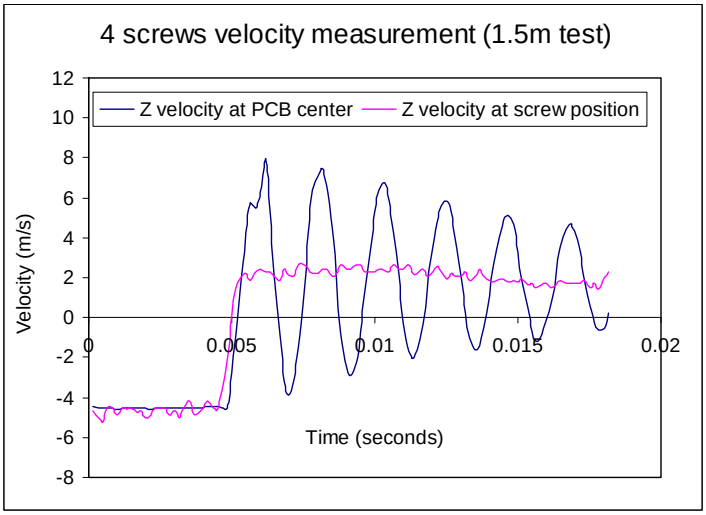

Figure 4.9: Plot of velocity against time for the 4-screw support case at PCB center and near screw support location

Besides monitoring the changes in deflection along the length (Y direction) of the PCB, the deflection along the width (X direction) was also recorded. Figure 4.10 shows the four tracking points used for velocity monitoring in the width direction of a typical 6-screw support setup. Point 1 is at the center along the width edge while Point 4 is at the screw support location and is assumed to indicate the velocity of the whole drop table. Points 2 and 3 are chosen to investigate the magnitude of fluctuation in velocity at different locations along the board width.

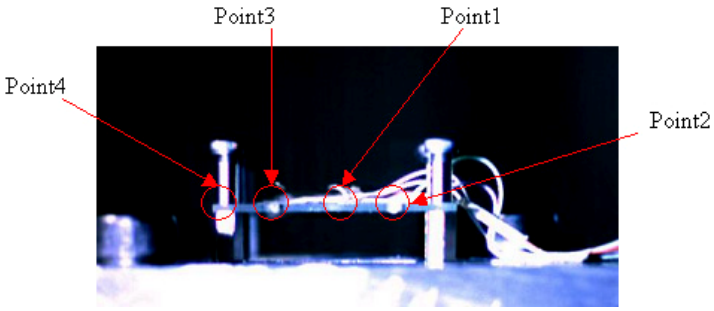

Figure 4.10: Location of four tracking points along width of PCB for the 6-screw support case

The high-speed images show relatively smaller bending of the PCB, as it is stiffer along the width of PCB. A velocity plot of the four points is shown in Figure 4.11. Point 1 (at the center of the width edge) shows a more significant fluctuation as compared with the other 3 location points although the trends are similar. The fluctuating trend is in a cyclical manner. The frequency of the fluctuation is about 1400Hz and agrees well with the frequency of the in-plane strain data as shown in Figure 4.4.

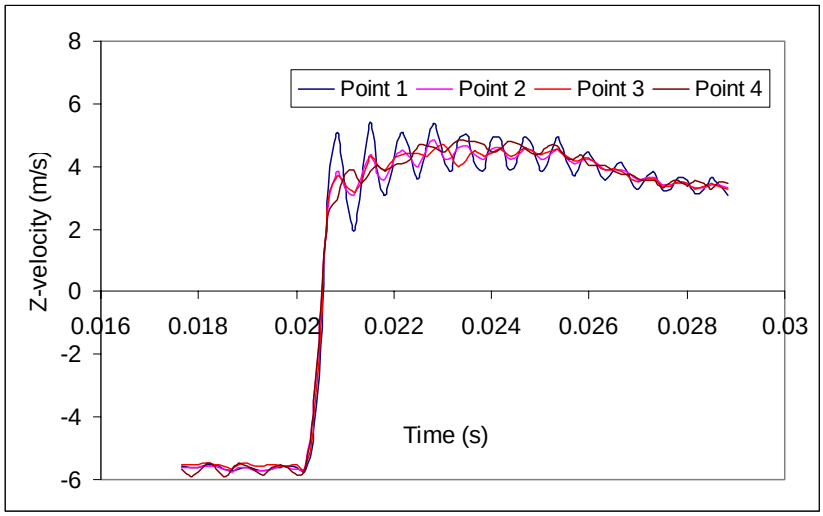

Figure 4.11: Plot of velocity against time for a 6-screw support at various locations along the width of the PCB

Since point 1 is at the center along the width edge, the extent of bending is expected to be greatest at this point. However, this fluctuation is not as great as that at the midpoint of the length edge. Points 2 and 3 do not show much fluctuation and is similar to Point 4. In general, the velocity profiles of all the location points imply that the degree of cyclic bending is at the greatest at the center of the PCB. Any component placed at the center region will experience the highest degree of deflection.

4.5 In-situ resistance monitoring of solder interconnect during board level drop test

4.5.1 Setting a failure criteria

During the board level tests, the solder interconnect resistance was monitored. The TFBGA component shows signs of failure when the 6-screw support case was carried out. Prior to this, the PCB has undergone a number of drop tests at 1.5 m drop height.

Figure 4.12 shows how the resistance of the TFBGA component (shown by R_x) is being monitored during the impact duration. A DC supply of about 3V is supplied in series with a dummy resistor (50Ω) and the TFBGA component. The potential difference across the TFBGA component is monitored by an oscilloscope. The sampling rate of resistance monitoring is equal to the sampling rate set on the oscilloscope. Thus, for the TFBGA component to undergo some failure, it would have to reach a resistance of some value much higher than 50Ω. This will be captured by the oscilloscope because of the increase in potential difference across the component.

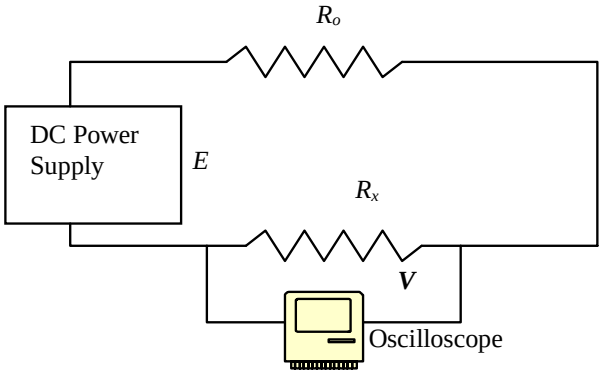

Figure 4.12: Circuit setup of resistance monitoring of TFBGA packaging

Compared with event detector, this method is much cheaper, easier to setup, and able to measure the actual value of dynamic resistance at real-time, which reflects the in-situ crack initiation and propagation of solder joints during drop impact. Event detector usually sets a threshold resistance (e.g., 300Ω) for failure to occur, and this simple pass/fail criterion is unable to describe the trend of solder joint reliability, and provide insufficient details for further analysis. Due to high frequency and short duration of PCB bending, event detector may fail to capture all the intermittent failures because of its long data acquisition period (minimum is 2 seconds/poll) and channel resetting. On

the other hand, manual probing can only check the static resistance of solder joints after drop impact. At this moment, the crack may close up again and the resistance measured may be lower

The common failure criteria used for determining failure in components are usually based on benchmarks like a 10 or 20% increase in resistance, manual probing, or event detector method (>300Ω). These criteria determine the final failure results of components or products and therefore not consistent for comparison if different criteria are used. The method discussed here tracks intermittent changes in resistance during impact even though the resistance values might seem acceptable after impact. In addition, it is able to determine all the possible failures from initial, intermittent to permanent failure.

4.5.2 Resistance monitoring during drop impact

In Figure 4.13, the vertical axis on the right denotes the voltage readings (potential difference across the component). Sharp increases represent a sudden open circuit in the component. For the 6-screw support, the X-direction strain dominates more than the Y-direction strain. However, there is no fixed trend as to where the intermittent failures will occur. For the first part of the graph, the component experiences intermittent losses in contact when the strain in the X-direction registers maximum compression.

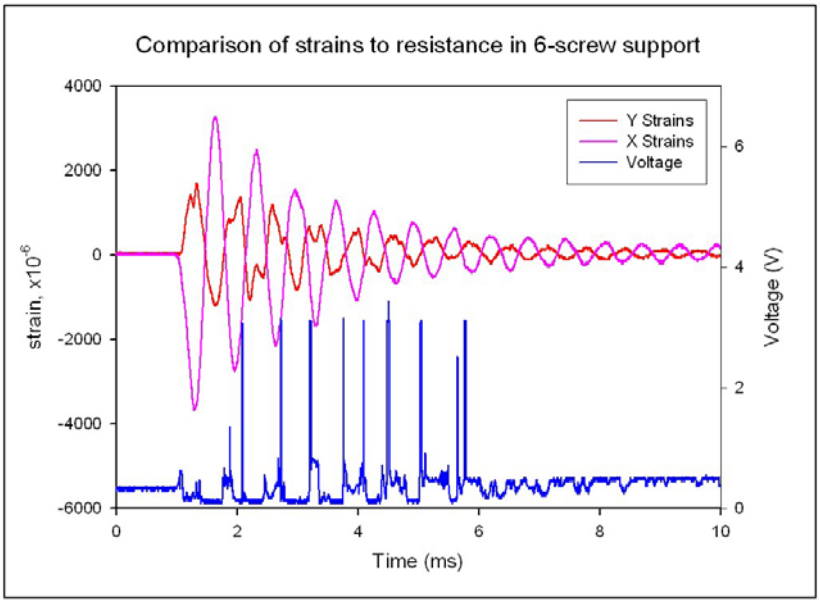

Figure 4.13: Plot of in-situ resistance and strain readings for a 6-screw support

In general, the failures usually occur when the strain gauge in the X-direction registers negative strains. Taking note that the strain gauges are mounted only on the top side of the PCB and the PCB undergoes flexing during impact. If the X-direction strain gauge registers a negative value (compression), it will mean the bottom side of the PCB where the IC package is mounted is under tension. A likely cause of failure will thus be peeling off of the solder joints due to solder joint-PCB mismatch in elasticity during the time when the board bends downwards.

To illustrate this, Figure 4.14 shows the PCB bending at two extreme deflections upwards and downwards. Maximum tensile or peeling stress is likely to occur at the outermost solder joints when the PCB is bending downwards. On the other hand, when the PCB is bending upwards, the outermost solder joints experience compressive stresses and thus cause the contacts to close up again. This kind of cyclic loading causes the solder material to undergo fatigue loading and thus ultimately to crack. When viewed under a microscope, it is found that most of the outermost solder joints have opened and thus further verifies the failure mechanism.

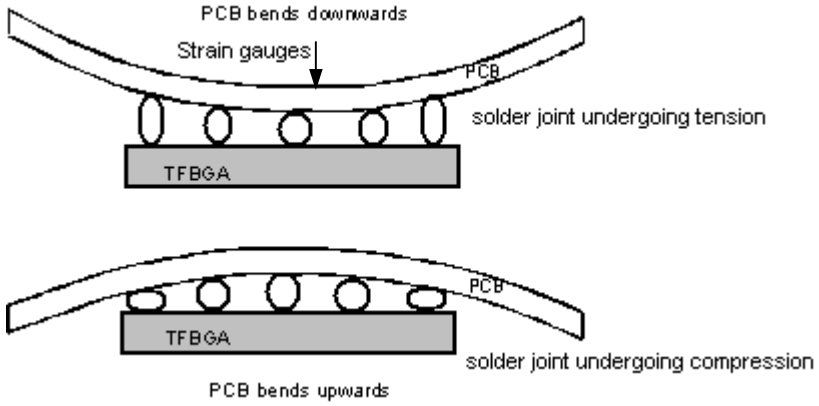

Figure 4.14: Stress induced in solder joints during PCB bending

Figure 4.15 shows another graph after several additional drops from Figure 4.13. The resistance measured is much higher than its operating resistance before the drop test. Upon impact, the flexing of the PCB closes back the open contacts at some points in time during the board level drop test. Thus, intermittent failure is prevalent in this case even though the component may register a normal operating resistance after impact. Usually after impact, the component's resistance is very sensitive to slight mechanical stress, e.g., touching and slight knocking.

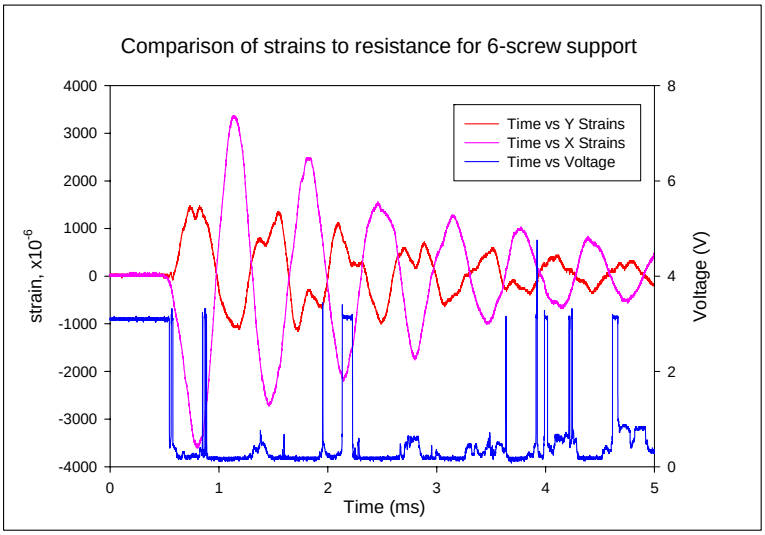

Figure 4.15: Plot of in-situ resistance and strain readings for 6-screw support (2)

4.5.3 Crack initiation, propagation and opening of solder interconnects

From in-situ resistance monitoring of solder interconnect, the failure process can be divided into three main stages (see Figure 4.16) - crack initiation (stage 1), crack propagation (stage 2), and crack opening (stage 3). At stage 1, both static and dynamic resistances increase gradually with number of drops. It implies that an initial crack is initiated, and the cross-sectional area of the critical solder joint is reduced gradually. At stage 2, there are a few peaks which start to appear in the dynamic resistance curve, as crack is propagated, the cross-sectional area of solder joint is reduced, and thus the resistance is increased. The impact life (in terms of number of drops) at the first dynamic resistance peak is N_1. In subsequent drops and PCB bending cycles, the amplitude of dynamic resistance peak increases until an intermittent failure ($R \rightarrow \infty$) occurs at impact life, N_2. At this moment, the crack has just propagated through the entire solder joint interface and there is an electrical discontinuity occurring in a very short duration. The crack usually closes back after the impact testing, and the resistance is dropped. At stage 3 the duration of dynamic resistance peak increases with number of drops and opening gap of the crack gets larger. The crack is harder to close up again during PCB bending, and the resistance is likely to go to infinity. Finally, both the static and dynamic resistance goes to infinity permanently at impact life, N_3. This is the state of permanent solder joint failure.

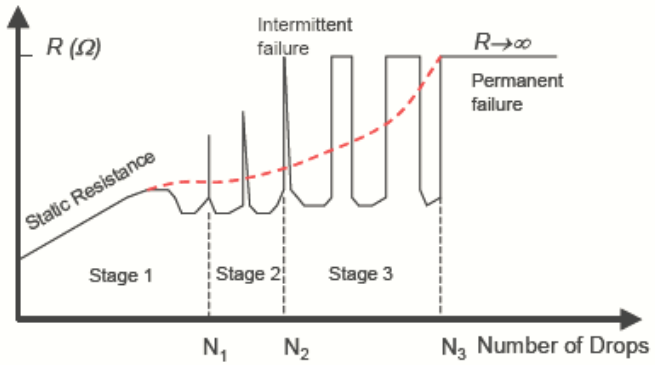

Figure 4.16: Solder joint failure process as described by the change in resistance curve

Therefore, there should be three different solder joint impact lifes - crack initiation (N_1), intermittent failure (N_2), and permanent failure (N_3), depending on the definition of solder joint failure criteria. The real-time dynamic resistance method is able to record down all the three impact lifes and display the three stages of solder joint failure process. However, it may not be easy to differentiate Stage 1 because slight increases in static resistance are hard to detect. Accuracy can be improved if the sensitivity and stability of the resistance monitoring equipment are excellent. N_1 and N_2 might only differ by a few drops as solder joint crack is propagated quickly during drop impact. Due to the dynamic nature of drop tests, sometimes N_1 and N_2 can occur at the same number of drops and thus the crack propagation stage can be totally ignored.

4.6 Batch testing on TFBGA/LFBGA packages

TFBGA and Low Profile Fine Pitch BGA (LFBGA) packages are subjected to 1500G with impact duration of about 0.5ms. The LFBGA packages only have a total thickness of 1.7mm including solder height. Some boards with TFBGA and LFBGA packages have gold (Au) on finger, organic solderability preservative (OSP) on ball pad (AFOP), where the finger is coated with a layer of gold for wire bonding and OSP is applied on the ball pad to prevent oxidization. The BGA balls are either made of eutectic solder or lead-free solder, SnAgCu. Each board has 10 components on it. Table 4.1 shows the drop test matrix of these boards. The boards are subjected to either 20 or 40 drops. Electrical continuity of the components is checked only during 20 or 40 drops.

Table 4.1: Drop test matrix of BGA packages

Batch no	Package	BGA balls	BGA AFOP	Drop tests
1	**LFBGA 8X8 64balls pitch 0.8mm ***	SnPb	yes	* 20 drops for 2 PCB * 40 drops for 3 PCB
2	**TFBGA 6X6 84balls pitch 0.5mm**	SnAgCu	yes	* 20 drops for 2 PCB having 5 units AFOP + 5 units without AFOP * 40 drops for 4 PCB (1 PCB AFOP + 1 PCB without AFOP)
3		SnAgCu	no	
4	**TFBGA 10X10 244balls pitch 0.5mm**	SnAgCu	yes	* 20 drops for 2 PCB (1 PCB AFOP + 1 PCB without AFOP) * 40 drops for 2 PCB (1 PCB AFOP + 1 PCB without AFOP)
5		SnAgCu	no	
6	**LFBGA 8X8 64balls pitch 0.8mm**	SnPb	yes	* 20 drops for 1 PCB * 40 drops for 3 PCB
7	**LFBGA 8X8 80 balls pitch 0.8mm**	SnPb	yes	* 20 drops for 1 PCB * 40 drops for 3 PCB
8	**LFBGA 10X10 120balls pitch 0.8mm**	SnPb	yes	* 20 drops for 1 PCB * 40 drops for 2 PCB
9		SnAgCu	yes	* 20 drops for 1 PCB * 40 drops for 2 PCB
10		SnAgCu	no	* 20 drops for 1 PCB * 40 drops for 2 PCB

* **8X8 64balls pitch 0.8mmmeans a 8x8mm BGA with 64 solder balls with 0.8mm separation**

In general, not many failures occurred after the drop tests. The results are summarized in Table 4.2. For the TFBGA packages (batches 2 to 5), the packages with lower ball count (batches 2 and 3) do not suffer failure easily as TFBGA packages with higher ball count (batches 4 and 5) of 244 balls. The same trend occurs in the LFBGA packages as well. Failures occur in the batches with higher ball count (batch 7 to 10). The effect of leaded solder and lead-free solder on drop reliability could not be determined in this test. In addition, it seems that AFOP has no significant improvement in drop reliability. Thus, lower ball count has better drop reliability probably because of the bigger size of each individual ball and the contact area for each ball on the pad is bigger.

Table 4.2: Drop test results of BGA packages

Batch Number	Drop Tests	Results
1	* 20 drops for 2 PCB * 40 drops for 3 PCB	0 defects out of 5 PCB
2	* 20 drops for 2 PCB having 5 units AFOP + 5 units without AFOP * 40 drops for 4 PCB (1 PCB AFOP + 1 PCB without AFOP)	0 defect out of 6 PCB
3		
4	* 20 drops for 2 PCB (1 PCB AFOP + 1 PCB without AFOP) * 40 drops for 2 PCB (1 PCB AFOP + 1 PCB without AFOP)	After 20 drops - AFOP / Lead free: 1defect / 10 (unit 5) After 40 drops - AFOP / Lead free: 5defects / 10 (unit 1, unit 5, unit 6, unit 8, unit 10)
5		After 20 drops - not AFOP / lead free: 4 defects / 10 (unit 5, unit 7, unit 8, unit 10) After 40 drops - not AFOP / Lead free: 3def/10 (unit 5, unit 7, unit)
6	* 20 drops for 1 PCB * 40 drops for 3 PCB	0 defect out of 4 PCB
7	* 20 drops for 1 PCB * 40 drops for 3 PCB	After 20 drops - AFOP / SnPb: 0 def / 10 After 40 drops - AFOP / SnPb: 2 def/30: unit 1 on PCB #1 and unit 1 on PCB #2. Consomption defects. Cross section revealed cracks between BGA ball and BGA substrate + initial crack inside PCB
8	* 20 drops for 1 PCB * 40 drops for 2 PCB	After 20 drops - AFOP / SnPb: 2 def/10 (unit 5, unit 10) After 40 drops - AFOP / SnPb: 1 def/10 (unit 10 for one PCB) and 2 def/10 (unit 5 and unit 10) for 2nd PCB
9	* 20 drops for 1 PCB * 40 drops for 2 PCB	After 20 drops - AFOP / Lead free: 2 def /10 (unit 5 and unit 10) After 40 drops - AFOP / Lead free: 2def/10 (unit 5 and unit 10) for both PCB
10	* 20 drops for 1 PCB * 40 drops for 2 PCB	After 20 drops - not AFOP / Lead free: 1 def/10 (unit 5) After 40 drops - not AFOP / Lead free: 2def/10 for one PCB (unit 5 and unit 10) and 1 def/10 for 2nd PCB (unit 5)

Chapter 5 Board Level Drop Tests for CABGA Packages

The demand for fine-pitch CSP is becoming higher as it satisfies the need for low cost, miniaturization, and high performance requirements of mobile phones, notebooks, PDAs, and other handheld electronic products. For such device, board level solder joint reliability due to drop test is a great concern to many manufacturers. The mechanical shock resulted from mishandling during transportation or customer usage may cause solder joint failure, which leads to malfunction of product. Under different combined loadings of operating conditions, the operating life of CSP may be limited. The effect of underfill on solder joint performance under various board level tests is also investigated.

CABGA packaging is used for this CSP test. The solder ball material used is that of the Eutectic 63/37 SnPb. The solder ball pitch is 0.5mm and the package thickness is 1.34mm. For every CABGA PCB, there are 10 components mounted on it. The schematic arrangement of the CABGA packages is shown in Figure 5.1.

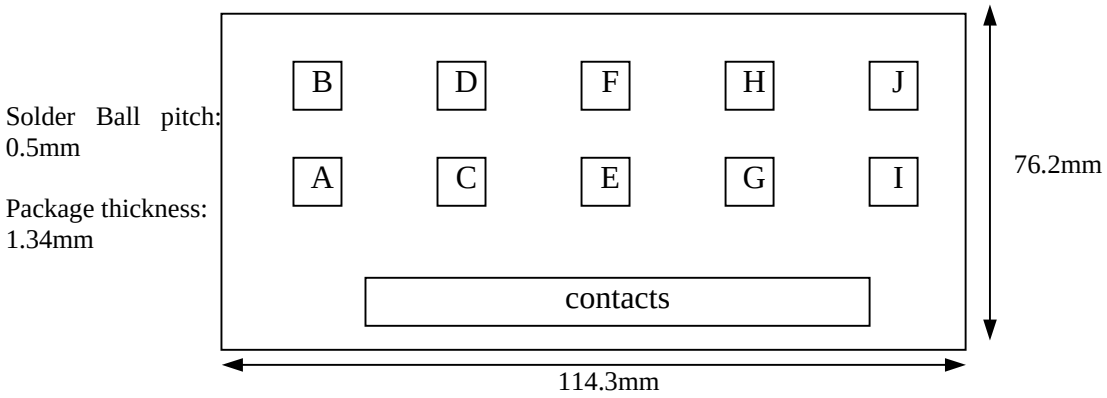

Figure 5.1: Mounting and labeling of CABGA components in the PCB

5.1 Effect of drop height on drop responses of CABGA PCB

Drop tests were conducted at 1.0, 1.2 and 1.4m drop heights. As the drop height increases, the resultant G level also increases. This increase in the input G level will affect the failure rates of the CABGA components. Other factors that may affect the failure rates are the positions of the components on the PCB, the type of screw support configuration on the PCB and the type of underfill material used for the packages.

Figure 5.2 shows the drop responses of the PCB. Each PCB houses 10 CABGA components. Each board contains a specific kind of underfill material for the components. A pair of strain gauges is mounted at the center of the PCB on the opposite side to where the components are located. The PCB is fixed using 4 screws near the corners of the PCB held by spacers with 10mm height allowance. The in-plane strains are monitored and compared with the failure trends of the components. Strains measured in the X- and Y-directions refer to the strains induced along the width and length of the board, respectively.

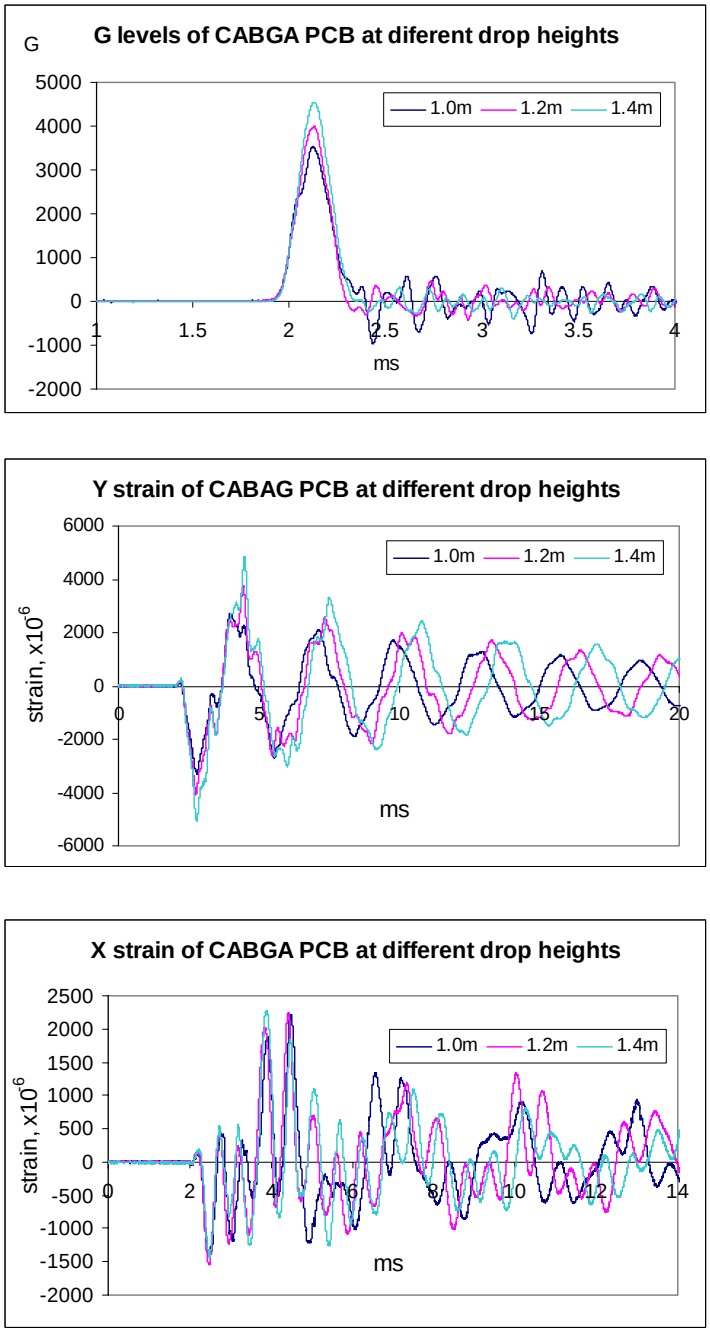

Figure 5.2: Drop responses of CABGA mounted PCB at 1.0, 1.2 and 1.4m drop height

The dimensions of the CABGA PCB are 114.3 x 76.2 x 1.6mm. From Figure 5.2, the frequency of fluctuation in the Y-strain is about 2.5 times slower than in the X-strain. The hole-to-hole (center to center of holes) distance is 104.3mm in the length direction and 66.2mm in the width direction. The aspect ratio of the length-to-width distance of holes is about 1.58. The PCB bends downwards due to its own inertia upon impact and bends upwards after maximum deflection has been reached. This behavior occurs subsequently in an oscillatory manner.

The Y strain experiences some damping after drop impact. The damping effect is quite different as shown from the Y-strain graph because the Y-strain at 1.0m drop height tend to oscillate faster than at 1.4m drop height. This could be due to the higher inertia loading at higher drop heights that may loosen the fixing screws. The X-strain also exhibits different trend patterns where X-strains of 1.2m and 1.4m are quite similar and X-strain at 1.0m tends to fluctuate lesser.

5.2 Effect of board bending during drop impact

Using simple beam mechanics as a comparison to PCB bending for the 4-screw support case, the Euler-Bernoulli beam equation is given by $\frac{d^4w}{dx^4} = \frac{q}{EI}$, where q is the distributed load (force per unit length) acting in the same direction as y (and w), E is the Young's modulus of the beam, and I is the area moment of inertia of the beam's cross section, assuming constant cross section along the length. For a beam with its ends clamped and applying boundary conditions, the maximum deflection of the beam is given as follows:

$$w_{\max} = \frac{qL^4}{384EI}$$

Hence, L denotes the length of the beam. The radius of curvature is related to the second derivative of its deflection function. The curvature at the center of the beam is given as:

$$\frac{1}{R} = \frac{d^2w}{dx^2} = -\frac{qL^2}{24EI}$$

The curvature of the beam will be similar to that of the PCB bending if the PCB length-width aspect ratio is high. Therefore from the equation, if the length is long,

deflection at the center of the beam will be high. From the graphs in Figure 5.2, the magnitudes of the peaks and troughs in the Y-strain graphs are much higher than that of the X-strain. Compared with simple beam theory, the curvature is also greater if the length of the PCB is longer, thus bending is more dominant along the length of the PCB that is manifested by the higher amplitudes of the in-plane strains in Y direction than in the X-direction.

Additional strain gauges were mounted at the corner as well as at the center of the edge along the length of the PCB. The PCB is dropped at a height of 1.2m and the PCB is mounted using the 4-screw support configuration. The in-plane strain data is acquired using an oscilloscope. Figure 5.3 shows the strain data during impact. The Y strain at the corner fluctuates in a cyclical manner that is opposite to that of the Y-strain at the midpoint of the longer edge of the PCB.

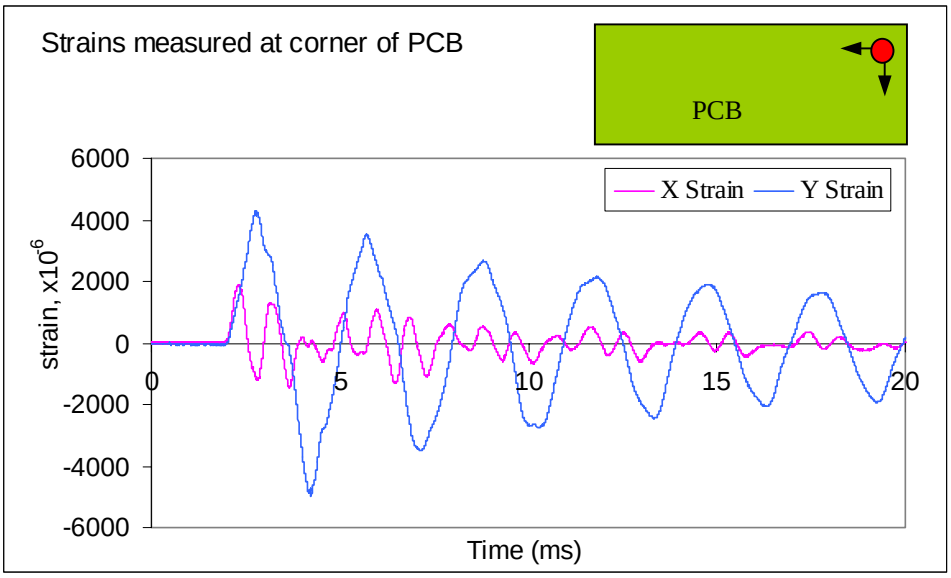

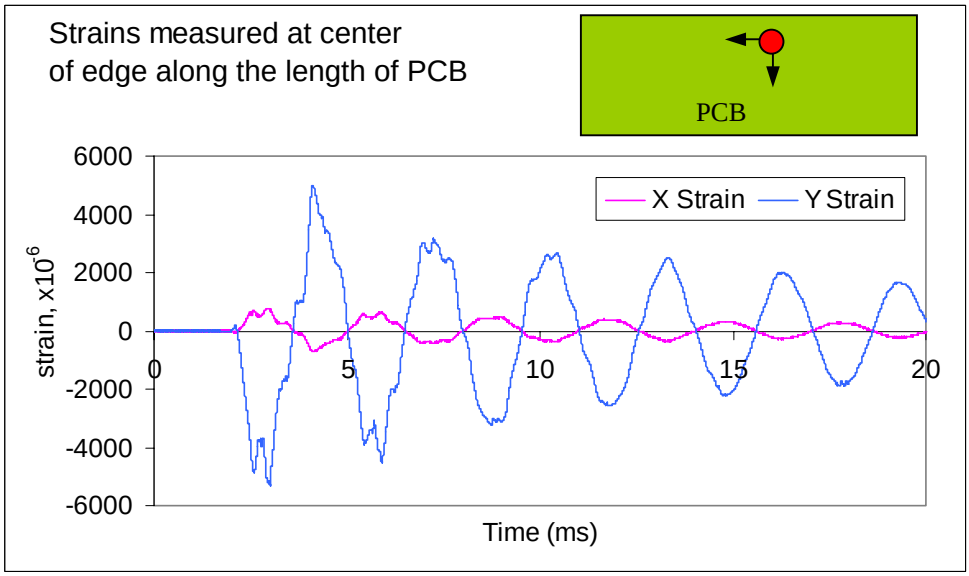

Figure 5.3: Plot of in-plane strains against time at different locations of the PCB

The opposite trend of the Y-strains is due to the change in curvature at different positions of the PCB during drop impact. Figure 5.4 shows the length edge of the PCB under maximum bending from simulation and a high-speed image of the PCB undergoing its fundamental mode of vibration. The regions at the corner screws are fixed so that no displacements or rotations are possible. Since the cyclic bending is the greatest along the length, it implies that the curvature changes the most along the length of the PCB. Looking at the top (no components side) surface of the PCB in Figure 5.4, the region near the fixed corner screws is experiencing extension while the PCB is bending downwards. At that same instant, the region at the top center of the PCB is experiencing contraction, thus explaining the opposite trend in experimental strain data shown in Figure 5.3.

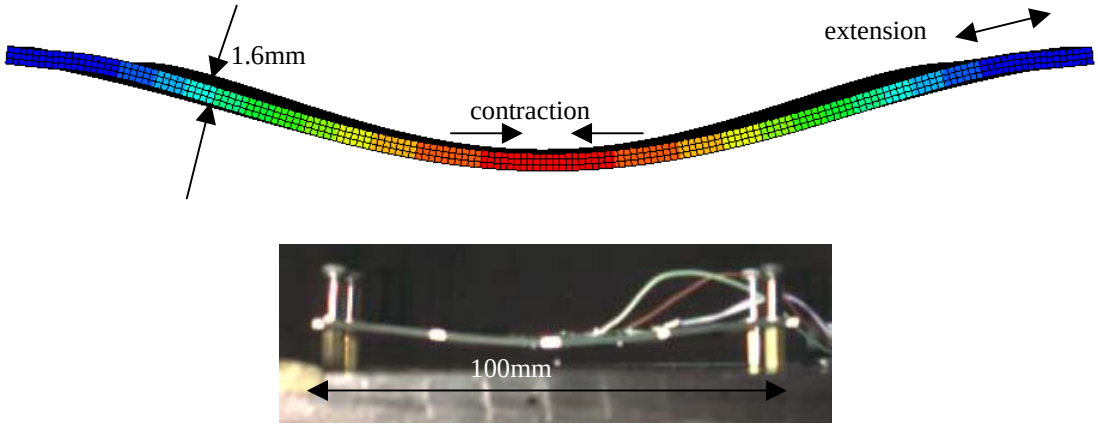

Figure 5.4: Curvature of the bending of PCB during drop impact

5.3 Effect of different screw support configurations

Other types of screw support configuration are also tested. 5-screw support consists of the normal 4 shoulder screws at the corners with one extra shoulder screw mounted at the center of PCB. 6-screw support consists of the usual 4 corner shoulder screws and 2 additional shoulder screws at the center of the edges along the length of the PCB. The location of the co-axial strain gauges used in the experiment is shown in Figure 5.5. Strain gauges 3 and 4 monitor the strains at the center of PCB for 4/6-screw support. For the 5-screw support, strain gauges 3 and 4 are mounted at the center but near the longer edge of the PCB. This is due to the center screw which does not allow the strain gauges to be mounted there. Channels 1 to 6 will determine if any asymmetrical bending may occur during impact by comparing the readings of strain gauges 1 with 5 and 2 with 6.

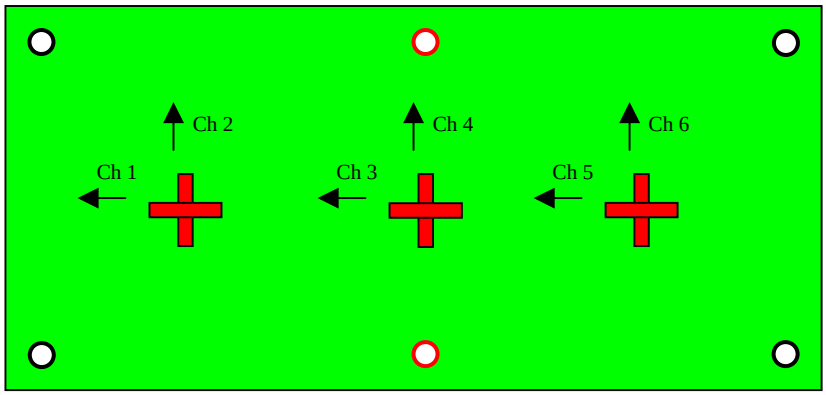

Figure 5.5a: Position of strain gauges mounted for 4/6-screw support

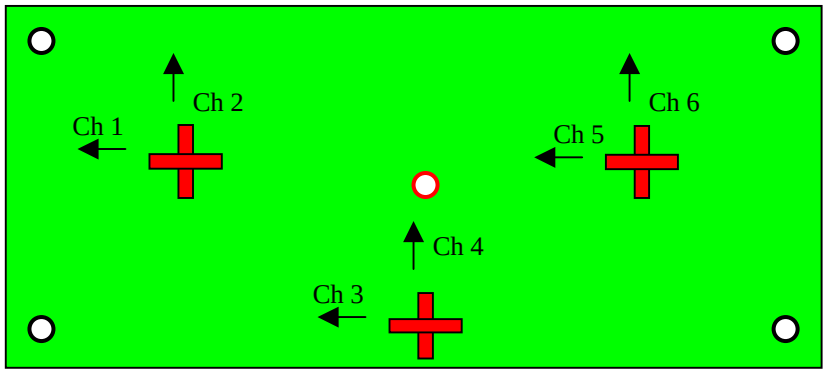

Figure 5.5b: Position of strain gauges mounted for 5-screw support

Tests are conducted with drop heights ranging from 0.3 to 1.5m and at increments of 0.2m. Drops are repeated 3 times for each drop height to determine good repeatability. The strain data is presented in Figure 5.6.

Generally for the PCB mounted CABGA packages, strain gauges 1 and 2 show similar readings with that of strain gauges 5 and 6 indicating symmetrical bending of the PCB during the drop test. This implies very little or no oblique impact of the drop table onto the impact surface.

For the 4-screw support, the variations in the Y-strain are found to be higher in magnitude than the X-strain as shown in Figure 5.6a. The trend in the Y-strain shows that bending along the length is predominantly larger. Trend in the X-strain suggests higher modes of vibration exits although this is very limited in the in-plane direction. The trend for the 6-screw support is quite different from the 4-screw support at the same positions where the strains are monitored. The magnitude of the variations in the strains for the 6-screw fixation is higher for the X-strain than in the Y-strain as shown in Figure 5.6c. In addition, the trend in the Y strain shows possible multiple modes of vibration while the X-direction is dominated by Mode #1 vibration.

For the 5-screw support in the Y direction, the variation in the strains in strain gauge 3 is higher than the other two positions (strain gauges 1 and 5). This is the opposite to that of the X-strain. The magnitude of the X- and Y-strains at the other two positions are comparable. For the X-strain, the second peak in strain gauges 2 and 6 (symmetrical) is much higher than the first peak. This might be due to the complicated bending modes upon drop impact for the 5-screw support. The full study of the drop height effects is being reported in Appendix B Figures B.9 to B.11.

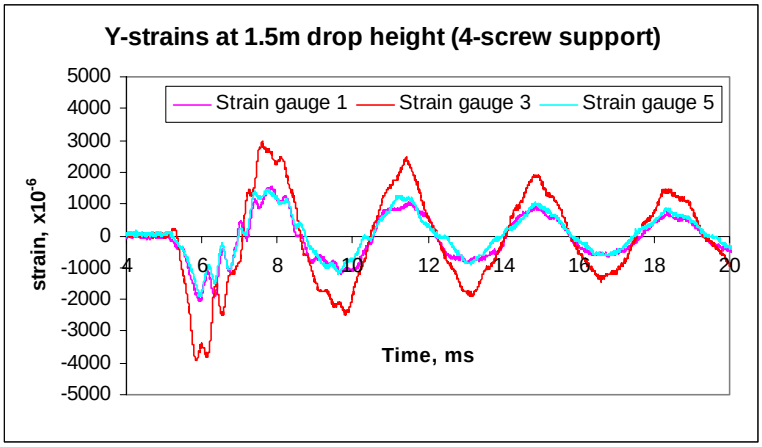

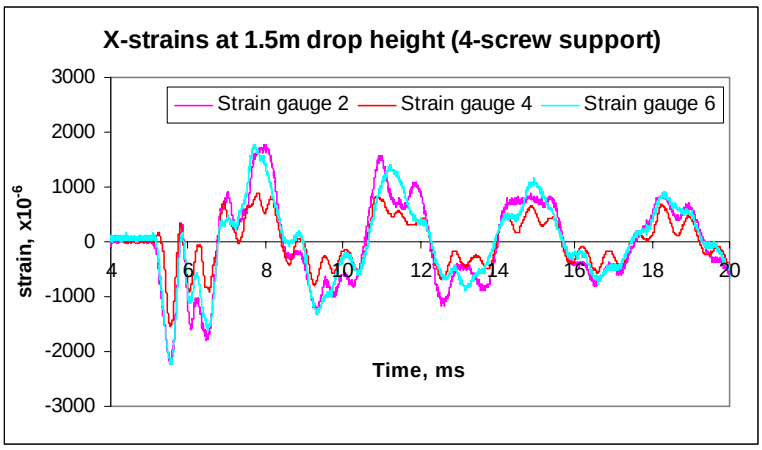

Figure 5.6a: Plots of X- and Y-strains against time for the 4-screw support

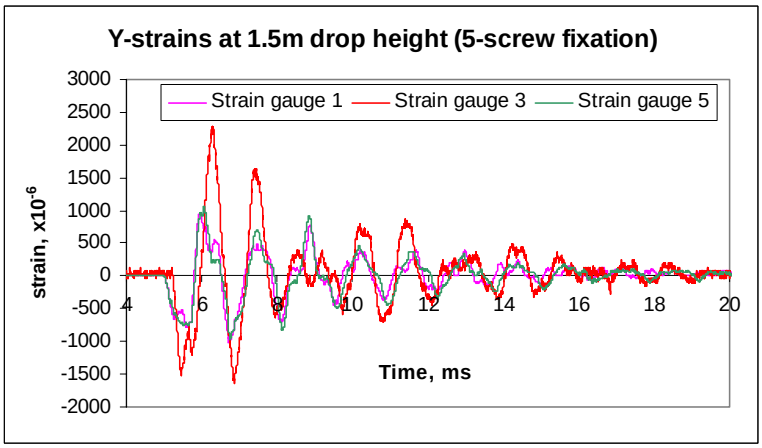

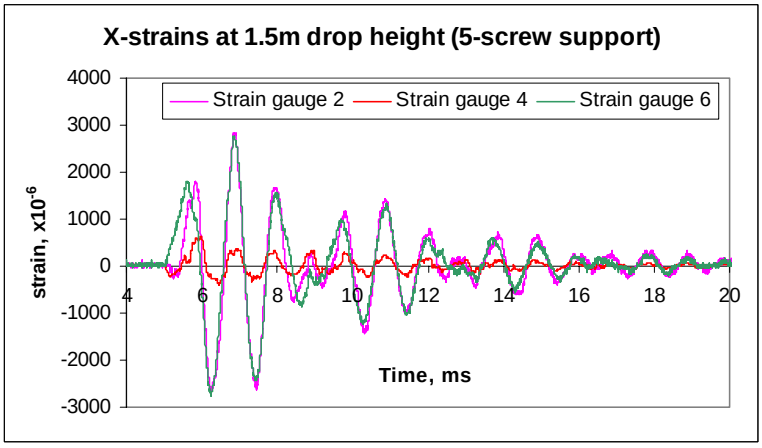

Figure 5.6b: Plots of X- and Y-strains against time for the 5-screw support

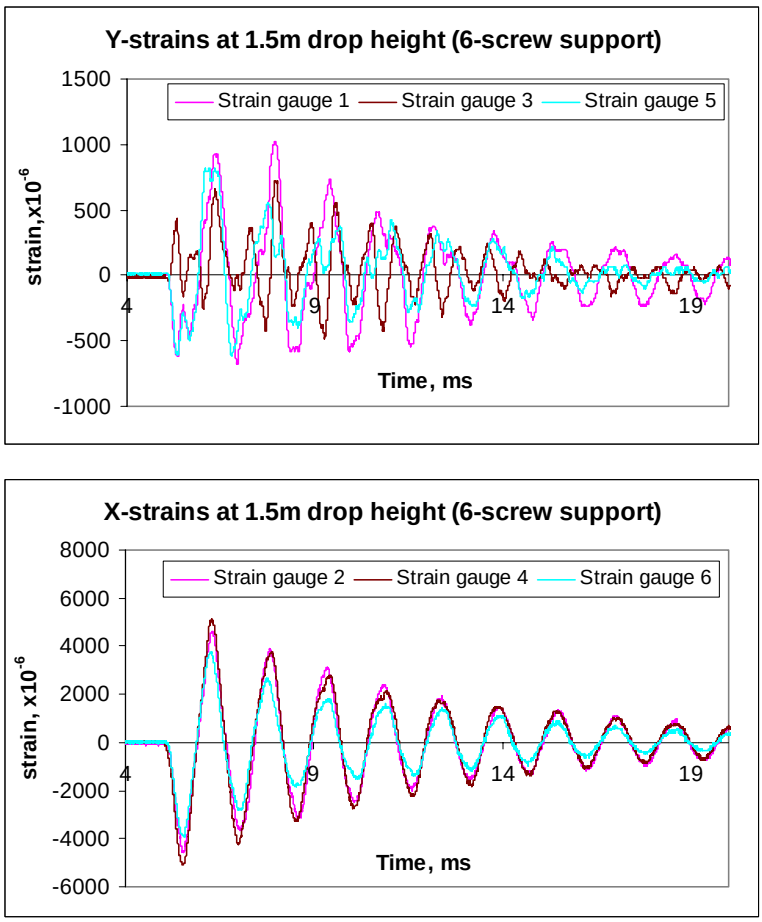

Figure 5.6c: Plots of X- and Y-strains against time for the 6-screw support

5.4 Effect of other clamp fixations

The strain gauges for this test are mounted in the same manner as in Figure 5.5b as the same PCB has been used (hole drilled at center for the 5-screw fixation). The center strain gauge rosette is placed off center and close to the edge. Clamp bars hold the PCB's edges and are screwed on to the drop table. Figures A.6 and A.7 of Appendix A shows the technical drawings of these clamping bars. The PCB is either clamped on its length or width. Figure 5.7 shows the picture of the PCB being clamped at the lengths or at the width. The clamped region is about 7mm from the edge. If the PCB is clamped at its length, the dominant strain will be in the X direction and if it is clamped at its width, the dominant strain will be in the Y direction. Figure 5.8 shows the dominant strain graphs for the two configurations of clamping at a drop height of 1.5m.

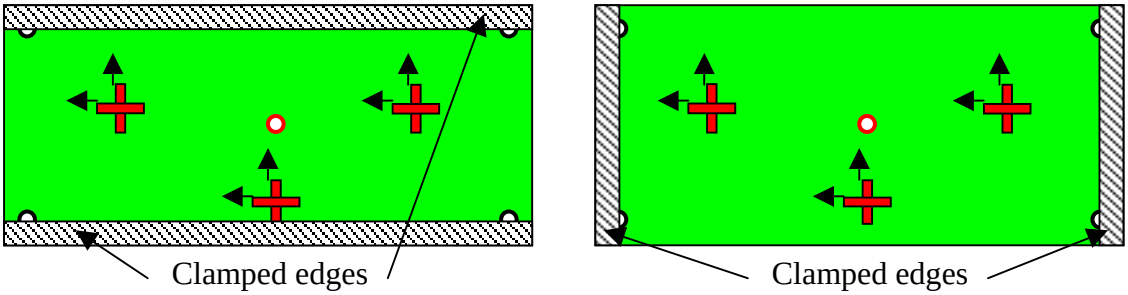

(a) (b)

Figure 5.7: (a) Clamping along lengthwise and (b) along the widthwise edges of PCB

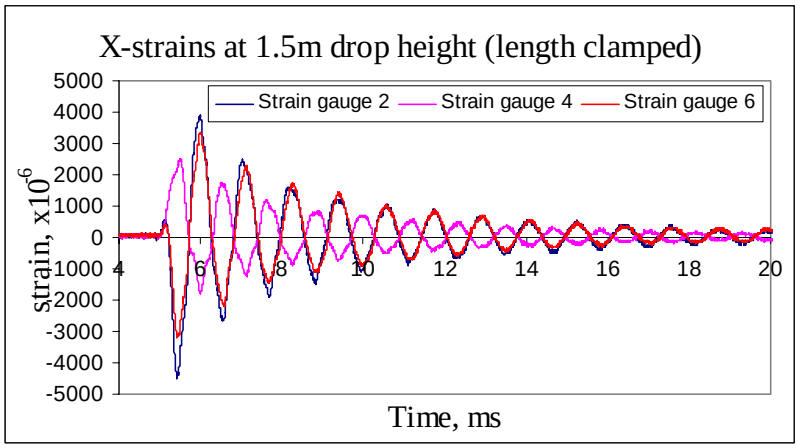

(a)

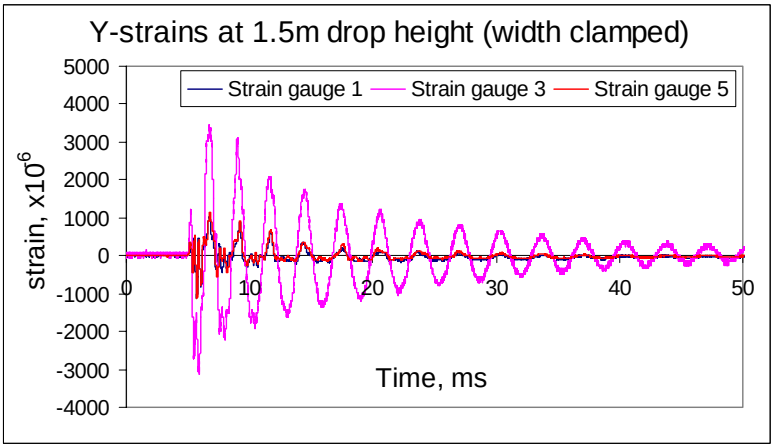

(b)

Figure 5.8: Strains in length / width clamped configurations

An interesting observation from Figures 5.7(a) and 5.6(c) is that the X strain of the 6-screw support varies at a frequency of about 670 Hz, while the X strain clamped PCB at its lengths is about 900Hz. Thus, the PCB flexes much faster for the clamped support than in the 6-screw support due to its increased stiffness. However, the

magnitude of the variations for the clamped support is smaller then the 6-screw support as a stiffer configuration will reduce the extent it can bend.

Likewise, comparing clamping along the widths of the PCB with that of the 4-screw support shows that as the dominant mode of bending is in the Y-direction. The first mode bending frequency of 4-screw support is about 290Hz, while it is about 460Hz for the clamped-width fixation. The same explanation of higher stiffness could be used to explain for the higher bending frequency.

5.5 Dynamic resistance measurement

There are 10 packages (2x5 matrix) mounted on the PCB (see Figure 5.9). The components are placed in a facedown orientation that is the worst condition for failure of components to occur fairly easily. For board level drop test, solder joint failures are induced by shock and PCB bending. Therefore, packages at PCB center (*E* and *F*) are more likely to fail first as the center of the PCB undergoes maximum bending. The other packages away from the PCB center (*A, B, C, D, G, H, I and J*) can withstand higher number of drops (>50 drops) before failure. The PCB length (115mm) is larger than its width (77mm), thus packages will fail along the PCB length rather than the width, according to three Zones 1, 2 and 3. Packages located in the same zone will take around the same number of drops to fail.

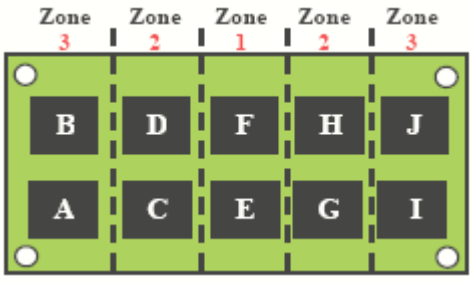

Figure 5.9: Package position on test board

Tests are compared with CABGA packages with and without underfill material. Figure 5.10 shows a graph with drop responses from PCB mounted with CABGA packages but without underfill material. Strain readings in Figure 5.10 are monitored on the non-component side and center of the board. The drop height used for this test is 1.4m. From Figure 5.9, components E and F are the closest to the center of the PCB. For the

4-screw support, the center of the PCB deflects the most and curvature of the PCB is found to be greatest.

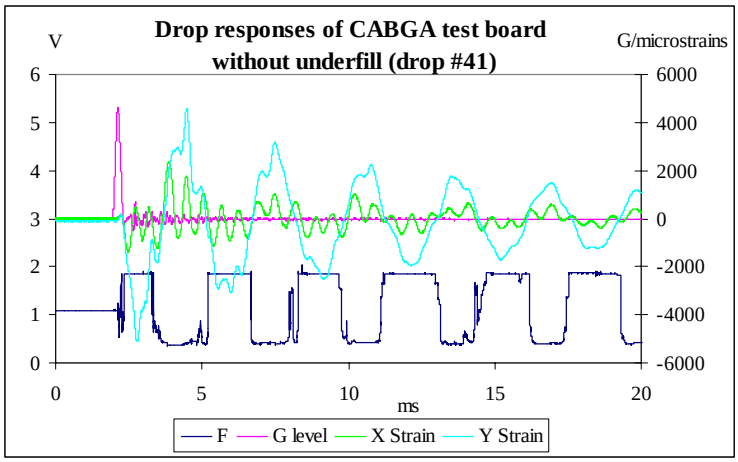

Figure 5.10: Drop responses of CABGA components without underfill material

From Figure 5.10, the graph F represents the dynamic resistance of component F during drop impact. The rise and fall of the G level plots represents the period of impact duration. After impact, the PCB will continue to bend cyclically for a number of cycles till it is completely damped out. As the PCB has already experienced a number of drops, the component F is reaching intermittent failure due to high cycle fatigue. The negative part of the Y-strain plot depicts compression that relates to the PCB bending downwards and the positive part relates to PCB bending upwards. This bending motion is shown in Figure 5.11.

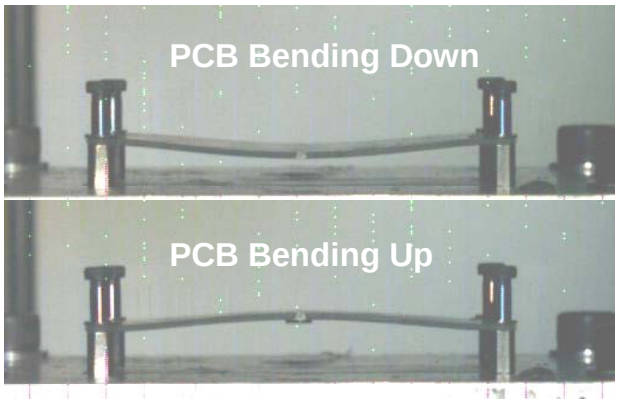

Figure 5.11: Bending of PCB for the 4-screw support case

Figure 5.11 is taken from the frames captured during the test by a high-speed camera. The high-speed images can be used for several purposes. It can be used to verify the cyclic bending frequency of the PCB, determine the impact velocity just before impact

and rebound velocity after impact, determine the relative velocity of bending of the PCB and gauge the maximum amount of deformation the PCB undergoes during impact.

The failure mechanism for the 4-screw support is mainly through bending fatigue. This is especially through for lightweight and small packages where inertia effect is not very large compared to packages equipped with heat-spreaders or bigger sized packages. The solder joints fail due to the mismatch in curvature of the PCB and the package. The mechanism is very similar to the failure mechanism explained in Chapter 4 for TFBGA packages. It is expected that failure will occur at the outermost solder joints.

5.6 Effect of board level mounted with components with underfill material

Figure 5.12 shows the peeling stress distribution of solder joints during drop test. The simulation results are able to correlate with experimental observations related to the failure location and failure interface. The stress concentration is along the solder/component interface, where actual failures are observed in testing. In the drop test model, four corner solder joints have the highest peeling stress, due to strong DNP (distance of the joint to neutral point) effect. In most assemblies especially flip-chip assemblies, the neutral point is usually at the center of the die. Thus, highest stress concentrations are located at the joints furthest from the neutral point, i.e. the outermost corner joints.

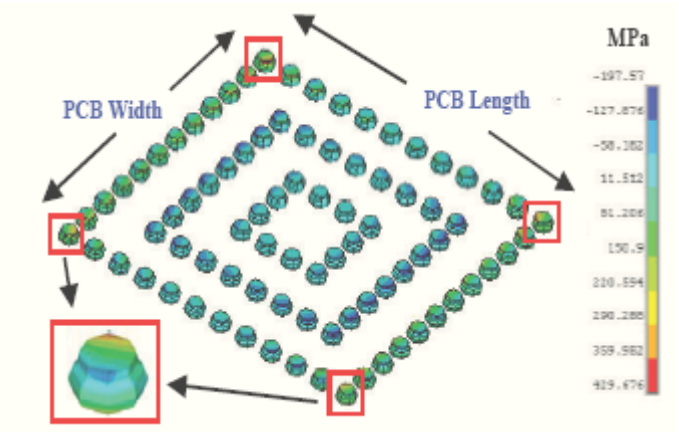

Figure 5.12: Distribution of solder joint peeling stresses in from a numerical simulation [13]

Board level underfill is a more general and practical design enhancement, when the effects of other package and board parameters are limited. Twelve batches of packages with underfill material have been tested at a drop height of 1.4m in the facedown orientation with 4-screw support. Each batch comprises two PCBs with ten components mounted each board. An additional batch of packages (two boards with ten packages each) is also tested where the packages do not have any underfill material.

The effects of underfill enhancement on drop testing are shown in Figure 5.13. The mean impact life (at 50% failure rate) and the first-failure life are summarized in Table 5.1. The mean impact life is taken of all the packages that failed in all three zones. The mean life of the failed packages with underfill at Zone 1 is about 101 drops. However, it should be noted that many of the packages with underfill did not fail after 300 drops. On the other hand, the packages without underfill failed more easily even at Zone 3. Therefore, good underfill material provides superb adhesion properties for the solder pads and package. Thus, it is able to prevent the solder balls from experiencing high bending fatigue stress during drop impact.

Table 5.1: Mean impact life and first failure life during drop test

Test	Drop Test (no. of drops)	
Lives	Mean Life	First Failure
W/o underfill	49	30
With underfill	205	35
Factor	4.18	1.17

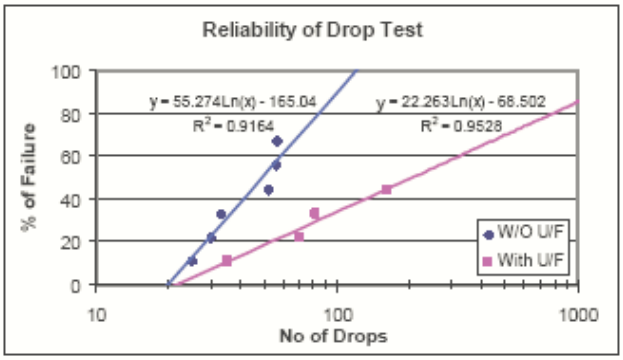

Figure 5.13: Comparison of reliability results of CABGA components during drop test (with and without underfill)

Figure 5.14 shows the mean impact life of drop test correlated to the maximum normal peeling stress of solder joint obtained from modeling. An impact life prediction model is formulated using power law approach to relate the maximum peeling stress of critical solder joint and mean impact life

$$N_{50} = C_1 \sigma_z^{C_2} \qquad (5.1)$$

where N_{50} is the mean impact life (number of drops to failure at 50% failure rate), σ_z is the maximum peeling stress (MPa) in the critical solder ball, C_1 and C_2 are the correlation constants, 174052 and –1.328, respectively.

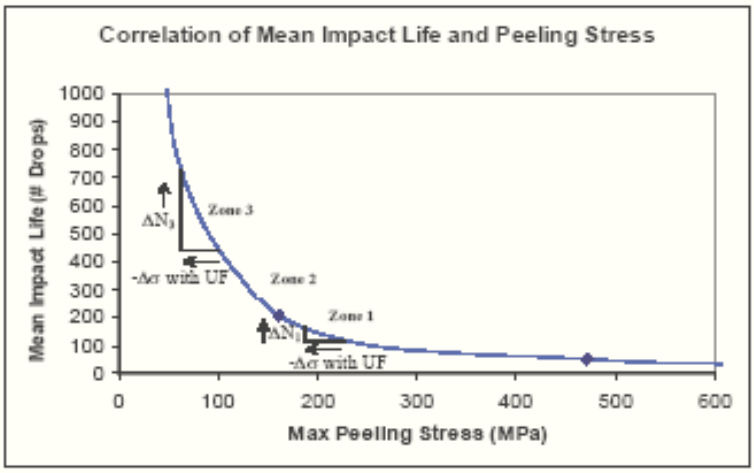

Figure 5.14: Impact life prediction for CABGA components [13]

5.7 Effect of knocking of the PCB

Tests were conducted to study the knocking effects on PCB. In actual small handheld products, the spacing between the packages and the chassis may be too small such that the packages on the PCB actually impacts against the battery or housing during accidental drops due to PCB bending. In board level drop tests, especially for 4-screw support, the spacing between the PCB packages and the fixture must be enough so that the packages in the facedown orientation do not impact on the fixture during PCB bending. In general, the larger the PCB is, more clearance is required to prevent the packages knocking on the fixture.

In these tests, the PCB is to undergo some knocking during drop impact to evaluate changes in the drop responses. Small cylindrical aluminum pieces are placed at the center of fixture one at a time where the center of the PCB will knock against during

impact. These aluminum pieces are shown in Figure 5.15. The drop height used is 1.5m with a single layer of felt as the strike surface. A 4-screw fixation is adopted and a spacing of 10mm is still maintained.

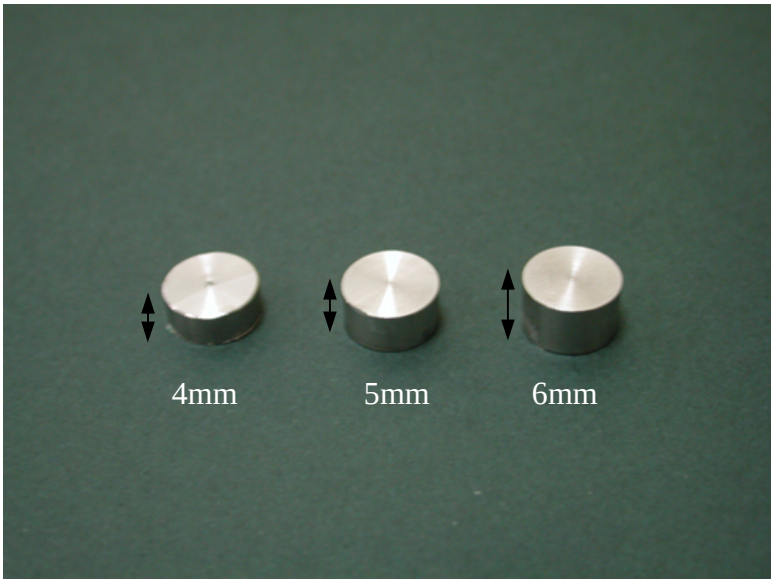

Figure 5.15: Picture of knocking objects used at the fixture

The effect of knocking is studied by varying the heights of the aluminum pieces (of 4, 5 and 6mm height with a diameter of 10mm) as shown in Figure 5.15. Thus, the actual clearance at the center of the PCB to the fixture is 6, 5 and 4 mm respectively. No packages are mounted at the center of the PCB in this case. Figure 5.16 shows a schematic diagram of a side view of the PCB during drop impact. As time progresses, the PCB will bend downwards upon impact and hit on the aluminum piece that is on the fixture. The aluminum pieces are held on tightly to the fixture by means of cyanoacrylate (a strain gauge glue).

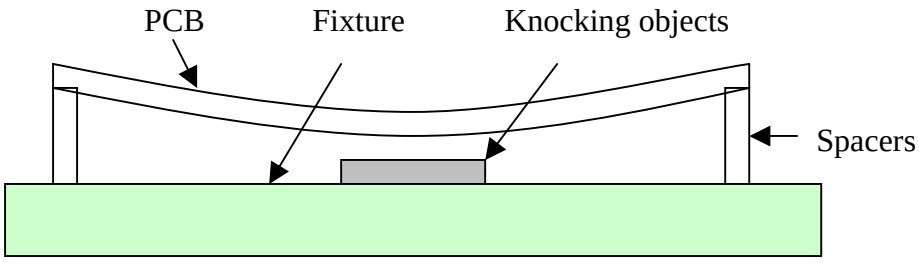

Figure 5.16: Schematic diagram of side view during drop impact

A pair of strain gauges is mounted at the center of the PCB at the reverse side. The in-plane strains are monitored during drop impact. Figure 5.17 shows the Y and X strains of the PCB for the different clearance heights of the aluminum pieces. The legends show the height of the aluminum piece used. For the Y-strain graph, the initial trough of the graph using a 6mm height piece fluctuates more than the other two. Generally, the higher the knocking object is, the earlier the PCB will hit on the object during drop impact. This will cause the PCB to flex back faster and other bending modes might be induced as shown by the fluctuations in the initial cycle of the Y-strain plot. The cycles after the first impact tend to be similar as the PCB is unable to hit the aluminum piece anymore.

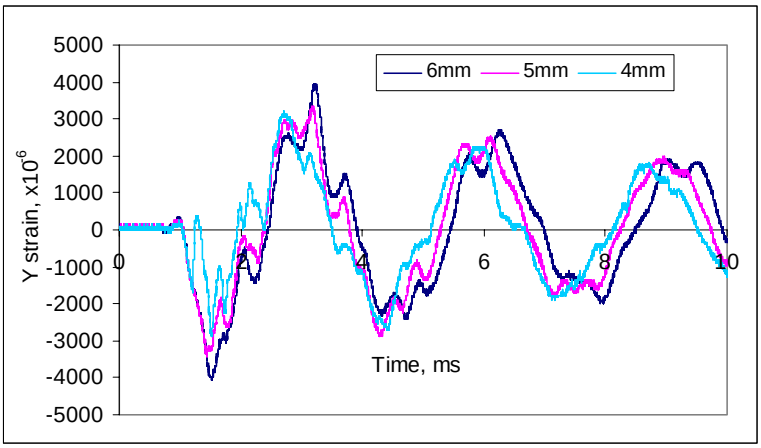

Figure 5.17a: Plot of Y-strain with different clearance heights

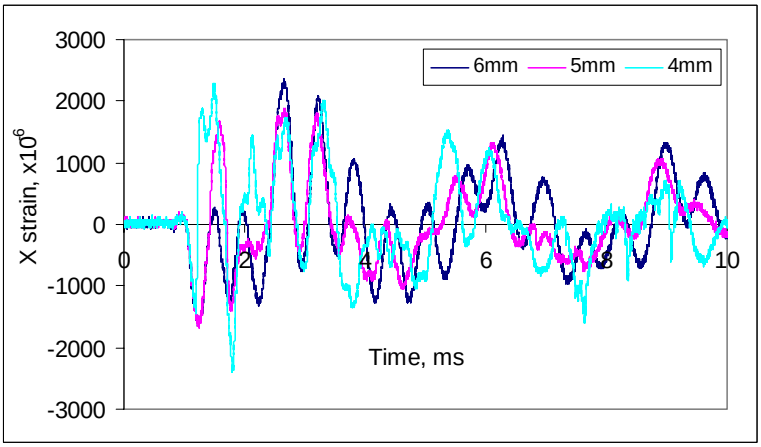

Figure 5.17b: Plot of X strain with different clearance heights

5.8 Effect of the tightness of screws at the spacers

The boundary conditions of PCB during drop impact include the number of PCB mounting screws as well as the tightness of these screws. The tightness of mounting

screws will be reduced after a certain number of drops due to the flexing of the PCB. Figures 5.18 show the strain in PCB length direction at the PCB center under tightened and loosened screw conditions. In this case, the M3 mounting screws were loosened by half a pitch for the loosened screw case.

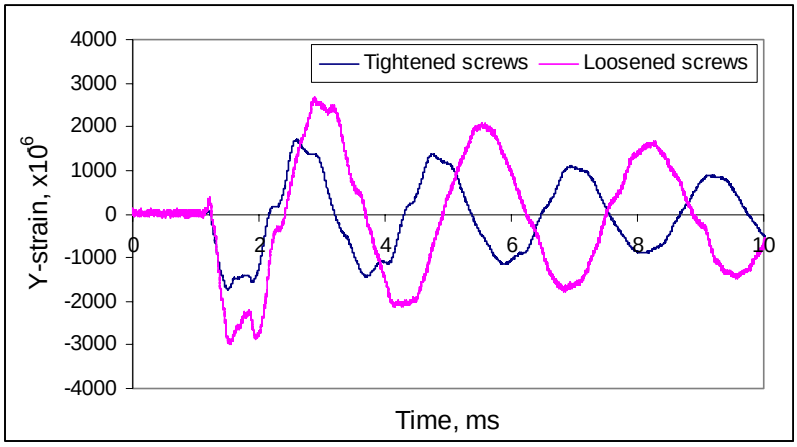

Figure 5.18: Plot of Y-strain for both tightened and loosened screw configurations

The results show that the period of PCB bending cycle for the case of loosened screws (3ms) is larger than that of tightened screw configuration (2.125ms). Besides, for loose screw condition, the negative strain peaks are higher than the tightened screw configuration. Due to lesser constraint, the displacement at PCB center is larger for loose screw. The test board can be simplified as a beam with two supports at each end. The loosened screw case has less constraint, and therefore, the natural frequency of its first mode is definitely lower. The differences in dynamic responses affect the stresses induced in solder joints. Therefore, regular check and torque wrench are required during drop test to avoid inconsistent or random test results.

Chapter 6 Numerical Simulation of Board Level Drop Tests

It is usually very costly and it takes more than three months (including board design, fabrication, assembly and testing) to conduct an actual drop test for package qualification or improving board layout. Due to the pressures of short time-to-market, testing by itself is not sufficient in assessing a product prototype. There is a need for faster and cheaper solutions. Hence, there is an increasing demand for validated drop impact models which are accurate and reliable.

In general, a validated drop impact model can be classified under three levels: 1) good correlation to dynamic responses of PCB (system's structural behavior), 2) good correlation to trend of solder joint stress/strain (qualitative), and 3) good correlation to actual impact life (quantitative). As it is difficult to measure stress/strain in solder joints, correlation at the second level is difficult. Quantitative impact life prediction requires sophisticated material models, and thus, correlation at the third level is also very challenging. A good correlation of drop impact models with dynamic responses is a prerequisite for accurate solder joint reliability analysis and impact life prediction. Good correlation at the first level has been successfully achieved using the Input-G method reported by Tee et al [14]. Hence, it is applied here for second level correlation.

6.1 Input-G method

Since the input impact pulse can be monitored during testing for package qualification, it can be used as a PCB boundary condition in drop test simulation. The Input-G method uses the impact pulse to prescribe the acceleration at the PCB mounting screw locations. The advantages of this method are that it disregards drop height, friction effects along sliding rods and type of strike surface material used as the impact pulse is derived from the actual impact tests.

Figure 6.1 shows a schematic of the drop test simulation. The drop table, fixture, contact surface, and friction of guiding rods are not simulated, but their complex effects are considered indirectly by using the impact pulse recorded from experiments.

The same impact pulse can be applied for design analysis of PCB/package geometry and material.

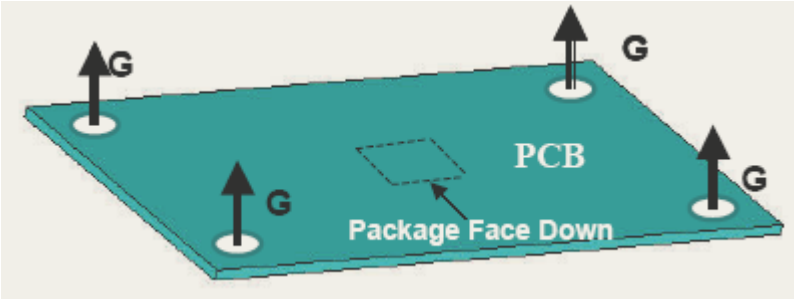

Figure 6.1: Input-G method for 4-screw PCB subassembly

In this study, board level drop test simulation of 0.75mm pitch TFBGA46 (see Figure 6.2) is performed. Only one quarter of the board is modeled using solid elements due to symmetry (horizontal drop, component facing downwards). The package size is 6.39x6.37mm, die size is 4.6 x 3.5 x 0.235 mm, and board size is 100 x 48 x 1.6 mm with 46 I/O. Detailed package geometry, solder balls, and pad design are included in the model. Because only a quarter of the BGA is modeled, the full model represents a full array of 48 solders balls instead of the 46 solder balls in the actual TFBGA. However, this is not expected to give rise to significant errors. The test board is mounted on four screws with one package (facing downwards) mounted at PCB center. The pad design is SMD on the component side and NSMD on the PCB side.

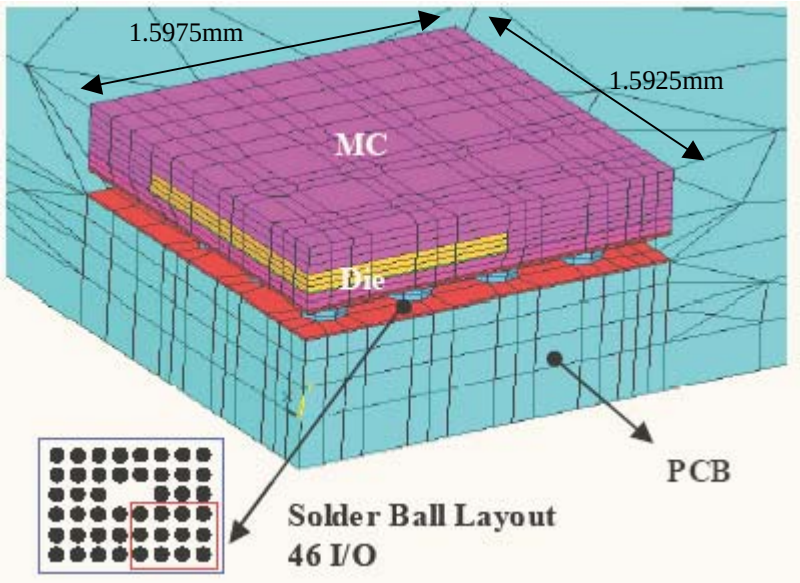

Figure 6.2: Board Level Drop Test for TFBGA46

ANSYS/LS-DYNA with drop test module is used for the pre/post-processing and solution of the dynamic drop test simulation. For simplification, only linear elastic material model is applied. Therefore, only basic mechanical properties are required. The mechanical properties are shown in Table 6.1.

Table 6.1: Material properties used in model

Materials	Modulus (MPa)	Poisson Ratio	Density x 10^{-9} (Mg/mm^3)
Die	131000	0.3	2.33
Die Attach	5000	0.3	2.2
Mold Compound	25506	0.3	1.97
Cu Pad	117000	0.3	8.94
PCB	16850	0.11	1.82
Al Block	70000	0.33	2.7
Steel Screw	200000	0.3	7.8
Eutectic Solder	34000	0.363	8.41
Solder Mask	5000	0.3	1.15

There are a total of 5183 elements and 5483 nodes. In the experiment, a layer of felt is used as the strike surface to generate a sinusoidal type of acceleration curve. Figure 6.3 shows the impact pulse measured experimentally for a drop height of 1.5m. The peak acceleration is 3700G and the pulse duration is about 0.4ms. Assuming the G level is the same for the whole fixture, this impact pulse is input as boundary condition to the four PCB mounting screws.

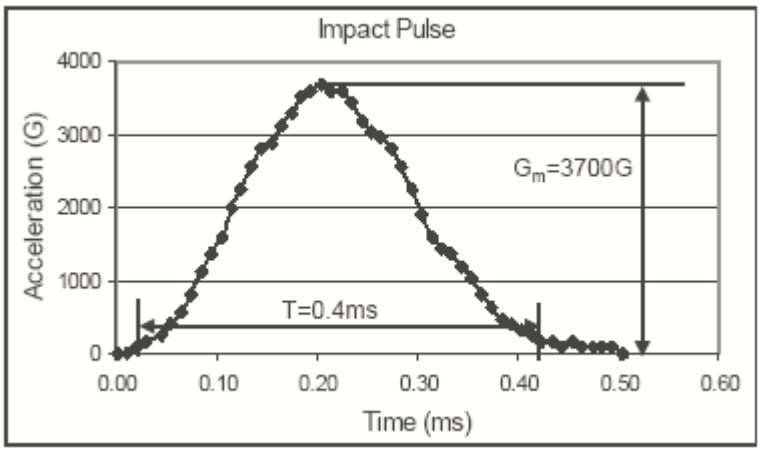

Figure 6.3: Input acceleration curve for FE simulation

6.2 Correlation with dynamic responses of actual tests

6.2.1 PCB strain in the length direction

The predicted strain along the PCB length direction at the center of the PCB is shown in Figure 6.4. It correlates very well with actual strain gauge readings. The amplitude of the PCB vibration decreases gradually with time, with a damping ratio of about 0.036 as mentioned in Chapter 4. The period or frequency of vibration is almost the same for both simulation and actual tests.

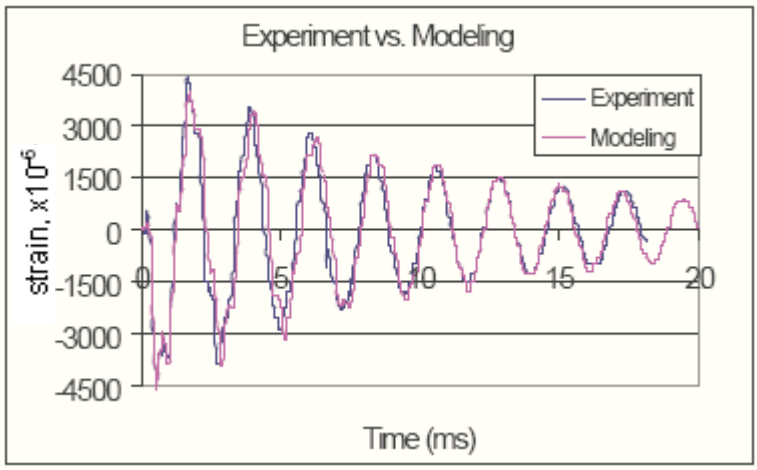

Figure 6.4: Comparison of strain (length) curves

The trend of the strain curve is similar to that of a free vibration system with linear viscous damping. The equation for the out-of-plane displacement free vibration system with viscous damping is:

$$z(t) = e^{-\varsigma\omega_n t}\left\{ z_o \cos\sqrt{1-\varsigma^2}\,\omega_n t + \frac{\dot{z}_o + \varsigma\omega_n z_o}{\sqrt{1-\varsigma^2}\,\omega_n} \sin\sqrt{1-\varsigma^2}\,\omega_n t \right\} \qquad (6.1)$$

where $z(t)$ is the out-of-plane displacement of the vibrating system at any time t, ζ is the damping ratio, ω_n is the natural angular frequency, z_o and $\dot{z}_o$ are the out-of-plane displacement and velocity at time 0 respectively. Using suitable boundary conditions similar to the graph in Figure 6.4, eqn (6.1) can also be used to approximate the experimental and simulated strain along the length of the PCB as the strain in Fig. 6.4 shows the dominant fundamental bending mode.

Figure 6.5 shows the comparison of strain (lengthwise) from actual test and the graph obtained from eqn (6.1). In this case, the initial condition is z_o=0 and $\dot{z}_o$ is estimated

to be 11 s^{-1} from the initial slope of the graph. The strain curve of the free vibrating system with viscous damping shows fairly good correlation. It is more accurate during the initial few cycles of the PCB bending, when the PCB experiences more deformation and higher curvature than in the subsequent cycles.

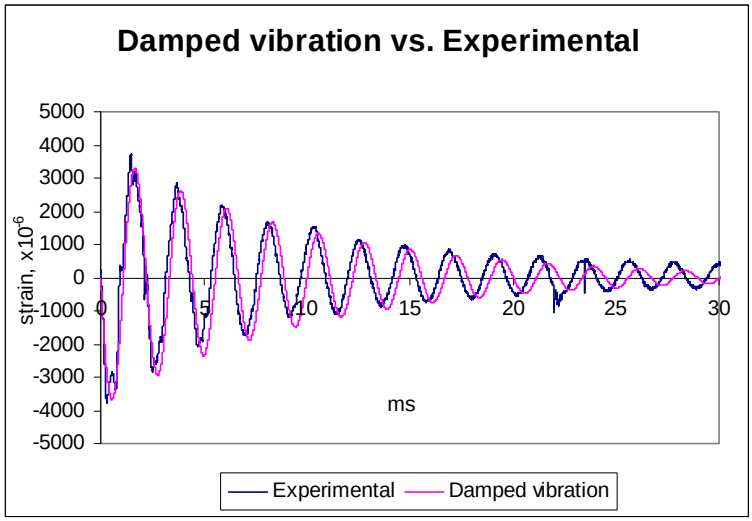

Figure 6.5: Comparison of a damped vibration system and experimental result

6.2.2 PCB strain in the width direction

Figure 6.6 shows the strain in the width direction from experiment and simulation. The correlation is not as good as the strain in the length direction shown in Figure 6.4. The magnitude of the strain is much smaller in the width direction than in the length direction. The signal-to-noise ratio is also higher than in the strain (length) curve.

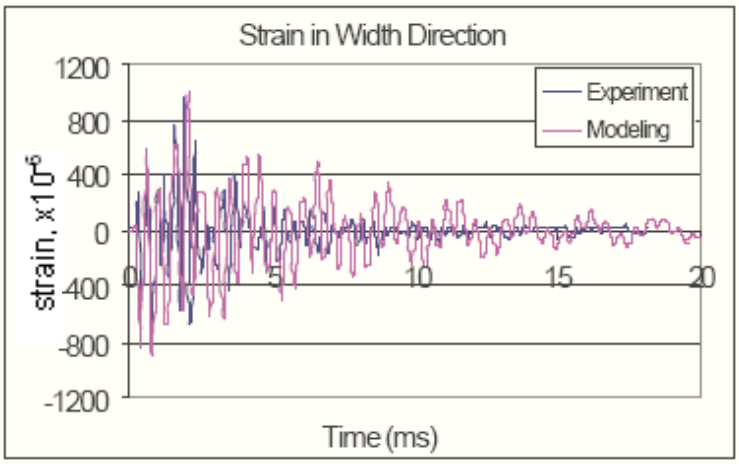

Figure 6.6: Comparison of strain (width) curves

6.2.3 Acceleration at PCB center package

In order to further verify the Input-G method, the acceleration signal from another test is used as input to the model. The input peak acceleration is about 2400G with pulse duration of 0.36ms. A small accelerometer is attached to the package at the center of the PCB. The accelerometer has to be very lightweight and small so that its mass can be neglected. Owing to the small size of the accelerometer, it is not possible to test at high drop heights as the shock limit of the small accelerometer of only about 10,000G. Thus, only a drop height of 1m is tested.

The dynamic strain in length direction and output acceleration of PCB center are computed and compared with the experimental measurements. Graphs with long time duration of 50ms are captured to understand the overall drop process. Figure 6.7a again shows good correlation in the dynamic strain between model and actual tests. The output acceleration is the out-of-plane acceleration at the center package. The output acceleration also matches well for both experimental and simulation with both showing the same trend (see Figure 6.7b).

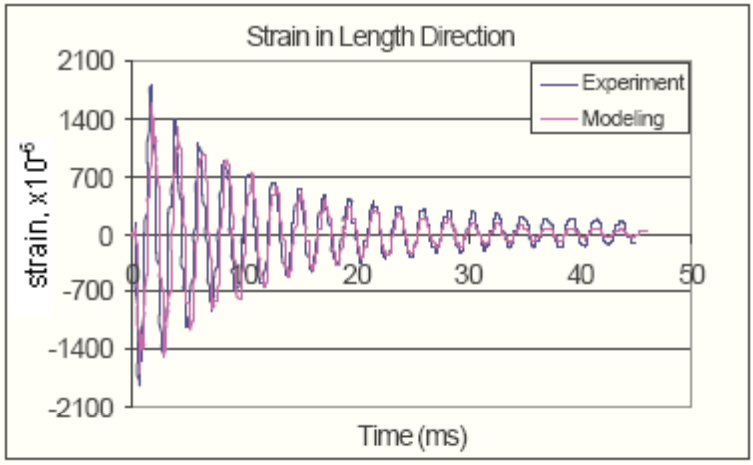

Figure 6.7a: Comparison of strain (length) curves from actual tests and simulation

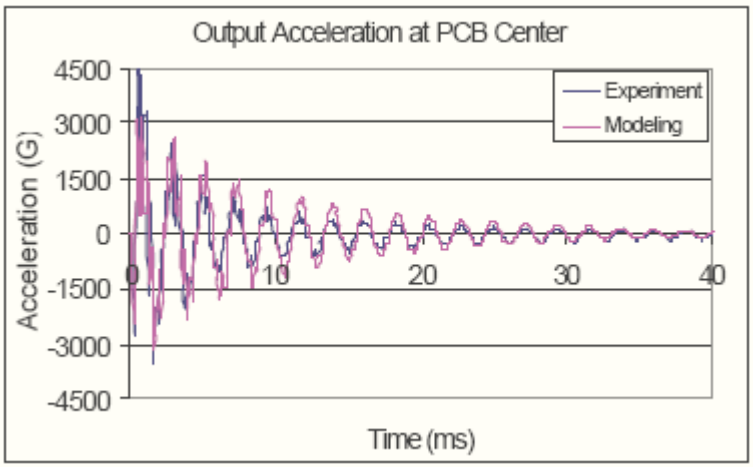

Figure 6.7b: Comparison of acceleration from actual tests and simulation

6.3 Failure analysis of the model

The maximum solder joint stress does not occur at the instant of maximum input acceleration at 0.2ms as shown in Fig. 6.3. Instead, the stress level is the highest at 0.74ms, and the critical solder ball is located at the outermost corner of the ball grid array, with stress concentration along the solder/PCB pad interface as shown in Fig. 6.8 (quarter 3D model). This is the instant when PCB has the largest deflection and bending stress, induced by the inertia force after impact. The location of the stress concentration predicted by modeling agrees with the actual failure mode and the critical solder ball location observed in cross-sectioned solder specimens. All the solder balls are cross-sectioned row by row, and only the outermost corner solder ball is observed to have failure. It is a brittle crack in solder intermetallic layer along the PCB pad-solder interface.

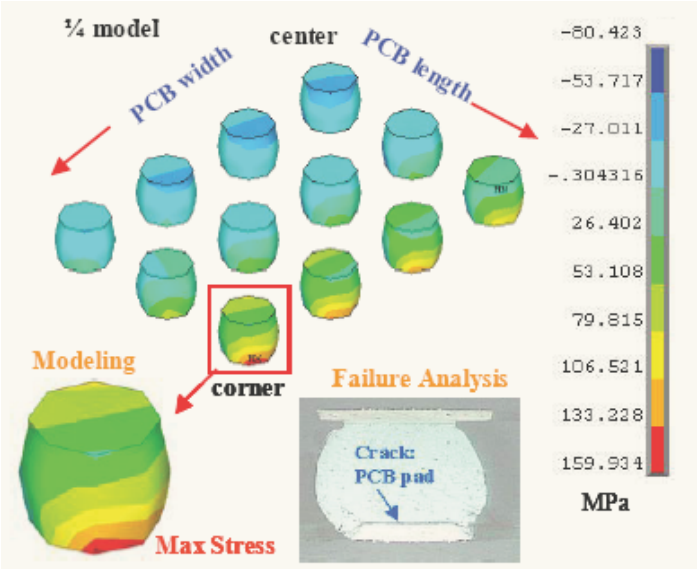

Figure 6.8: Location of critical solder ball and failure interface

The solder ball interfacial failure is induced by a combination of stress waves propagating through it and PCB bending. The bending stress is critical to solder joint reliability. Figure 6.9 shows the deflection of PCB during bending. There is an in-plane stretch of 3.35mm in the length direction from the center of the board to the shorter edge. This is much larger than in the width direction (0.33mm), measured from the center of the board to the longer edge. As a result, the outer row of solder balls in the PCB length direction deforms more and has higher bending stress level. Therefore, the DNP (Distance to Neutral Point) effect and the ball grid array layout are important design considerations for components under drop impact.

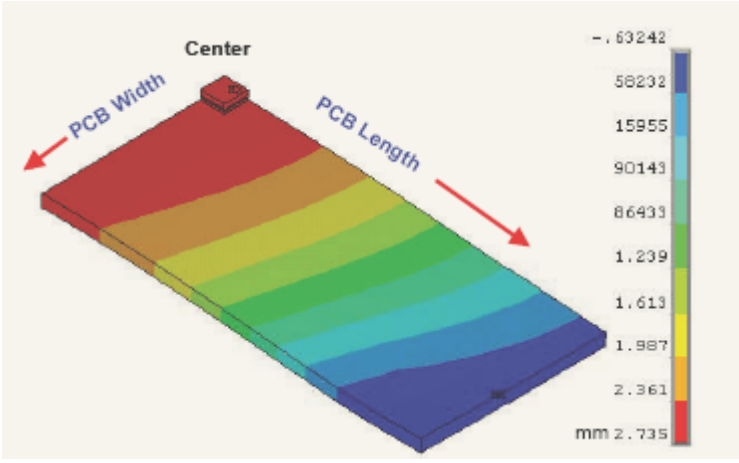

Figure 6.9: PCB out-of-plane displacement distribution at maximum bending

The reliability of solder joints during the drop impact is a main factor in determining the impact life of the packages. Figure 6.10 shows the variation of stresses in the critical solder joint with impact time, including normal stress in PCB length direction (S_y), first principal stress (S_1), vertical normal stress or peeling stress (S_z), shear stress (S_{yz}), and Von Mises stress (S_{eqv}). The maximum solder stress is found to be at the bottom interface of solder close to the PCB side. All the stresses vary cyclically under PCB vibration, corresponding to the measured dynamic strain of PCB. Among them, the peeling stress has the highest amplitudes in positive and negative directions. The peeling stress shows an amplitude-declining cyclic stress trend. The peeling stress is the dominant stress component that causes the intermetallic layer to peel off. The horizontal normal stress (S_y) and shear stress (S_{yz}) are much lower in magnitude. Therefore, the solder joint peeling stress can be used as a failure criterion for the purpose of design optimization, although the shear stresses would probably be much higher in ball shear tests. Since the peeling stress is induced mainly by PCB bending or vibration, it can also be concluded that the PCB bending is the major failure mechanism of PCB subassembly under drop impact, especially for components mounted at PCB center with 4-screw fixation.

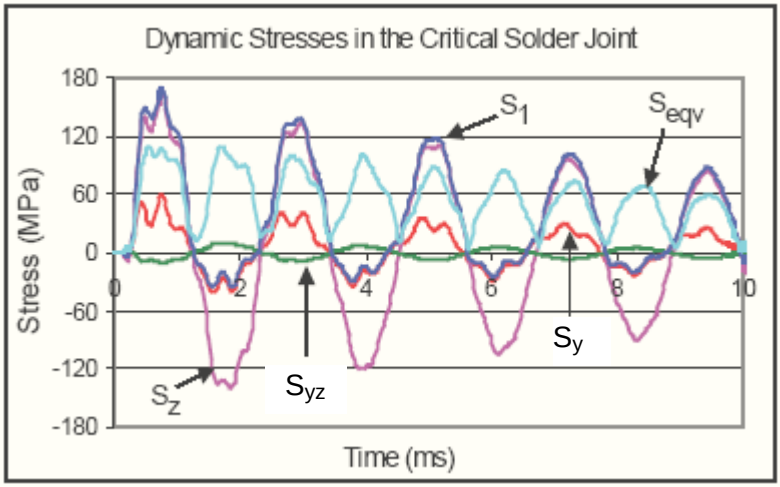

Figure 6.10: Dynamic stresses during drop impact

6.4 Natural bending frequency of PCB

On impact, the velocity of the drop table is reduced to zero, while the PCB assembly is still traveling downwards. The PCB bends downwards and upwards cyclically until the vibrating amplitude is damped to zero. The PCB assembly can be regarded as a uniform beam, as mentioned in Chapter 5, to estimate its response to drop impact.

The natural frequencies of beams with uniform section and uniformly distributed loads can be obtained from a handbook by Cyril [63]. This is shown in Equation (6.2).

$$f_n = \frac{1}{2\pi} A \sqrt{\frac{EI}{\rho\, a^4}} \qquad (6.2)$$

where f_n is the natural frequency of the beam, A is the coefficient used for different boundary conditions, E is the Young's Modulus, I is the area moment of inertia of beam cross section, ρ is the mass per unit length of beam and a is the length of the beam. The two boundary conditions used here are shown in Figure 6.11. A fixed-fixed beam and a simply supported beam are used to approximate the cyclic bending conditions of a PCB.

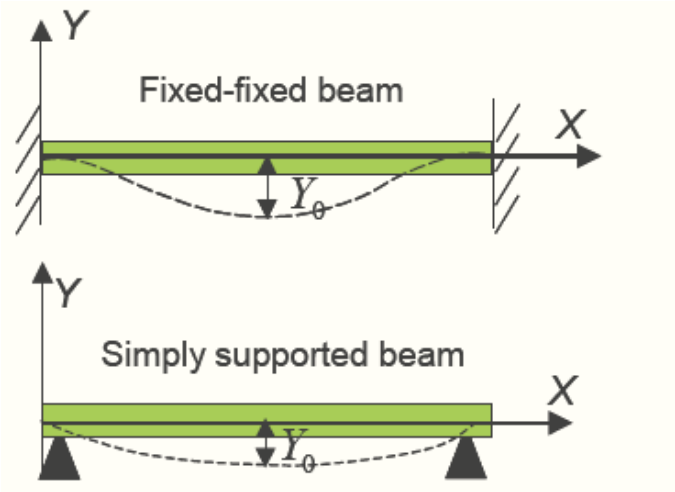

Figure 6.11: Beams with different boundary conditions

For a fixed-fixed beam, the coefficient A is 22.4 and for a simply supported beam, the coefficient is 9.87. It is clear that the natural frequency of PCB assembly is mainly dependent on PCB dimensions, mass inertia, moment of inertia, elastic modulus and its boundary condition.

Typical material properties of PCB assembly are:

E = 16850 MPa

ρ = 0.182 kg/m

and moment of inertia, I, of PCB is described as

$$I = \frac{bh^3}{12} \qquad (6.3)$$

where *b* is the width of PCB, *h* is the thickness of PCB. For fixed-fixed beam, the natural frequency is 460Hz, and the maximum deflection is 1.51mm. As for simply supported beam, its natural frequency is 203Hz. The natural frequency measured by experiment is about 450Hz and is between the range of a uniform beam that is simply supported and one that is fixed but closer to that of a fixed-fixed beam.

A discrete Fourier Transform is performed on the signals of the in-plane board strains of the TFBGA board in the time domain to obtain signals in the frequency domain. Figure 6.12 show the longitudinal strains in the frequency domain after FFT for a typical 4-screw fixation on the TFBGA board. The frequency domain shows only one dominant frequency at about 460Hz. This is again between the range of a uniform beam that is simply supported and one that is fixed.

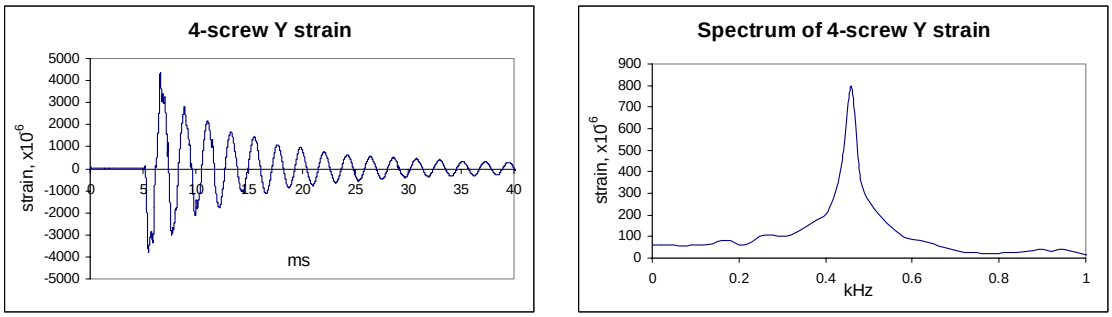

Figure 6.12: FFT of 4-screw fixation longitudinal strain

Chapter 7 Conclusions

7.1 Drop test methodology

A new design for the drop table is implemented. It is more lightweight and is easy to install. For board level drop testing, thin layers of felt are used for strike surface. This is to achieve a high G level that is required if the drop test requires components to fail after a reasonable number of drops. The strike surface used is curved to ensure a single point of impact throughout the test. However, the point of impact must be aligned with the drop mass center of gravity so that no turning moments will be induced after impact. Standardized mounting shoulder screws of size M3 and spacers of 10mm length are used for most types of boards. Pre-characterization of the drop tester is done before the start of the experiment. The Lansmont drop tester is also capable of accomplishing the JEDEC proposed standards [7].

7.2 Experiment findings using TFBGA board

Records of PCB strains, in-situ solder interconnect resistance and high-speed photographs were made. These records are used to verify with simulation results from a suitable model. The extent of bending was found to be the greatest for the 4-screw fixation set-up. It is shown in this test that in the 6-screw fixation, the PCB undergoes lesser degree of deflection upon drop impact. This suggests that in the actual product, it is always advisable to have more screws for fixing on the PCB. However, the limitation in space on a small PCB is an important consideration.

High-speed photography was deployed to determine the frequency and bending mode of the PCB bending. The photographs are consistent with the strains measured at the center of the PCB. In-situ resistance monitoring was conducted through a simple setup to determine the failure characteristics of the TFBGA component. Intermittent failure is found to be prevalent before the component totally failed. The component is believed to have failed when the PCB is bending downwards, causing the corner solder balls to peel off due to tensile stresses. These stresses are closely related to the strains measured by the strain gauges mounted at these positions.

7.3 Experiment findings using CABGA board

Other screw fixations and clamp fixations are studied using the CABGA board. Edged clamped fixations tend to have a higher frequency of bending as compared to the screw-mounted fixations. Clamped edge support also takes up more space at the edges just for mounting the boards. The effect of underfill is also studied on CABGA components. The components with underfill material are found to have better drop reliability than components without underfill. For CABGA boards, the effects of knocking between the PCB center and the fixture are studied. When knocking occurs, the components may fail due to direct impact in addition to failure at the interconnects. The effect of screw tightness at the mounting points is also studied and results show that loosened screws causes the PCB to bend larger in magnitude than tightened screw case.

7.4 Correlation of experimental results to modeling

A new modeling method is adopted where the input of the boundary conditions are the input G levels at the mounting screw positions. This method is advantageous as it eliminates friction errors when the drop mass slides along the rods and can used for any impact pulse waveform. The model showed good correlation with the experiment. This gives some insight on the solder ball stresses during impact. The peeling stress of the solder joints, being the dominant stress for solder joint failure, could thus be estimated using the model during drop impact.

7.5 Recommendations

During the course of the project especially in testing the CABGA packages, 300 drops were required to complete a batch test. There were 12 batches so the number of drops can be many. The work can be tedious as performing every drop requires the user to control the drop tester. Therefore, it will be advantageous that the drop tester can be automated to conduct the drops, saving the user's effort and time to operate the drop tester. In addition, resistances should also be measured automatically through an event detector after every drop. This saves the user's time to manually check the resistances using the multimeter.

Thermal loading can arise when the electronic products are in use. The temperature within the electronic components can reach in excess of 100^{o}C and this can seriously

affect the mechanical properties of the solder interconnects. While much work has been done on investigating the effects of thermal loading and aging on the static mechanical properties of solder interconnects, no such work is known to have been performed on the effects of thermal loading on the dynamic mechanical response of solder interconnect arising from drop impact. Further study should be done to investigate the influence of thermal loading and aging on the drop impact reliability of various electronic packages used in portable electronic products.

List of References

Drop Test Standards

1. EIA-364-27B, “Mechanical Shock (Specified Pulse) Test Procedure for Electrical Connectors,” Electronic Industries Association, Engineering Department, 1996.

2. MIL-STD-810F Method 516.5, “Military Standard: Test Method Standard for Environmental Engineering Consideration and Laboratory Tests,” U.S. Department of Defense, 2000.

3. MIL-STD-883C Method 2002.4, “Military Standard: Test Methods and Procedures for Microelectronics,” U.S. Department of Defense, 1983.

4. IPC J-STD-029, Performance and Reliability Test Methods for Flip Chip, Chip Scale, BGA and other Surface Mount Array Package Applications, 2000.

5. JESD22-B104-B, “Mechanical Shock Test Method,” JEDEC Solid State Technology Association, 2001.

6. JESD22-B110, “Subassembly Mechanical Shock Test Method,” JEDEC Solid State Technology Association, 2001.

7. JESD22-B111, “Board Level Drop Test Method of Components for Handheld Electronic Products,” JEDEC Solid State Technology Association, 2003.

Board Level Drop Test References

8. T.Y. Tee, H.S. Ng, C.T. Lim, E. Pek, and Z.W. Zhong, “Application of Drop Test Simulation in Electronic Packaging”, 4th ASEAN ANSYS Conference, 2002.

9. T.Y. Tee, H.S. Ng, C.T. Lim, E. Pek, and Z.W. Zhong, “Board Level Drop Test and Simulation of TFBGA Packages for Telecommunication Applications”, 53rd ECTC, 2003.

10. T.Y. Tee, H.S. Ng, C.T. Lim, E. Pek, and Z.W. Zhong, “Board Level Drop Test and Simulation of QFN Packages for Telecommunication Applications”, ICEP Conference, 2003.

11. T.Y. Tee, H.S. Ng, C.T. Lim, E. Pek, and Z.W. Zhong, “Drop Test and Impact Life Prediction Model for QFN Packages,” Journal of Surface Mount Technology, 2003.

12. T.Y. Tee, H.S. Ng, C.T. Lim, E. Pek, and Z.W. Zhong, “Impact Life Prediction Modeling of TFBGA Packages under Board Level Drop Test,” Microelectronics Reliability Journal vol. 44, 2004.

13. T. Y. Tee, H.S. Ng, J.E. Luan, D. Yap, K. Loh, E. Pek, C.T. Lim, and Z.W. Zhong, “Integrated Modeling and Testing of Fine-pitch CSP under Board Level Drop Test, Bend Test, and Thermal Cycling Test”, ICEP Conference, 2004.

14. T. Y. Tee, J.E. Luan, E. Pek, C.T. Lim, and Z.W. Zhong, “Novel Numerical and Experimental Analysis of Dynamic Responses under Board Level Drop Test,” EuroSIME Conference, 2004.

15. T. Y. Tee, J.E. Luan, E. Pek, C.T. Lim, and Z.W. Zhong, “Advanced Experimental and Simulation Techniques for Analysis of Dynamic Responses during Drop Impact”, 54th ECTC, 2004.

16. J.E. Luan, T.Y. Tee, E. Pek, C.T. Lim, and Z.W. Zhong, “Modal Analysis and Dynamic Responses of Board Level Drop Test,” 5th EPTC, 2003.

17. T.Y. Tee; H.S. Ng; Z.W. Zhong, “Design for enhanced solder joint reliability of integrated passives device under board level drop test and thermal cycling test,” 5th EPTC, 2003.

18. L.B. Tan, C.T. Lim, E.H. Wong, V.B.C. Tan, S.K.W Seah and X .W. Zhang, “Board level solder joint failures of MCM by static and dynamic loads,” 5th EPTC, 2003.

19. Liping Zhu, “Submodeling Technique for BGA Reliability Analysis of CSP Packaging Subjecting to an Impact Loading,” IPACK’01, July 2001.

20. Takahiro Sogo and Satoru Hara, “Estimation of Fall Impact Strength for BGA Solder Joints”, ICEP Proceedings, 2001.

21. Nokia’s report, “Reliability of ST TFBGA 224 and TFBGA 228 components”, Presentation Paper, 2001.

22. Ahmer Syed, “Interconnect Reliability: Board Level Drop Test Considerations”, Amkor Technology, Inc, Presentation Paper, 2001.

23. A. Kujala, T. Reinikainen, W. Ren, “Transition to Pb-free Manufacturing Using Land Grid Array Packaging Technology”, 52nd ECTC, 2002.

24. Dongji Xie, Minna Arra, Sammy Yi, Dan Rooney, “Solder Joint Behavior of Area Array Packages in Board Level Drop for Handheld Devices”, 53rd ECTC, 2003.

25. Masazumi Amagai, Yoshitaka Toyoda, Takeshi Tajima, “High Solder Joint Reliability with Lead Free Solders”, 53rd ECTC, 2003.

26. Leon Xu, Janjun Wang, Tommi Reinikanen, “Numerical Studies of the Mechanical Response of Solder Joint to Drop/Impact Load”, 5th EPTC, 2003.

27. Y.Q. Wang, K.H. Low, F.X. Che, H.L.J. Pang, S.P. Yeo, “Modeling and Simulation of Printed Circuit Board Drop Test”, 5th EPTC, 2003.

28. Kinuko Mishiro, Shigeo Ishikawa, Mitsunori Abe, Toshio Kumai, Yutaka Higashiguchi, Ken-ichiro Tsubone, “Effect of the drop impact on BGA/CSP package reliability,” Microelectronics Reliability Journal vol. 42, 2002.

29. Q. Yu, H. Kikuchi, S. Ikeda, M. Shiratori, M. Kakino, N. Fujiwara, “Dynamic behavior of electronics package and impact reliability of BGA solder joints,” The Eighth Intersociety Conference, ITHERM 2002.

30. K. Hiraiwa, M. Minamizawa, “Advanced LSI Packaging Technologies,” Fujitsu Sci. Tech. J. 36, 1, 2000.

31. W. Ren; J.J. Wang, “Shell-based simplified electronic package model development and its application for reliability analysis,” 5th EPTC, 2003.

32. Sidharth, V. Valluri, R. Gannamani, Meilu Zhang, “Characterization of a novel fine-pitch ball grid array package for flash memory application,” 50th ECTC, 2000.

33. A. Yoshida, Young-Ho Kim, K. Ishibashi, T. Hozoji, “An extremely thin BGA format chip-scale package and its board level reliability,” 52nd ECTC, 2002.

34. T.Y. Tee, H.S. Ng, D. Yap, X. Baraton, Z.W. Zhong, “Board level solder joint reliability modeling and testing of TFBGA packages for telecommunication applications,” Journal of Microelectronics Reliability vol. 43, 2003.

35. Se-Young Jang, Soon-Min Hong, Min-Young Park, Dong-Ok Kwak, Jae-Woo Jeong, Sang-Hoon Roh, Young-Jun Moon, “FCOB (Flip Chip on Board) Reliability Study for Mobile Applications,” 54th ECTC, 2004.

36. Nael Hannan, Arni Kujala, Vinod Mohan, Paul Morganelli, Jayesh Shah, “Investigation of Different Options of Pre-Applied CSP Underfill for Mechanical Reliability Enhancements in Mobile phones,” 54th ECTC, 2004.

37. S. Irving, Y. Liu, “Free Drop Test Simulation for Portable IC Package by Implicit Transient Dynamics FEM,” 54th ECTC, 2004.

38. T.C. Chiu, K.J. Zeng, R. Stierman, D. Edwards, K. Ano, “Effect of Thermal Aging on Board Level Drop Reliability for Pb-free BGA Packages,” 54th ECTC, 2004.

39. Sambit K. Saha, Sesil Mathew, Sridhar Canumalla, “Effect of Intermetallic Phases on Performance in a Mechanical Drop Environment: 96.5Sn3.5Ag Solder on Cu and Ni/Au Pad Finishes,” 54th ECTC, 2004.

40. Pradeep Lall, Dhananjay Panchagade, Yueli Liu, Wayne Johnson, Jeff Suhling, "Models for Reliability Prediction of Fine-Pitch BGAs and CSPs in Shock and Drop-Impact," 54th ECTC, 2004.

41. Masazumi Amagai, Yoshitaka Toyoda, Tsukasa Ohnishi, Satoru Akita, "High Drop Test Reliability: Lead-free Solders," 54th ECTC, 2004.

Product Level Drop Test References

42. C.T. Lim and Y.J. Low, "Drop Impact Testing of Portable Electronic Products," 52nd ECTC, 2002.

43. C.T. Lim, C.W. Ang, L.B. Tan, S.K.W. Seah, E.H. Wong, "Drop Impact Survey of Portable Electronic Products," 53rd ECTC, 2003.

44. S.K.W. Seah, C.T. Lim, E.H. Wong, V.B.C. Tan, V.P.W. Shim, "Mechanical Response of PCBs in Portable Electronic Products During Drop Impact," 4th EPTC, 2002.

45. Y.C. Ong, V.P.W. Shim, T.C. Chai, C.T. Lim, "Comparison of Mechanical Response of PCBs Subjected to Product-Level and Board-Level Drop Impact Tests," 53rd ECTC, 2003.

46. Y.J. Low, "Drop Impact Testing of Cellular Products", B.Eng. Thesis, National University of Singapore, 2000/2001.

47. Y.P. Teo, "Study of Physical Robustness of Small Electronic Consumer Products", B.Eng. Thesis, National University of Singapore, 1997/1998.

48. S.M. Lee, "Experimental Investigation Of The Impact Behavior of Electronic Pagers and Components", B.Eng. Thesis, National University of Singapore, 1995/1996.

49. Yasuhisa Yamaji, Takehiro Suzuki, Hirofumi Yamasaki, Tsukasa Ohishi, Yasunori Chikawa, Noritoshi Kako, “New Evaluation Method of CSPs Board Level Reliability using Strain Gauge”, 50th ECTC, 2000.

50. Liping Zhu, “Modeling Technique for Reliability Assessment of Portable Electronic Product Subjected to Drop Impact Loads”, 53rd ECTC, 2003.

Board Level Vibration and Cyclic Bending Tests References

51. T.Y. Hin; K.S. Beh; K.N. Seetharamu, “Development of a dynamic test board for FCBGA solder joint reliability assessment in shock & vibration,” 5th EPTC, 2003.

52. P. Geng, W.M. Beltman, P.H. Chen, G. Daskalakis, D. Shia, M.H. Williams, “Modal analysis for BGA shock test board and fixture design,” 5th EPTC, 2003.

53. J.D. Wu, S.H. Ho, P.J. Zheng, C.C. Liao, S.C. Hung, “An Experimental Study of Failure And Fatigue Life of a Stacked CSP Subjected to Cyclic Bending”, 51st ECTC, 2001.

54. Jiansen Zhu, Stephen Quander, Tommi Reinikainen, “Global/Local Modeling for PWB Mechanical Loading”, 51st ECTC, 2001.

55. F.X. Che, H.L.J. Pang, F.L. Wong, G.H. Lim, T.H. Low, “Vibration Fatigue Test and Analysis for Flip Chip Solder Joints”, 5th EPTC, 2003.

56. Andrew Skipor, Larry Leicht, “Mechanical Bending Fatigue Reliability and Its Application to Area Array Packaging”, 51st ECTC, 2001.

Other References

57. S.K.W. Seah, C.T. Lim, V.B.C. Tan, “S.E. Quah, “Study of Microvia Failure Under PCB Flexing Loads,” 53rd ECTC, 2003.

58. Phil Geng, Philip Chen, Yun Ling, “Effect of Strain Rate on Solder Joint Failure under Mechanical Load”, 52nd ECTC, 2002.

59. Santosh Shetty, Tommi Reinikainen, “Three and Four-Point Bend Testing for Electronic Packages”, Journal of Electronic Packaging, 2003.

60. P.Z. Zheng, J.Z. Lee, K.H. Liu, J.D. Wu, S.C. Hung, “Solder Joint Reliability of TFBGA Assemblies with Fresh and Reworked Solder Balls,” Microelectronics Reliability Journal vol. 43, 2003.

61. M. Date, T. Shoji, M. Fujiyoshi, K. Sato, K. N. Tu, “Impact Reliability of Solder Joints”, 54th ECTC, 2004.

62. Murali Hanabe, Sridhar Canumalla, “Package to Board Interconnection Shear Strength (PBISS) behavior at High Strain Rates Approaching Mechanical Drop,” 54th ECTC, 2004.

63. Cyril M. Harris, “Shock and Vibration Handbook” 4th Edition, 1995

Appendix A: Technical Drawings

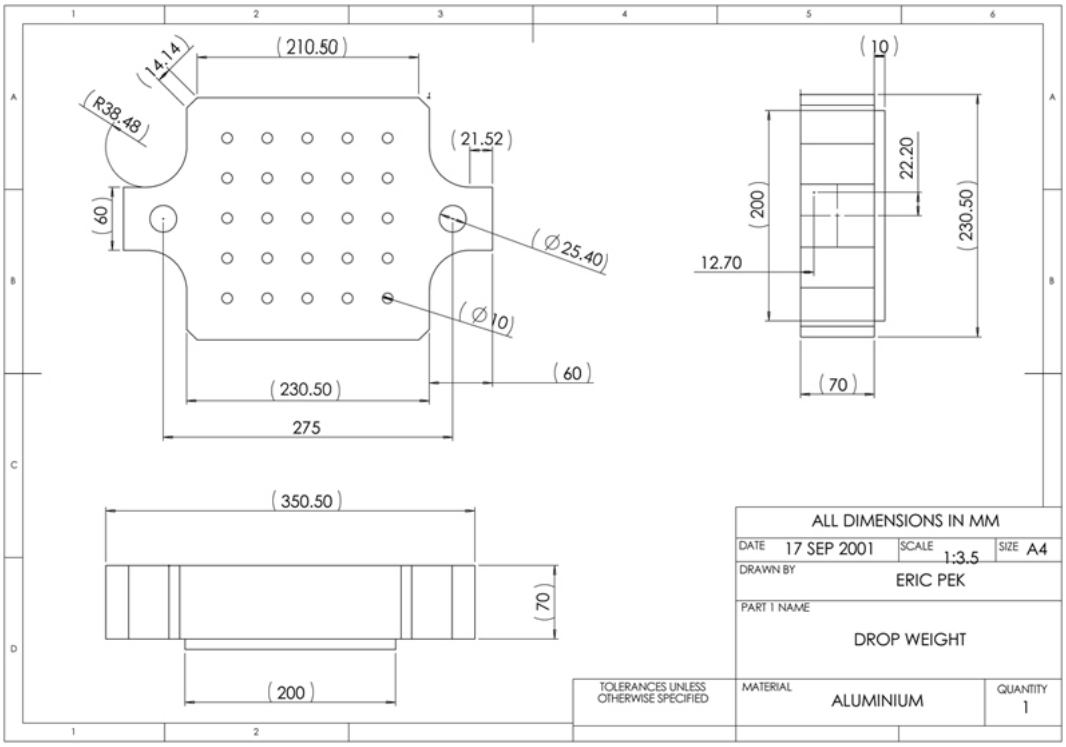

Figure A.1: Drop table drawing

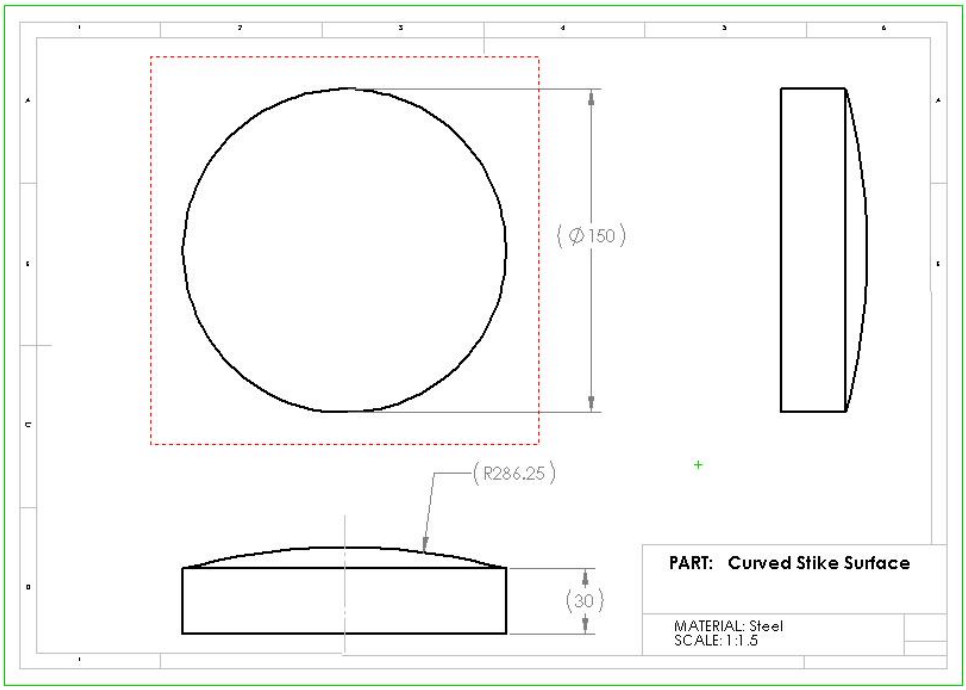

Figure A.2: Curved strike surface drawing

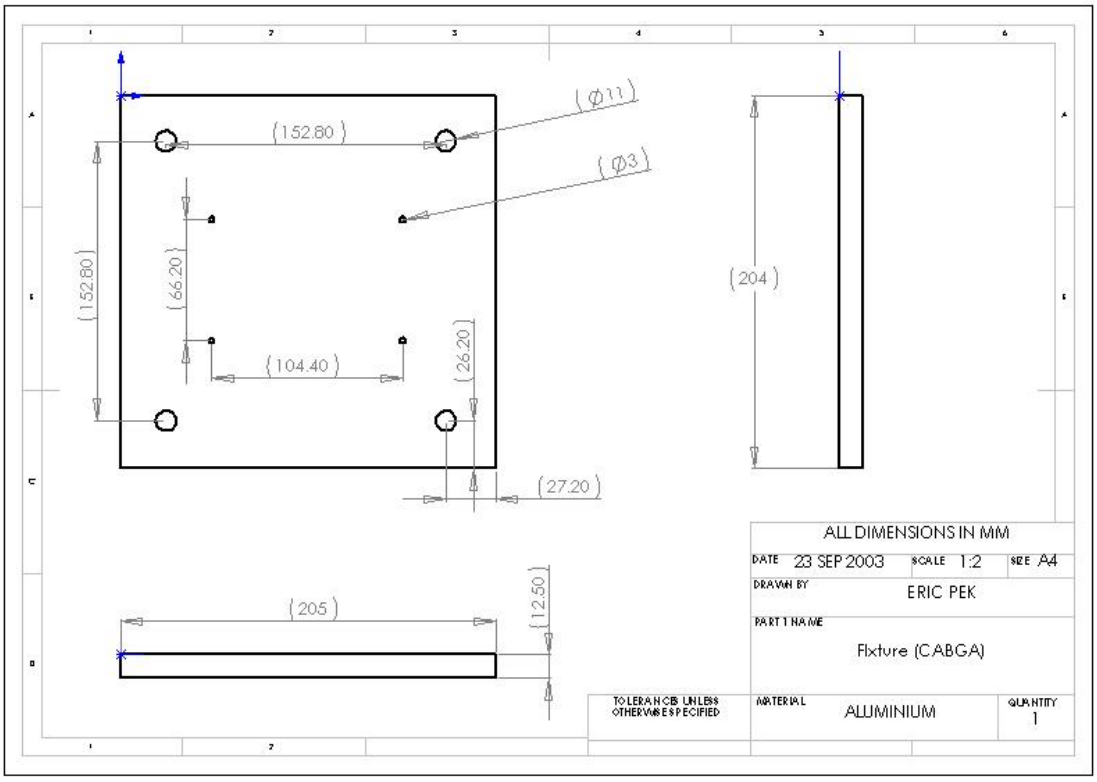

Figure A.3: Fixture for CABGA board at center

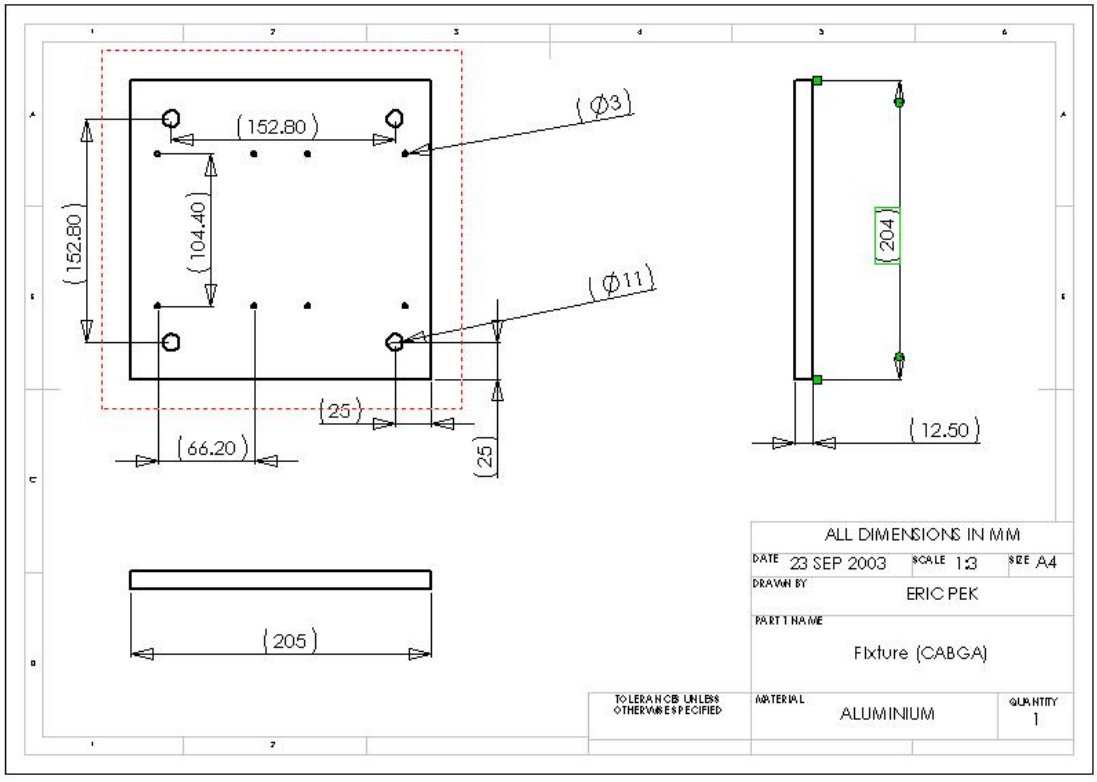

Figure A.4: Fixture for 2 CABGA boards

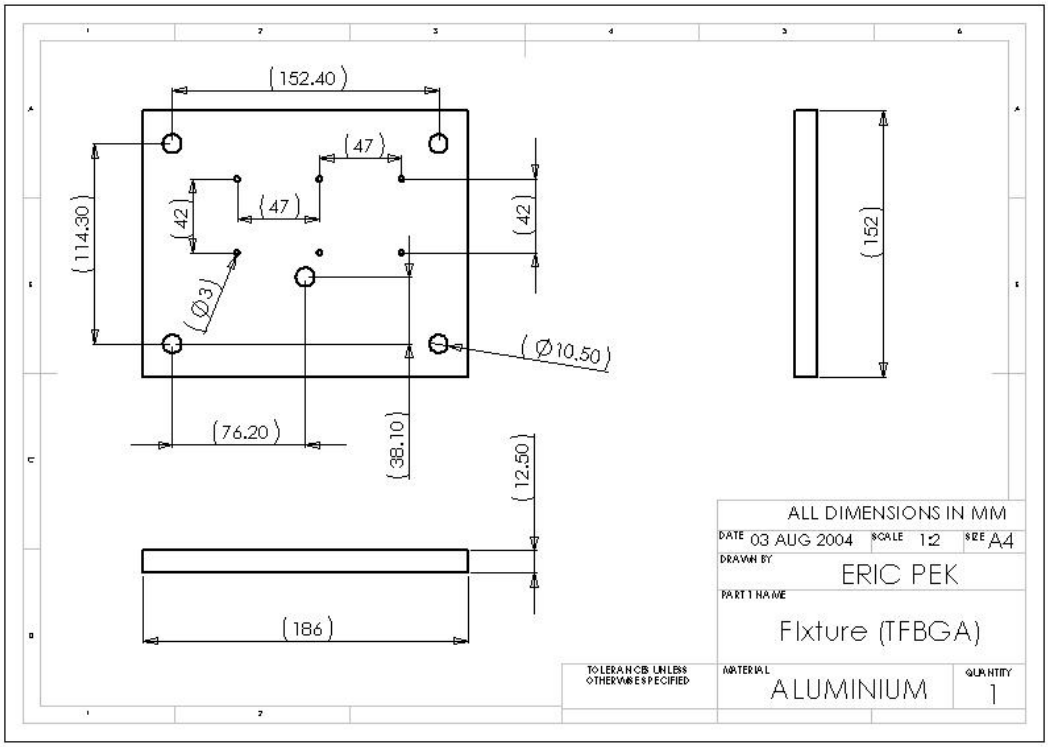

Figure A.5: Fixture for TFBGA board

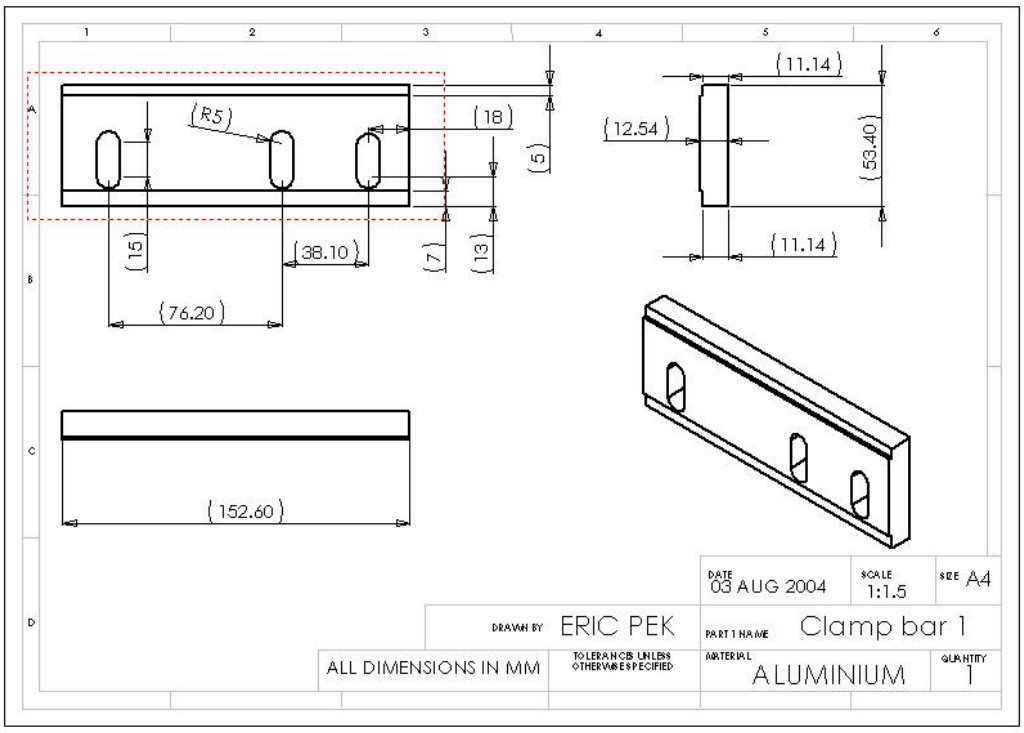

Figure A.6: Clamping bar type 1

Figure A.6 shows a fixture bar for clamping the TFBGA or CABGA board edge. The grooves at the edges are used to lock the board edges in place. Two clamping bars are

required to tighten an edge of the board. The other bar is the same as in Figure A.6 except that it has no grooves so that the edge could be tightened. The hole-slots are to fixture the bars to the drop table in various positions so that either the width or length of the CABGA/TFBGA boards could be clamped. Figure A.7 shows the other clamp bar required to clamp the other edge of the board.

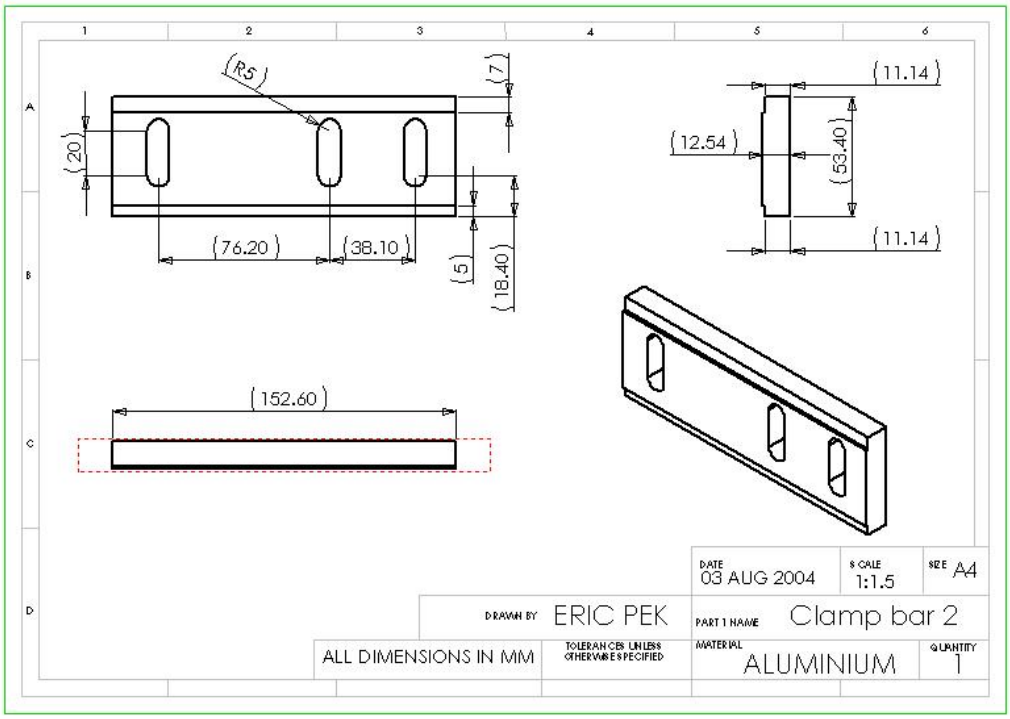

Figure A.7: Clamping bar type 2

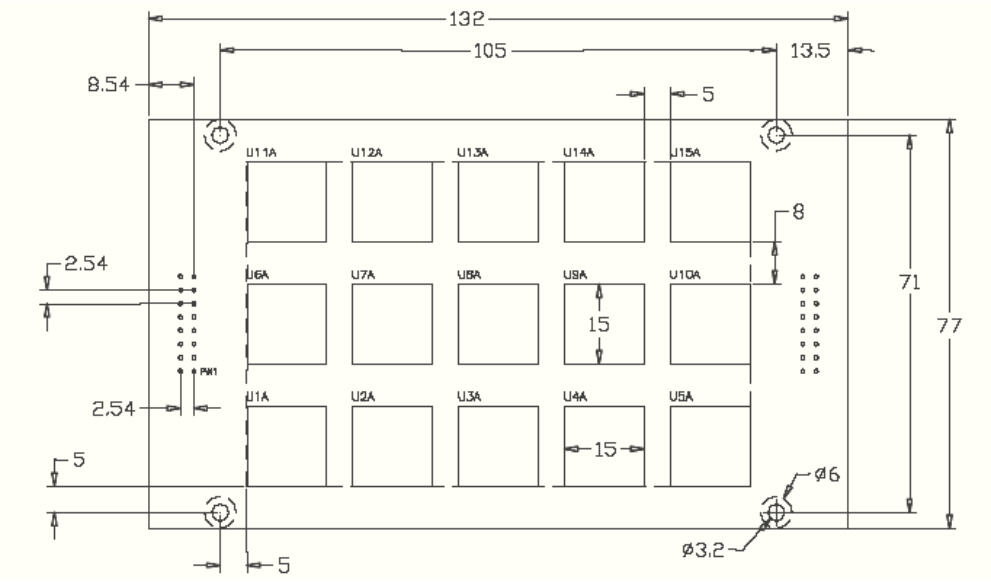

Figure A.8: JEDEC Proposed Test Board Size and Layout

Table A.1: X, Y coordinates for the centers of the components
(Center of lower left screw hole used as datum)

Component ID	X location of component center (mm)	Y location of component center (mm)
U1	5 + CompX/2	5 + CompY/2
U2	28.75 + CompX/4	5 + CompY/2
U3	52.5	5 + CompY/2
U4	76.25 - CompX/4	5 + CompY/2
U5	100 - CompX/2	5 + CompY/2
U6	5 + CompX/2	35.5
U7	28.75 + CompX/4	35.5
U8	52.5	35.5
U9	76.25 - CompX/4	35.5
U10	100 - CompX/2	35.5
U11	5 + CompX/2	66 - CompY/2
U12	28.75 + CompX/4	66 - CompY/2
U13	52.5	66 - CompY/2
U14	76.25 - CompX/4	66 - CompY/2
U15	100 - CompX/2	66 - CompY/2
CompX & CompY: Component length and width.		

Table A.2: Component locations for test boards

Group	Number of components in the group	Component locations on the board	Sample size	
			Side A Assembly	Side B Assembly
A	4	U1, U5, U11, & U15	8	8
B	4	U2, U4, U12, & U14	8	8
C	2	U6 & U10	4	4
D	2	U7 & U9	4	4
E*	2	U3 & U13	4	4
F*	1	U8	2	2

Table A.3: Component Test Levels

Service Condition	Acceleration Peak (G)	Pulse Duration (ms)
H	2900	0.3
G	2000	0.4
B	1500	0.5
F	900	0.7
A	500	1.0
E	340	1.2
D	200	1.5
C	100	2.0

Appendix B: Experimental Plots

Table B.1: Effect of drop height on peak acceleration / area under G(t) graph

H, Drop height (m)	A, Area under G(t) graph	G_m, Peak Acceleration
0.5	0.4656	1540
0.6	0.5125	1680
0.7	0.59	1960
0.8	0.6235	2040
0.9	0.6689	2240
1	0.713	2440
1.1	0.7554	2640
1.2	0.8051	2840
1.3	0.8246	2840
1.4	0.838	2960
1.5	0.8737	3080

The area under the G(t) graph is estimated using the trapezium rule. The time step used is the same resolution as the capture rate of the oscilloscope used. It is about 0.0004985ms. The G(t) graph is in terms of Gs where 1G is 9.81m/s^2. The area is also expressed in terms of Gs.

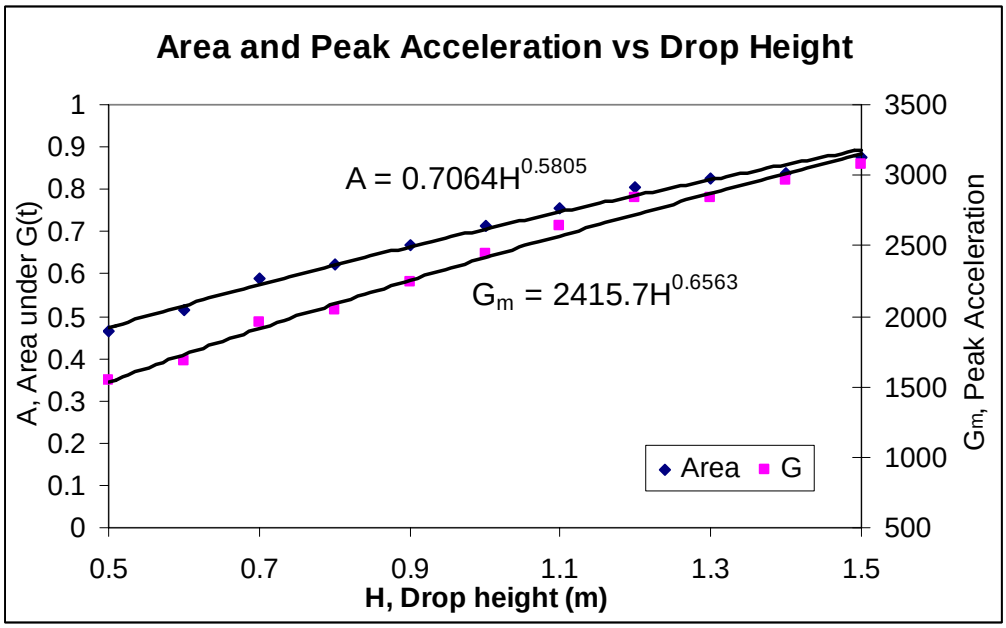

Figure B.1: Plot of *A* and G_m vs. drop height

Additional drop test was conducted on a 2-screw support for the TFBGA board. The board is mounted on two shoulder screws in a position shown in Figure B.2. This is similar to a 4-screw support but the in-plane strains registered at the center of the board is slightly higher for the 2-screw support case (see Figures B.4 and B.5).

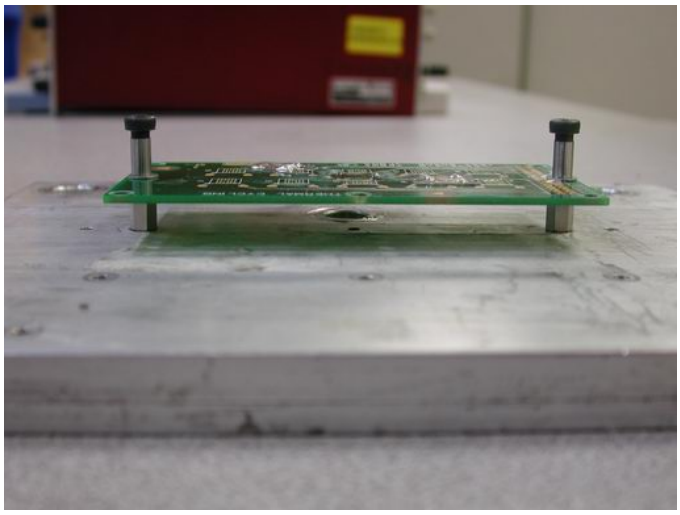

Figure B.2: 2-screw support for TFBGA board

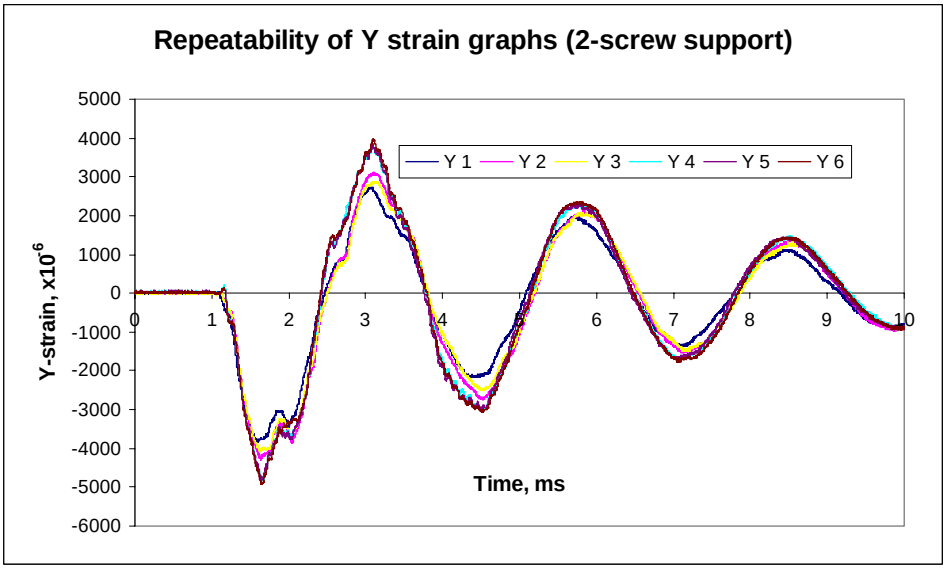

Figure B.3: Plot vs time for Y-strain reading at the center of the board (2-screw support)

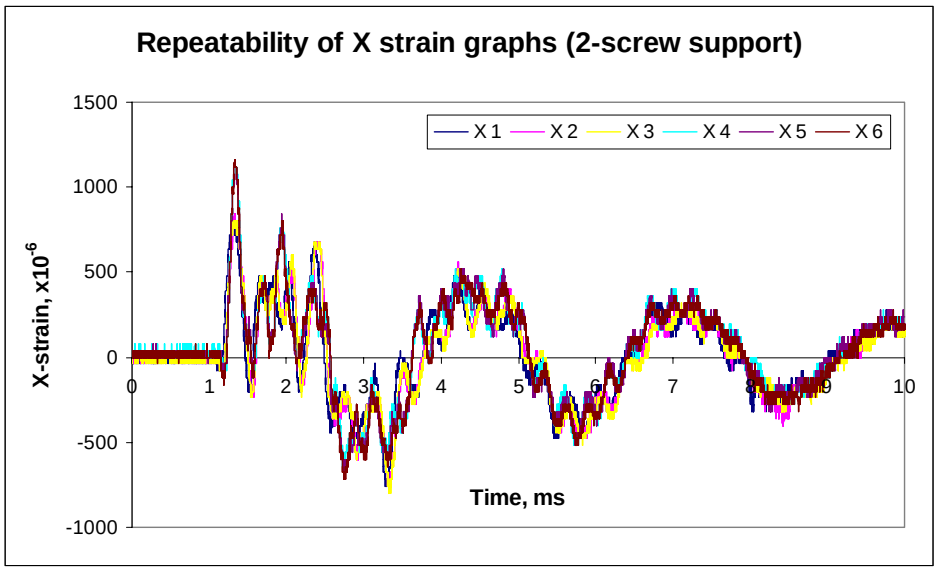

Figure B.4: Plot vs time for X-strain reading at the center of the board (2-screw support)

Figures B.5 to B.7 show the output acceleration trends of the TFBGA board at the board center, where a package is located. The accelerometer is mounted using cyanoacrylate glue to the top of a package facing down. At higher drop heights, the high G levels exceed the maximum limit of the accelerometer's specifications.

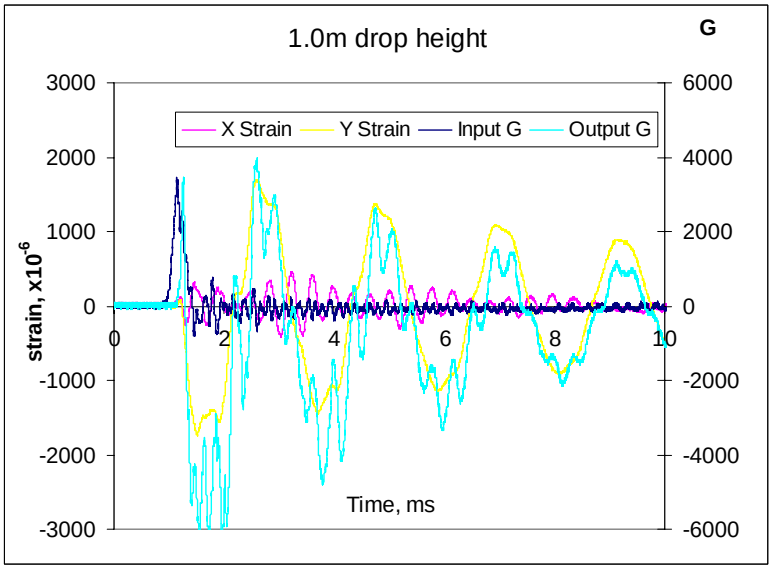

Figure B.5: Plots of strains and output acceleration vs time for test on CABGA board conducted at 1m drop height

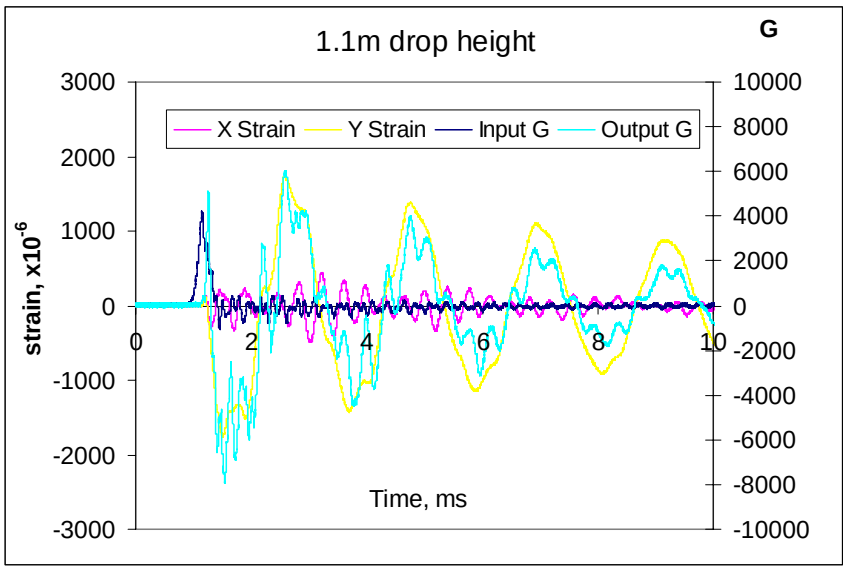

Figure B.6: Plots of strains and output acceleration vs time for test on CABGA board conducted at 1.1m drop height

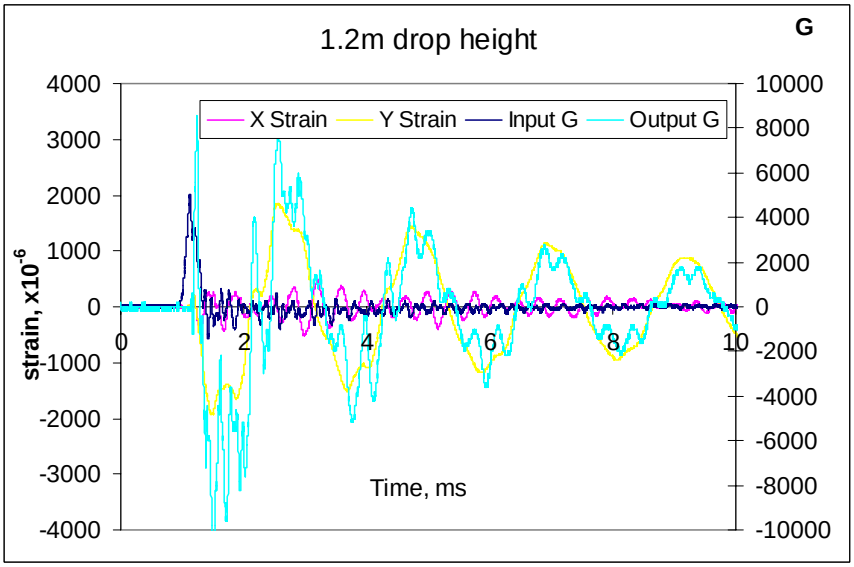

Figure B.7: Plots of strains and output acceleration vs time for test on CABGA board conducted at 1.2m drop height

Figure B.8 shows the output acceleration for a loose screw case. The conditions are kept the same for the TFBGA board except that the screws are loosened. The output acceleration in a loose-screw configuration acts the same as the in-plane strain in the length direction, where the peaks and troughs occur slightly later due to the slower bending of the board.

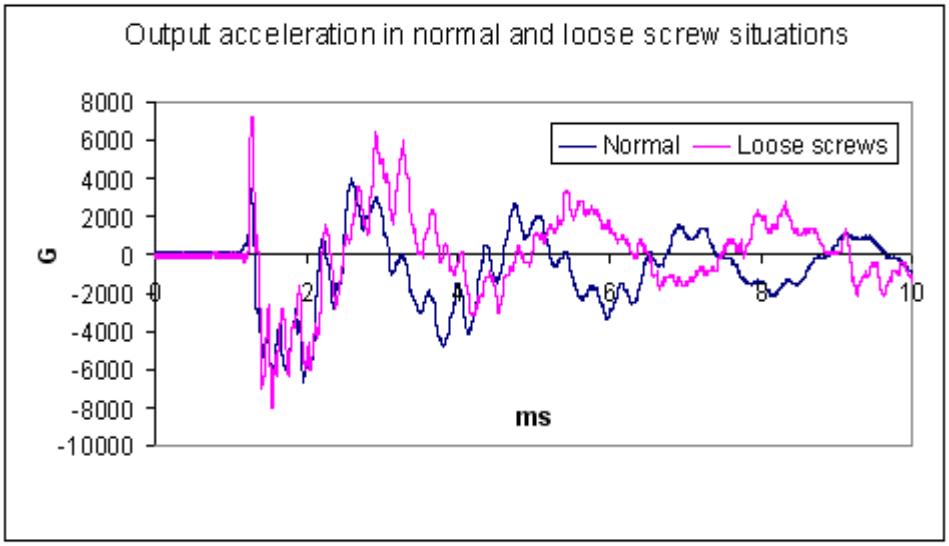

Figure B.8: Plots of output acceleration vs time for tightened and loosened screw mounting

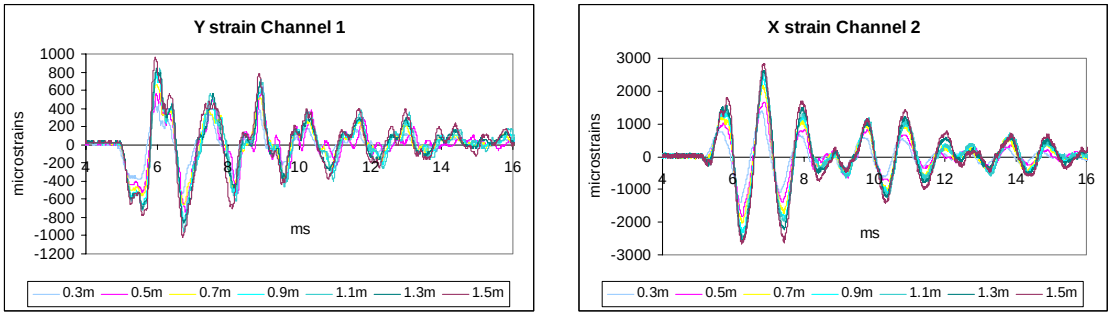

Figure B.9: Drop height study of 5-screw support on CABGA board (ch 1 and 2)

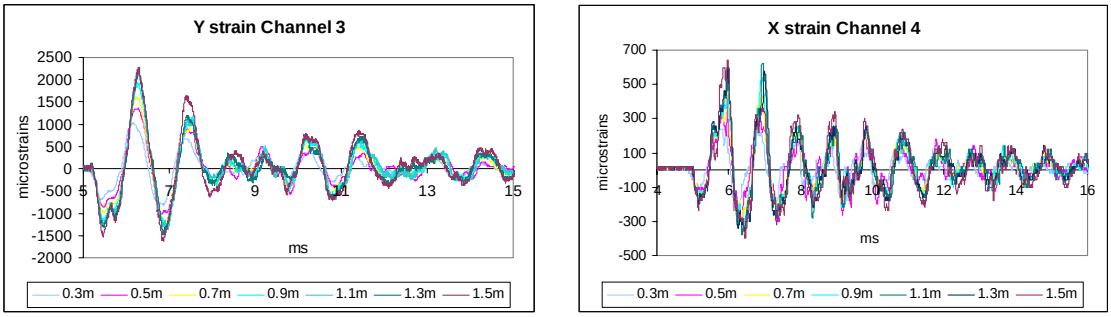

Figure B.10: Drop height study of 5-screw support on CABGA board (ch 3 and 4)

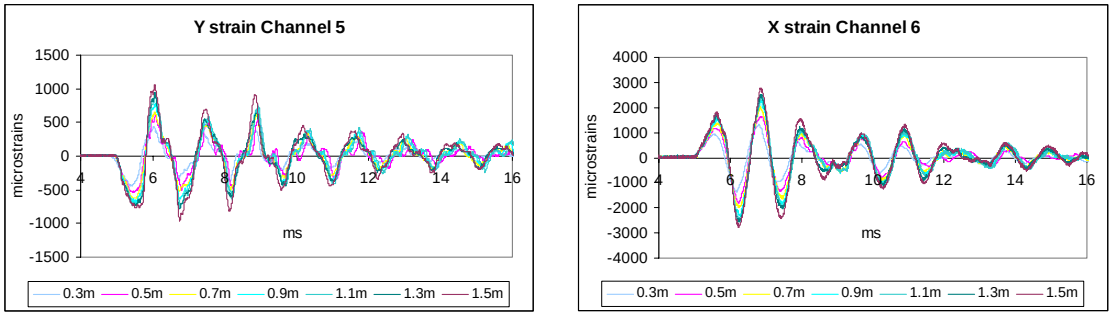

Figure B.11: Drop height study of 5-screw support on CABGA board (ch 5 and 6)

Appendix C: High-speed camera images

The high-speed images shown are taken at a frame rate of 6000 frames per second. Each picture shown is taken from every two frames for simplicity. The images shown are taken during the first impact of the drop weight on the strike surface.

C.1: High-speed images of PCB knocking effect

		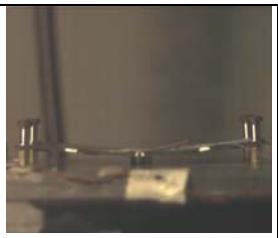	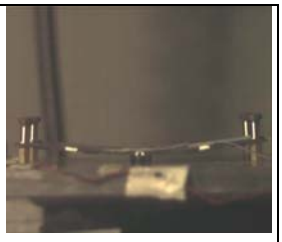
t = 0ms	t = 0.33ms	t = 0.67ms	t = 1ms
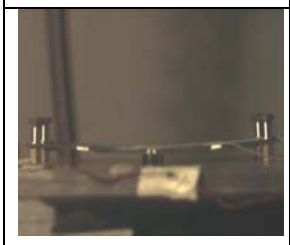	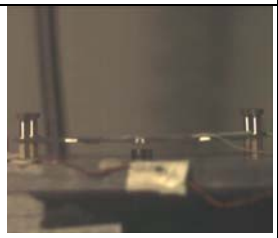	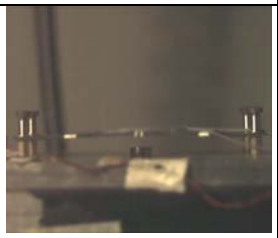	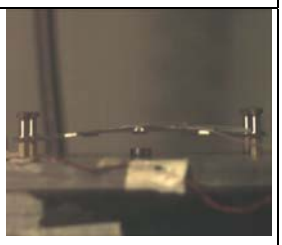
t = 1.33ms	t = 1.67ms	t = 2ms	t = 2.33ms
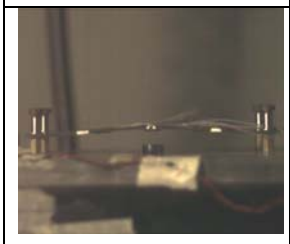	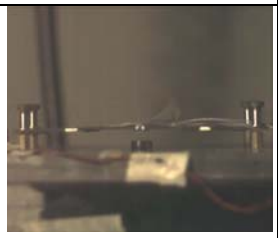	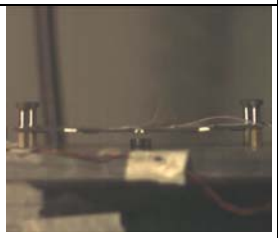	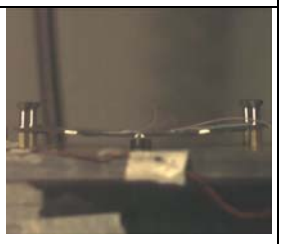
t = 2.67ms	t = 3ms	t = 3.33ms	t = 3.67ms
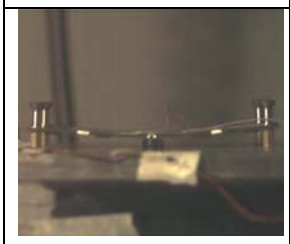	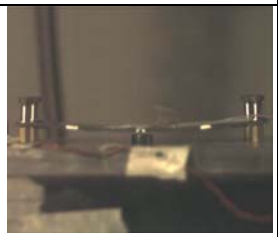	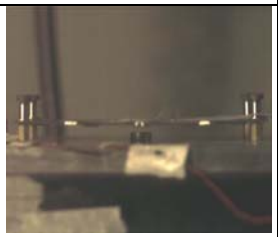	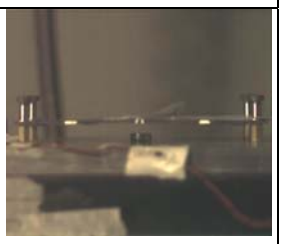
t = 4ms	t = 4.33ms	t = 4.67ms	t = 5ms

Figure C.1: Investigating the knocking effect of PCB arising from clearance height of 6mm conducted at 1.5m drop height

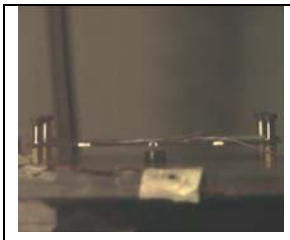	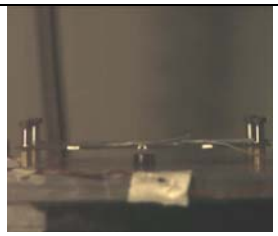	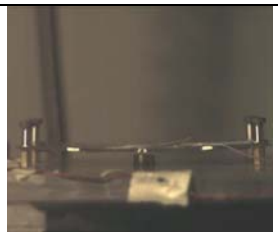	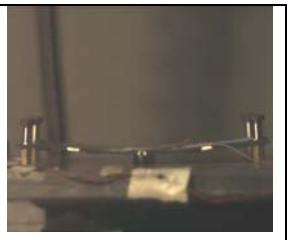
t = 0ms	t = 0.33ms	t = 0.67ms	t = 1ms
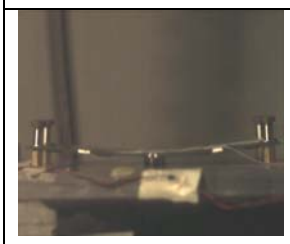	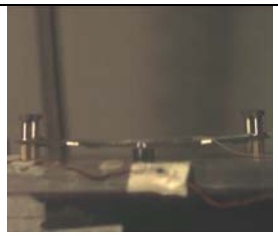	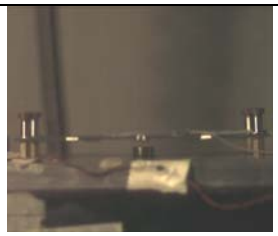	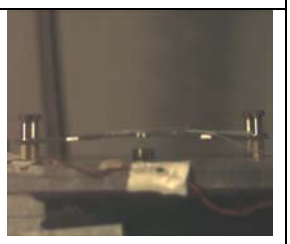
t = 1.33ms	t = 1.67ms	t = 2ms	t = 2.33ms
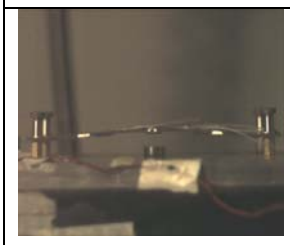	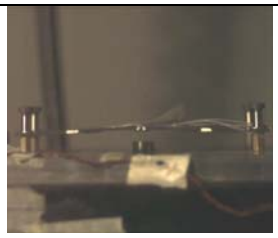	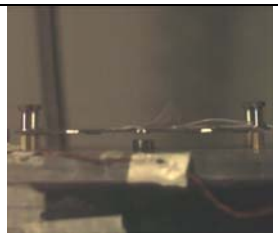	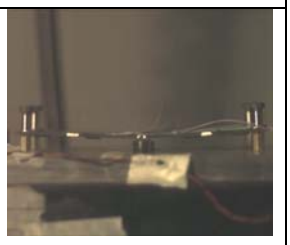
t = 2.67ms	t = 3ms	t = 3.33ms	t = 3.67ms
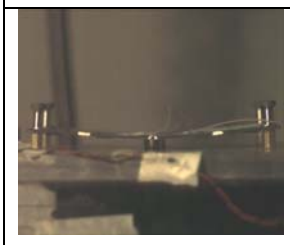	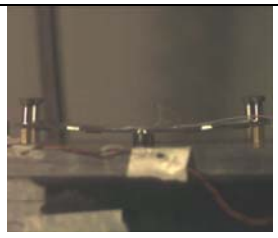	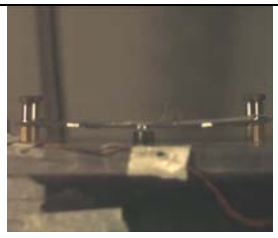	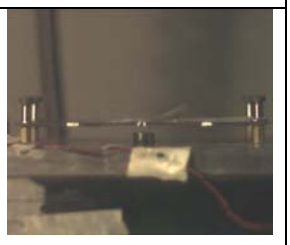
t = 4ms	t = 4.33ms	t = 4.67ms	t = 5ms

Figure C.2: Investigating the knocking effect of PCB arising from clearance height of 5mm conducted at 1.5m drop height

		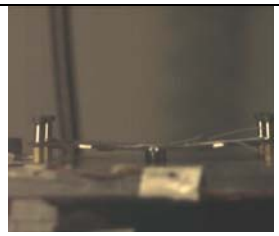	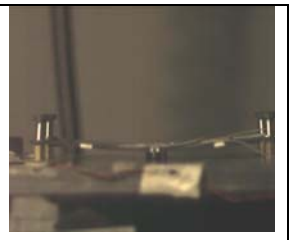
t = 0ms	t = 0.33ms	t = 0.67ms	t = 1ms
			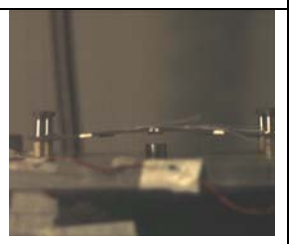
t = 1.33ms	t = 1.67ms	t = 2ms	t = 2.33ms
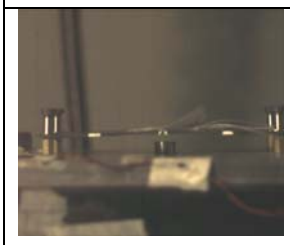			
t = 2.67ms	t = 3ms	t = 3.33ms	t = 3.67ms
	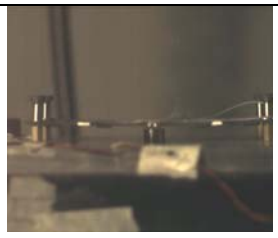	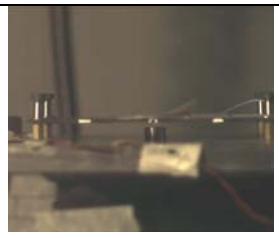	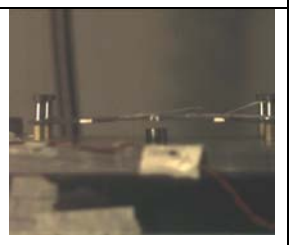
t = 4ms	t = 4.33ms	t = 4.67ms	t = 5ms

Figure C.3: Investigating the knocking effect of PCB arising from clearance height of 4mm conducted at 1.5m drop height

C.2: High-speed images of TFBGA board width side

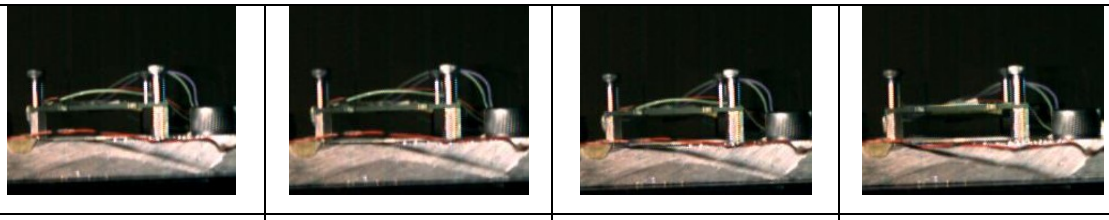

t = 0ms	t = 0.33ms	t = 0.67ms	t = 1ms

t = 1.33ms	t = 1.67ms	t = 2ms	t = 2.33ms

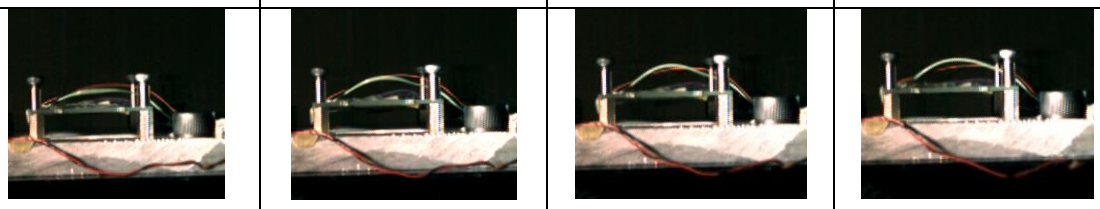

t = 2.67ms	t = 3ms	t = 3.33ms	t = 3.67ms

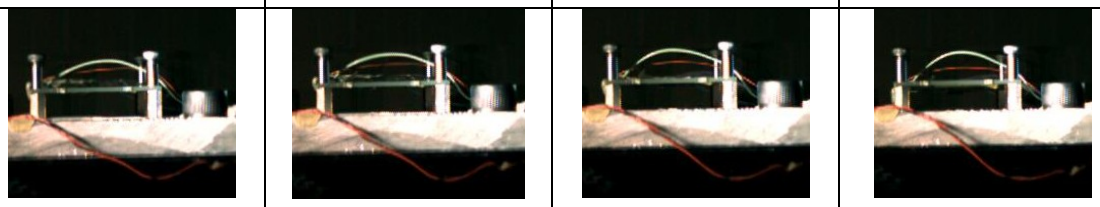

t = 4ms	t = 4.33ms	t = 4.67ms	t = 5ms

Figure C.4: Investigating the TFBGA mounted PCB viewed from the board width at 1.5m drop height

C.3: High-speed images of TFBGA board mounted on nuts and screws

Figure C.3 shows a TFBGA board that uses nuts as spacing. The nuts are then tightened by means of screws. The nuts used might pose a problem, as the amount of spacing might not be enough for board bending. In fact, it is likely that the board might impact on the fixture during the drop impact. If there is any package that is situated at the center of the board, it might cause impact on the package directly if the package is positioned facedown. Frame 3 might be a situation where the package is likely to impact on the fixture. As a result, it may not be a good board level drop test to use nuts for spacing.

			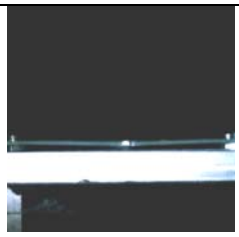
t = 0ms	t = 0.33ms	t = 0.67ms	t = 1ms
			
t = 1.33ms	t = 1.67ms	t = 2ms	t = 2.33ms
			
t = 2.67ms	t = 3ms	t = 3.33ms	t = 3.67ms
			
t = 4ms	t = 4.33ms	t = 4.67ms	t = 5ms

Figure C.5: Examining the knocking effect of a TFBGA mounted board using nuts for spacing

Appendix D: Experimental Procedures

Standard Operating Instructions for the Lansmont Drop Tower

1. Ensure the drop table is at the rest position before switching on the power. Ensure no loose equipment is placed on the drop table or fixture.
2. Check that the bushings of the drop table are tightly in place inside.
3. Raise the drop table slightly and align the strike surface with the drop table. Screws or strong adhesives should secure the strike surface tightly.
4. Ensure the fixture is also tightly fixed and adequately screwed to the drop table.
5. Ensure that all wires, especially accelerometer cables, are properly secured by beeswax and masking tape to avoid flexing during impact. Ensure the wires at the sharp edges of the fixture and drop table are properly added with beeswax.
6. Adjust the height gauge to the correct drop height setting. The measuring tape is at the side for reference.
7. Ensure that all wires are adequately long enough to prevent pulling of wires when raised to a high drop height.
8. Pay caution to the trigger level as pressing the up button on the control unit might cause some signal noise that may set off the trigger and may result in pre-triggering of signal before impact.
9. After impact, ensure the bushings are back in place and that the secured areas (masking tapes, double-sided tapes, beeswax etc) are still secured.

High-speed camera operating instructions

1. Start up control unit of APX high-speed camera and turn on the LCD monitor and spotlight(s).
2. Adjust spotlight(s) to focus on the specimen for best clarity of images.
3. Adjust the aperture of the camera lens for correct lighting and the focusing of the lens. Make sure the camera lens is securely fixed.
4. Trigger ‘Record Ready’ mode and set to endless recording with external trigger if possible. The external trigger is useful in controlling the recording while conducting the experiment.
5. Raise the drop table to desired drop height and release. After the drop table impacts fully on the strike surface for a few seconds, press the trigger to stop recording.
6. Switch off all lighting. Check the high-speed images via a laptop to ensure the drop process has been recorded.
7. Download the range of frames in video or jpeg format from just before to after drop impact of the drop table.
8. Switch off all equipment after use. Close back the lens with a lens cover to prevent water and dust particles from entering.

Accelerometer setup procedures

1. Use beeswax for mounting bigger size accelerometers like the Model 2252-02 and petrol wax for small accelerometers.
2. Ensure there is sufficient beeswax or petrol was for mounting and the wires near the terminals to sit on.
3. Scotch tape the wires tightly on the fixture so that they do not flap around during drop test.
4. Connect the wires to the charge amplifier and adjust to the correct settings (like sensitivity, scaling, high-pass frequency).
5. Ensure wires are given enough slag and space for the drop height tested. Ensure any objects do also not obstruct the wires during drop test.

Strain gauge preparation procedures

1. Grind and sand away the rough area of the PCB or specimen where the strain gauges will be mounted. Make sure the area is smooth and not too dug in. Clean with alcohol or acetone.
2. Stick the strain gauge to a piece of scotch tape such that the mounted side is not in the scotch tape.
3. Tape it on the PCB and release it partially so that the mounted side is exposed.
4. Apply cyanoacrylate glue to the exposed area of the strain gauge and press it to the PCB with a piece of tracing paper for about a minute.
5. Remove the scotch tape slowly making sure the strain gauge wires are not broken. Place pieces of scotch tape underneath the strain gauge wires if they touch any metallic surfaces. This is to ensure insulation of the wires.
6. Place metal contacts beside the strain gauge and connect the wires to the contacts by soldering. The contacts are connected to another set of wires that connect to the strain bridges.
7. Wait for a few hours for the glue to be completely cured.